# BIO-ENGINEERING OF A TRACHEAL CONSTRUCT-IDENTIFICATION OF APPROPRIATE BIOMATERIAL SCAFFOLDS AND CONDITIONS

**RAHUL V.G**

**Ph.D. THESIS**

**2022**

**SREE CHITRA TIRUNAL INSTITUTE FOR MEDICAL**

**SCIENCES AND TECHNOLOGY**

**THIRUVANANTHAPURAM**

**INDIA**

# BIO-ENGINEERING OF A TRACHEAL CONSTRUCT-IDENTIFICATION OF APPROPRIATE BIOMATERIAL SCAFFOLDS AND CONDITIONS

**A THESIS PRESENTED BY**

**RAHUL V.G**

**TO**

**SREE CHITRA TIRUNAL INSTITUTE FOR MEDICAL**

**SCIENCES AND TECHNOLOGY**

**THIRUVANANTHAPURAM**

**INDIA**

**IN PARTIAL FULFILMENT OF THE REQUIREMENTS**

**FOR THE AWARD OF**

**DOCTOR OF PHILOSOPHY**

**2022**

# DECLARATION

I, **Rahul V.G**, hereby certify that I had personally carried out the work depicted in the thesis entitled, **"Bio-engineering of a tracheal construct- identification of appropriate biomaterial scaffolds and conditions"**, except where due acknowledgement has been made in the text. No part of the thesis has been submitted for the award of any other degree or diploma prior to this date.

**Date:** 28-03-2022

**Signature**

**Rahul V.G**

**SREE CHITRA TIRUNAL INSTITUTE FOR MEDICAL SCIENCES & TECHNOLOGY**
THIRUVANANTHAPURAM – 695012, INDIA
(An Institute of National Importance under Govt.of India)
Phone-(91)0471-2520242 Fax-(91)0471-2341814
Email- prabha@sctimst.ac.in Web site – www.sctimst.ac.in

**Dr. Prabha D. Nair,**PhD, FRSC, FBAIO
Scientist G (Senior Grade)
Division of Tissue Engineering and Regeneration Technologies
BMT Wing, SCTIMST
Thiruvananthapuram

This is to certify that **Mr. Rahul V.G** in the **Division of Tissue Engineering and Regeneration Technologies** of this Institute has fulfilled the requirements prescribed for the Ph.D. degree of the Sree Chitra Tirunal Institute for Medical Sciences and Technology, Thiruvananthapuram. The thesis entitled **"Bio-engineering of a tracheal construct - identification of appropriate biomaterial scaffolds and conditions"** was carried out under my direct supervision. No part of the thesis was submitted for the award of any degree or diploma prior to this date. Clearance was obtained from the Institutional Animal Ethics Committee for carrying out the study.

**Date:** 28.3.2022

**Signature**

The thesis entitled

**Bio-engineering of a tracheal construct - identification of appropriate biomaterial scaffolds and conditions**

Submitted by

**Rahul V.G**

for the degree of

**Doctor of Philosophy**

Of

SREE CHITRA TIRUNAL INSTITUTE FOR MEDICAL SCIENCES AND TECHNOLOGY,

Thiruvananthapuram

Is evaluated and approved by

Dr. Prabha D. Nair
(Name of the Guide)

Dr. Sourabh Ghosh (IIT Delhi)
(Name of thesis examiner)

## *ACKNOWLEDGEMENTS*

***I would never have been able to finish my dissertation without the guidance, help, support and encouragement of numerous people around me. I would like to thank all those who made this thesis possible and it is a pleasant task to express my thanks to all those who contributed in many ways to the success of this study.***

***At this moment of accomplishment, first of all I express my sincere and deepest gratitude to my guide Dr. Prabha D. Nair. This work would not have been possible without her guidance, support and encouragement. Under her guidance I successfully overcame many difficulties. I remember my first oral presentation where she sat beside me and taught me patiently how to prepare and perform a scientific presentation which was a lesson for me for my future presentations. I thank her and I am indebted to her for the patience, motivation and enthusiasm shown to me in my failures and difficulties.***

***I am grateful to the present Director, former Directors of this Institute and also The Head, BMT Wing for giving me the opportunity as well as for providing the facilities to carry out my research in this Institute.***

***I would like to thank my Doctoral Advisory Committee members, Dr. H.K. Varma and Dr. P.R Umashankar for their valuable suggestions throughout my study.***

***I thank the Deputy Registrar, Academic Division and Project Cell for their help in academic affairs. I acknowledge SCTIMST for providing financial assistance in the form of research fellowship throughout the tenure.***

***Most of the results described in this thesis would not have been obtained without the support and help of many Scientists and staff of SCTIMST. I am thankful to Dr. Renjith. S and Dr. Radhakumary C, Central Analytical Facility for the DSC, TGA experiments. I thank Dr.Nishad, Bioceramics Laboratory for the SEM imaging. I am grateful to Dr. Sachin Shenoy, Dr. Hari, Mr. Manoj, Mr. Sunil and all staff of DLAS for their help in giving the cadaver organs. I also thank Dr.Lissymol P.P, Dr. Deepu D. R, Dental Products Laboratory for the mechanical testing experiments. I also thank Dr. P.R. Anilkumar for helping me with the confocal imaging. I express my gratitude to the entire***

*faculty who took effort in spending their valuable time and sharing their knowledge in the course work conducted.*

*I also extend my gratitude to The Director, Rajiv Gandhi Centre for Biotechnology, for giving the permission to use the confocal microscope facility and my sincere thanks to Kerala University, CLIF unit for the NMR experiments.*

*On a personal note, I would like to thank every member of the Division of Tissue Engineering and Regeneration Technologies (DTERT). Most of all I sincerely thank my seniors Dr. Neethu Mohan, Dr. Lynda, for teaching me the basics as well as for their expert advice, help and friendship. I would also like to thank the ex-members of DTERT, especially Dr. Shiny, Mrs. Nimi, Dr. Dhanesh for helping me with their valuable suggestions. My special thanks to Dr. Babitha and Ms. Jijo for their valuable friendship and help throughout. I thank you all- Dr. Bindu, Mrs. Geetha, Dr. Resmi, Dr. Rakhi, Dr. Merlin, Dr. Neelima, Dr. Sivadas and Dr. Amrita for their cooperation and help throughout my work. I warmly thank all other fellow colleagues for their care and concern. Besides this, several people have knowingly and unknowingly helped me in the successful completion of this project. I would also like to express my respect to Ms. Alexandra Elbakyan for her constant effort in making knowledge free.*

*It's my fortune to gratefully acknowledge the support of my family. Words fail me to express my appreciation to my beloved parents, my brothers, my friend Cuckoo and her family, who were beside me during the happy and hard moments to push me and motivate me. I owe everything to them.*

*Last, but not the least, I thank the Almighty for the wisdom and perseverance that he has bestowed upon me during this research project and throughout my life.*

***Rahul V.G***

# TABLE OF CONTENTS

# LIST OF FIGURES

# LIST OF TABLES

# ABBREVIATIONS

| | |
|---|---|
| 2D | Two dimensional |
| 3D | Three dimensional |
| AFM | Atomic force microscope |
| BMP | Bone morphogenetic protein |
| CAD | Computer aided design |
| cAMP | Cyclic adenosine monophosphate |
| DAPI | 4,6-diamidino-2-phenylindole |
| DMEM | Dulbecco's minimal essential medium |
| DSC | Differential scanning calorimetry |
| ECM | Extracellular matrix |
| FBS | Fetal bovine serum |
| FGF | Fibroblast growth factor |
| FOX | Forkhead box |
| FTIR | Fourier transform infrared |
| GAG | Glycosaminoglycan |
| Gata | Guanine adenine thymine adenine |
| Gli | Glioma associated oncogene |
| GPa | Giga pascal |
| GPC | Gel permeation chromatography |
| HDI | Hexamethylenediisocyanate |
| iPSC | Induced pluripotent stem cells |
| kDa | Kilo dalton |
| MPa | Mega pascal |
| NMR | Nuclear magnetic resonance |
| PAMPs | Pathogen-associated molecular patterns |
| PBS | Phosphate buffered saline |
| PCL | Polycaprolactone |
| PGA | Polyglycolic acid |

| | |
|---|---|
| PLA | Polylactic acid |
| PLCL | Poly(lactide-co-caprolactone) |
| PLGA | Poly(lactide-co-glycolic acid) |
| Ppm | Parts per million |
| Pr | Printability |
| PRRs | Pattern recognition receptors |
| PUU | Polyurethane urea |
| RNA | Ribonucleic acid |
| SEM | Scanning electron microscope |
| Shh | Sonic hedgehog |
| Tc | Temperature of crystallization |
| Td | Degradation temperature |
| Tg | Glass transition temperature |
| TGA | Thermo gravimetric analysis |
| TGF | Transforming growth factor |
| Tm | Melting temperature |
| UTM | Universal testing machine |
| Wnt | Wingless related integration site |

# SYNOPSIS

The thesis entitled **"Bio-engineering of a tracheal construct - identification of appropriate biomaterial scaffolds and conditions"**, deals with the development of a tissue engineered tracheal construct having 3D cell distribution and comparable mechanical properties as that of the native trachea. The study explores the synthesis of elastomeric materials and the feasibility of fabricating them into a 3D tracheal scaffold, emphasizing on the mechanical properties and 3D cell distribution of the tracheal construct. The major requirement of a tracheal scaffold is its elastic property, as implanting a mechanically rigid structure may cause mechanical mismatch and its failure. Having a 3D cell distribution is another important feature required for the successful regeneration of the cartilage rings. Having these mechanical properties and 3D cell distribution in one system is a challenge. Hence, in this work we explore different biomaterials and their fabrication methodologies along with studies of cell distribution so as to have all these properties incorporated as a single system which would be the potential tracheal construct.

Tracheal disorders can occur due to many reasons like congenital, trauma, iatrogenic or neoplastic. In case of small injuries, the human body has the ability to repair itself, but in case of major defects it has to be treated using different strategies. Presently the most commonly used strategy is tracheal resection and end-to-end anastomosis. But this has its limitations, the technique can be used only if the defective part is less than 50% of the total tracheal length and in the case of infants it's less than 30% of the tracheal length. Hence these presently available treatment strategies have limitations and are not applicable in all instances.

Another effective method is allogenic tracheal transplantation;even though its success rate is high, there is not enough donor tracheas available to meet the clinical needs and size mismatch is also often a problem, especially when the implant is to be used for small children. Hence a synthetic substitute would be a promising approach which can address all these problems.

There have been many biomaterials explored for the feasibility to be used for tracheal tissue engineering. An ideal biomaterial alone does not make a successful tracheal construct; an appropriate fabrication method is also required in order to include many features important for a functional trachea. Many materials like Polycaprolactone (PCL), Polylactic acid (PLA), Poly lactide-co-glycolic acid (PLGA) have already been tested for its efficacy to repair tracheal defects. But these materials lack cell adhesion moieties and hence have limited cell response. To bring cytocompatibility and mechanical property in one system requires an interdisciplinary approach such as "Tissue engineering approach" involving expertise and strategies from different fields like material science, engineering and biology.

In this study, two elastomeric materials were synthesized and tested for its efficacy to be used as a tracheal scaffold. Further, the feasibility of the synthesized materials to fabricate into a tracheal construct was explored.

The work is based on the hypothesis: "A 3D elastomeric biphasic tracheal scaffold which can support cells and have adequate mechanical strength is expected to bring both mechanical properties and cytocompatibility in one system".

The aims of the work are:

Synthesis of elastomeric biomaterial and its characterization.

Identification of a suitable fabrication method for the development of the tracheal construct.

Designing a biphasic construct to maintain the mechanical properties and 3D cell distribution in the tracheal construct.

To achieve the aims, the following objectives are set for the work,

- Synthesis of elastomeric biomaterial for tracheal tissue engineering.
  Part I: Synthesis of polyurethane urea (PUU).
  Part II: Synthesis of poly(lactide-co-caprolactone) (PLCL).
- Fabrication of the synthesized elastomeric biomaterial into a 3D scaffold system for tracheal tissue engineering.

- Development of a biphasic design having elastomeric framework and a hydrogel system having appropriate mechanical properties and cytocompatibility.

The work is presented in six chapters. Chapter 1 begins with an introduction to the tracheal anatomy, the disorders associated with it and its treatment modalities. It also briefly introduces different biomaterials, fabrication strategies and various methods to develop a tracheal substitute. Chapter 2 carries a wide literature review, concentrating on currently used treatment modalities to treat the disorders associated with trachea. The topics reviewed include history of tracheal substitutes, biomaterials, tissue engineering concepts and different treatment modalities.

Chapter 3 involves the materials and methods that have been used to achieve the aforementioned objectives. This includes detailed description of the experimental protocols, materials used, instruments utilized and preliminary cytotoxicity assays. The first section in this chapter describes essential chemicals and material synthesis protocols used for the study, analysis methods and different physicochemical characterization techniques which includes Fourier-transform infrared spectroscopy (FTIR), Nuclear magnetic resonance (NMR), Gel permeation chromatography (GPC), Differential scanning calorimetry (DSC), Scanning electron microscopy (SEM), Atomic force microscopy (AFM), *in vitro* cytotoxic analysis and mechanical tests based on UTM. The second section describes the fabrication methods like electrospinning, 3D printing and preparation of chitosan-HDA hydrogel and their characterizations like gelling time determination based on viscometer, DMMB assay, gel fraction, estimation of degree of cross linking by ninhydrin method etc.

Chapters 4 comprise of three parts and it involves results of the studies and is represented using figures, tables and graphs. The first part describes the chemical structure of the synthesized polyurethane urea (PUU) and poly(lactide-co-caprolactone) (PLCL) based on the FTIR and NMR results, and its molecular weight determined by GPC analysis. The

thermal analysis of materials was done by DSC and showed some characteristic peaks which is explained in this section. The hydrophilicity was tested by contact angle measurement which gave expected results. Most importantly, the mechanical properties were tested using UTM and its elongation at break, tensile strength, Young's modulus was determined from the stress-strain curve. Further the synthesized PUU and PLCL were proved to be non-cytotoxic by direct contact test, live/dead staining and MTT assay. The part two of this chapter discusses the feasibility of the synthesized elastomers to fabricate into a tubular scaffold. Electrospinning and 3D printing are the two fabrication methods used for this purpose, out of this a suitable material and a fabrication method is selected based on its mechanical properties and its ability to seed cells in a 3D manner. It was found both the synthesized materials possess desired mechanical properties; however, they differed in their ability to fabricate into the tubular scaffold. The PUU was found to be a good material for electrospinning and not suitable for 3D printing whereas PLCL was found to be a good material for 3D printing and only certain ratios of PLCL were suitable for electrospinning. The cells seeded on an electrospun scaffold failed to have proper 3D cell distribution while the 3D printing method could extend the flexibility to seed cells as per the design, hence 3D printing was selected over electrospining for the fabrication purpose. In Fused deposition modeling (FDM) based 3D printing it is not possible to seed cells along with the molten polymer being extruded; hence a biphasic design is proposed where cells are mixed with a hydrogel and delivered using an additional printing head by dual head 3D printing. Part 3 of this chapter discusses the preparation and properties of a chitosan-HDA hydrogel. The hydrogel is non-cytotoxic and could be used for delivering the cells. The dual head 3D printing parameters were next standardized for this design. Finally, chondrocytes seeded tracheal scaffold was evaluated for its ability to support chondrogenesis by immunostaining and histology studies and the efficacy of the biphasic structure to provide a three-dimensional cell distribution is evaluated by live dead staining.

The chapter 5 involves the analysis and discussion of the results with the aid of the currently available literature. The need for using an elastomeric material and the concept of biphasic design is discussed with the obtained results. Since most of the fabrication methods used has limited cell penetration, it affects the generation of a 3D cartilage. This biphasic design and the fabrication method provide generation of 3D cartilage structure of desired thickness without compromising its mechanical properties.

Chapter 6 summarizes the results and the conclusions which are drawn from the study. The studies among the materials PUU and PLCL showed that PUU is a good material to fabricate an electrospun nanofibrous scaffold whereas the PLCL is not. On the other side PLCL is found to be a good material for 3D printing, whereas as due to high melting point and degradation immediately after the melting point makes the PUU not a suitable material for 3D printing. This study describes the 3D printability of PLCL and also proposes a biphasic design for 3D printing the tubular construct which can be used as a tracheal substitute having a 3D cell distribution and comparable mechanical properties as that of the native trachea. The chapter also describes current limitations of this study and its future perspectives. The thesis ends with bibliography, list of publications and other research outputs.

# CHAPTER 1|
# INTRODUCTION

## 1.1 Background

The trachea is a tubular tissue connecting the upper respiratory tract to the lungs. It is responsible for conducting the air we breathe to the lungs, and it is also responsible for the filtration of the air. Hence any defect to the airway can be fatal. Clinically, tracheal injury is life-threatening, and rigorous interventional management is required. Tracheal pathology has different reasons; it ranges from traumatic to neoplastic and inflammatory diseases that cause tracheal stenosis, or it could be iatrogenic or congenital. Any pressure alteration in the airway can affect the remodeling of the airway system and affects the patient in the long run.

## 1.2 Trachea

The trachea is a membranous tissue connecting the larynx to the carina. Its main function is to conduct air from the upper respiratory system to the lungs. To keep the tube patent there are 'C' shaped cartilage rings placed alternatively along the length of the trachea (Premkumar et al., 2003) (Fig. 1.1). The trachea extends from cricoid cartilage and runs till the thoracic cavity where it bifurcates into left main bronchus and right main bronchus. The length of the trachea ranges from 10 cm to 13 cm with a coronal diameter of 2.3 cm, and sagittal diameter of 1.8 cm and a wall thickness of 3 mm. There are about 15-20 cartilage rings placed alternatively along the trachea, which are joined together laterally by annular ligament made of fibrous tissue and the ends of the 'C' shape is joined by trachealis muscle made of smooth muscle cells. The cross-sectional shape of the trachea is generally 'D' shaped but it may vary from person to person. Two-thirds of the membranous tube consists of the 'C' shaped cartilage, and the cartilages are approximately 5 mm apart (Brand-Saberi and Schäfer, 2014).

The anterior part of trachea is covered by cervical fascia and infrahyoid muscles. The posterior wall of trachea is where the cartilage rings end, and it is joined by the trachealis muscles. The posterior part of trachea also has esophagus running apposed to the proximal side of trachea. The trachea is responsible for conducting air we breathe into the lungs and clearing secretions. The trachea is also responsible for filtering, humidifying and warming of the air we breathe and makes it ready for the gas exchange (Allen, 2003).

Trachea receives its blood supply from the blood vessels from internal thoracic region, innominate, inferior thyroid, intercostal, subclavian and middle bronchial arteries. All these blood vessels interconnect to form longitudinal vascular anastomoss.

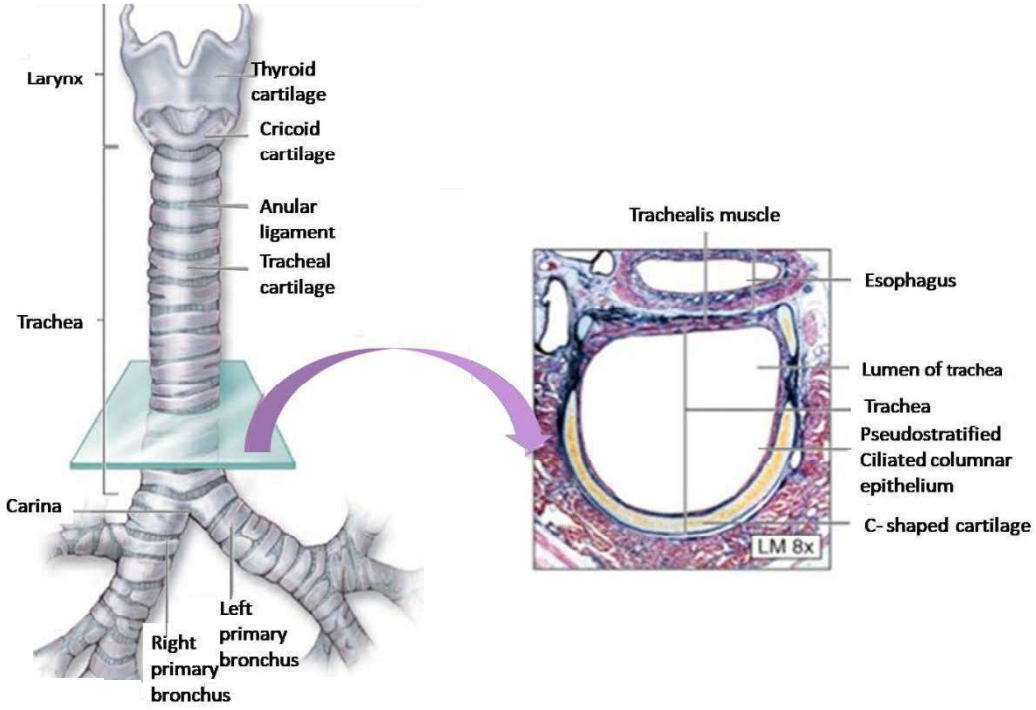


**Figure 1.1. Anatomy of trachea showing tubular structure with alternate 'C' shaped cartilages (Premkumar et al., 2003).**

which supplies blood to lateral and anterior walls and the esophageal arteries supply blood to the posterior region of the trachea (Furlow and Mathisen, 2018).

## 1.3 Histology

The trachea is composed of a fibrous membrane having 'C' shaped cartilages; the cartilages are of hyaline in nature and are arranged alternatively along the length of the membranous tube. The inner lumen is composed of pseudostratified columnar epithelium (G.S Shroff et al., 2016) (Fig. 1.2). Trachealis muscle made of smooth muscle cells connects the free ends of the 'C 'shaped cartilages at the posterior side of the trachea. The epithelium is composed of ciliated cells, neuroendocrine cells, goblet cells and basal cells. A slight variation in the

structure of the airway exists among the species. As the airway tube progresses, the epithelial layer becomes thinner and cells become cuboidal at the respiratory bronchioles (Drevet et al., 2016). At the terminal bronchiole the goblet cells decrease in number and they disappear and clara cells become more prominent, supplanting them. The mucous glands also follow the same pattern, they are maximum in number in the medium-sized bronchi and become fewer in number distally and disappear on reaching the bronchioles (Kuehne and Junqueira, 2000).

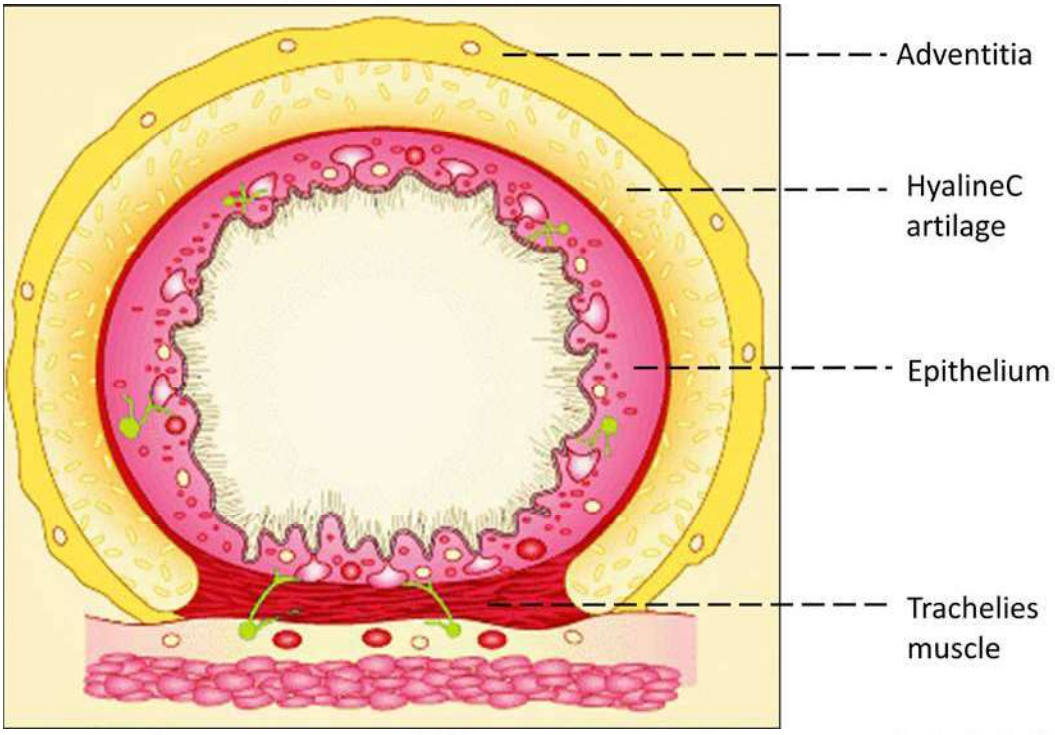


**Figure 1.2. Cross section of trachea showing three different layers of cells (G.S Shroff et al., 2016).**

The smooth muscle is seen as a spiral network or as bands in the large bronchi and trachea, whereas it encircles the smaller bronchi circumficially as a continuous layer. Such changes in the configuration are also present in the cartilages. The cartilages in the trachea are 'C' shaped with free ends at the posterior side. On reaching the bronchi, they become small and less in number and are absent in the bronchioles (Mabrut et al., 2001).

## 1.4 Developmental biology of airway

The development of the airway starts at the 3rd week of gestation with the appearance of a laryngotracheal groove with the anterior protrusion of the proximal foregut. This laryngotracheal groove progresses towards the posterior part and the tracheal ridges progress towards the anterior part and forms the primordium of the trachea. Further, the esophagotracheal septum separates the primordium from the foregut (Wailoo and Emery, 1982). The ventral part of the primordium forms the trachea and the lung bud and the dorsal part forms the esophagus. And by the end of sixth week of the gestation, the trachea and esophagus form separate tubes. The epithelial layer of the trachea, bronchi, alveoli and larynx is formed from the endothelial lining of the respiratory diverticulum. The cartilage and the muscle components of the airway and the lungs are formed from the splanchnic mesoderm. The cartilage appears in the trachea by the 10th week of the gestation and the esophageotracheal bifurcation moves downwards till the 4th vertebra. The interaction of epithelium with the mesenchyme plays an important role in development of the pulmonary and bronchial system. The development of larynx occurs separately from the bronchi and pulmonary development (Kumra et al., 2019).

## 1.5 Molecular pathway of airway development

The molecular mechanism behind airway development was mainly studied in the mouse system. The early expression of the transcription factors Gata6, Gata4, FoxA1 and FoxA2 are important for the foregut development and differentiation. The local expression of these factors by E8-9.5 along the anteroposterior axis of the gut endoderm marks the particular domains of the organ. The homeobox gene Nkx2.1 expressed in progenitors of lung, trachea, and thyroid is the early marker for respiratory region. The progenitor cells of the trachea and proximal lung have different lineages from that of the distal portion of the lung. The lung primordium is developed by the downregulation of Sox2 and by the induction of transcription factors Gli1, Gli2, Gli3, Foxf1, Tbx2, Tbx3 and Tbx4. Later Sox2 is highly expressed in the esophagus region. The Fgf10 which is under the regulation of sonic hedgehog (Shh) plays a role in tracheoesophagealbifurcation and in the development of the bronchi. Another regulator for the tracheoesophageal

separation is the Bmp4 which activates the foregut endoderm cells. Wnt signaling has a role in the morphogenesis of the distal region of the lungs (Morrisey et al., 2013).

## 1.6 Epithelial biology of the trachea

The tracheal mucosa has several functions, from filtering the air to moistening the air we breathe in. Hence the tracheal mucosa consists of several specialized cell types. Goblet and Clara cells are responsible for the secretions of the lumen. The ciliated cells are responsible for the mucociliary escalatory system. Apart from this, it also consists of neuroendocrine and intermediate cells (Reynolds et al., 2015).

The basal cells have rounded morphology and have low pyramid-like nucleus. They are known to express cytokeratins 5 and 4, CD44 and Trp-63. Ciliated cells have a characteristic columnar morphology and cilia, which can be identified by staining acetylated tubulins. The goblet cells and Clara cells also appear in columnar shape (Kim et al., 2012).

The submucosal glands present in between the cartilage and the epithelium are responsible for most of the secreted mucous and serous secretions. The serous and mucous tubules form a collecting duct which changes its shape into a ciliated form and opens into the epithelial lumen. Apart from the mucous and serous secretions the trachea also has neuroendocrine cells which are lesser in number and secrete hormones like serotonin, chromogranin A, calcitonin, cholecystokinin, calcitonin gene related peptide, gastrin releasing peptide (Rawlins and Hogan, 2008).

The foregut endoderm of the respiratory system has primary buds which consist of un-patterned epithelium having loosely packed mesenchyme and mesothelial cells around it. These mesenchyme and mesothelial layers activate the primary buds to undergo repeated branching and outgrowth. At the E10.5-E16.5 stage the airway conduit is formed having a lining of ciliated cells and secretory cells in it. The prenatal stem cells of the trachea are present in the surface of the lumen epithelium. They are capable of complete regeneration of the airway epithelium (Zhang et al., 2015).

The human prenatal stem cell of the airway resides in the surface epithelium and can restore a full repertoire of epithelial lining. In the early stages of development, the tracheobronchial epithelium is lined by a columnar cell type that probably represents the pluripotent stem cell precursor of the basal, ciliated, mucous, serous and neuroendocrine cells comprising the mature tracheobronchial epithelium. In the early stages of tracheal development, the epithelium is lined by columnar cells that are precursor cells for mucous, ciliated, serous, basal and neuroendocrine cells they further differentiate to form the mature epithelial layer (Perl et al., 2005).

## 1.7 Adult progenitor cells

The KRT5 and KRT14 positive cells present in the basal and the parabasal region are identified as the progenitor cells. Lineage tracing experiments have proved that these cells migrate onto the surface of the epithelium and are responsible for the renewal and regeneration of the lumen epithelium (Borthwick et al., 2001; Cole et al., 2010).

## 1.8 Terminally differentiated airway cells

Apart from the mucus secreted by the mucus glands, a small proportion is also secreted by the goblet cells scattered in between the epithelium. These secretions trap the inhaled foreign particles; the ciliated cells propel these particles along with the secretion towards the pharynx. The cilium is made of microtubule having 9+2 arrangement, two microtubules in the centre and nine double microtubules around them. The neuroendocrine cells secrete many bioactive peptides, and they also have an oxygen sensor protein coupled to an oxygen-sensitive potassium channel. They act as a chemoreceptor and helps in the detection of hypoxia. They are also known to play a role in epithelial growth and regeneration (Nettesheim et al., 1990).

## 1.9 Regeneration and repair mechanisms of airway epithelium

The pseudostratified epithelium of the airway is in constant contact with the outer environment, and is exposed to the foreign particles, gases, bacteria and other harmful agents. In a healthy individual there is a balance between the cells that shed off and cells that differentiate and replace them. Several growth factors and

intercellular communications through gap junctions, tight junctions and desmosomes are responsible for the regulation of this cellular turnover in the lumen. This intercellular communication network is also responsible for the secretion of ions, antibacterial, antioxidant and anti-inflammatory molecules, regulation of water balance and mucous clearance. Apart from the antibacterial secretion, the epithelial cells of the lumen express pattern recognition receptors (PRRs) and are responsible for the identification of pathogen associated molecular patterns (PAMPs). In normal conditions the airway epithelium has a slow turnover (Ganesan and Sajjan, 2013). They reside in the G0 phase and re-enter in the cell cycle only when active growth is required. There are several studies in the animal models showing the repair and regeneration of the epithelium during injury (Yahaya, 2012).

An acute injury in the airway epithelium results in loss of epithelial impermeability and results in denudation of the basement membrane. The first event in the epithelial repair involves flattening of migration of the basal cells and restoration of the tight junction, this happens within 12 hrs of the injury. The basal cells then dedifferentiate and undergo hyper proliferation along with mucus cells. And by 72 hrs there will be redifferentiation and forms ciliated cells and finally restore ciliogenesis. The growth factors like TGF-α, TGF-β, keratinocyte growth factor, insulin like growth factor and epithelial growth factor regulate the proliferation and differentiation of the epithelial cells (Puchelle et al., 2006).

## 1.10 Mesenchymal biology of trachea

During the embryonic stage, the mesenchymal stem cells undergo condensation and several stages of maturation to form mature chondrocytes. The growth factor FGF-10 induces the differentiation of mesenchymal stem cells into chondroblast, which under the control of the master transcription factor Sox-9, along with L-Sox5 and Sox6 proliferate and differentiate into collagen-II secreting mature chondrocytes. During this process, chondroblast cells differentiate into mature chondrocytes synthesizing highly sulfated proteoglycans and collagen II (Turcatel et al., 2013).

In this process of cartilage formation, several growth factors like bone morphogenetic proteins (BMP), transforming growth factor-β (TGF-β), insulin

like growth factors (IGF) and fibroblast growth factors (FGF) are required for the development of the functional cartilage. Apart from these growth factors, microRNA miR-125b and miR-30a/c also play a key role in the development of fully matured cartilage.

The cartilage in the body is of three types: hyaline cartilage, elastic cartilage and fibrocartilage. The cartilage rings found in trachea are of hyaline nature which is also found in articular cartilage. Compared to the other two types, hyaline cartilage is rich in collagen II and has a smooth surface with white color. The matured chondrocytes are suspended in cavities called lacunae. They are round in shape with oval nuclei and have a mean diameter of 13 μm. Even though the chondrocytes represent only 5-10% of the total cartilage, they are very important in maintaining the extracellular matrix. During the synthesis of extracellular matrix components, the cytoplasm of the chondrocytes become basophilic and the Golgi apparatus becomes large in size. The main components of the hyaline cartilage extracellular matrix are collagen II and aggrecan. The chondrocytes can anabolize and catabolize these matrix components and are responsible for maintenance of the matrix turnover (Fang et al., 2019).

The fibril collagen type II is responsible for the mechanical strength of the cartilage and the proteoglycan aggrecan is responsible for the cushioning property of the cartilage. The aggrecan is composed of a protein core and to which keratin sulphate and chondroitin sulphate are attached to form a brush structure, which is linked to hyaluronic acid through linker proteins. The aggrecan is negatively charged and attracts sodium ions which in turn attract water molecules. This gives the cartilage cushioning property for absorbing compressive load. Apart from these two components, small components like decorin, collagen VI, collagen XI, collagen IX, biglycan are responsible for organizing and holding these structures together. The outer surface of the cartilage is covered by a layer of collagen I embedded with progenitor cells called perichondrium. The chondrocytes receive nutrients by diffusion from the blood vessels present in the perichondrium. The tracheal cartilage is divided into three zones: deep, middle and superficial. In the deep zone the collagen fibers are arranged irregularly. In the superficial zone the collagen fibrils are arranged in an

ordered fashion oriented either longitudinally or circumferentially (Cassandras et al., 2020; Seguin et al., 2013).

## 1.11 Components of extracellular matrix

The extracellular matrix is responsible for the mechanical properties of the organ. The extracellular matrix (ECM) components are synthesized by the cells itself and are secreted outside by exocytosis, where they integrate with the existing ECM. The cells also secrete protease which cleave the ECM proteins and thus regulate the ECM remodeling. The ECM is made of 1) Proteoglycans, 2) Non-proteoglycans, 3) Fibrillar proteins, 4) Non-fibrillar proteins. As discussed earlier, proteoglycans are highly glycosylated proteins responsible for the load bearing capacity of the cartilage. The non-proteoglycan components form the polysaccharides hyaluronic acid on to which aggrecan is attached. The fibrous proteins collagen, elastin are responsible for its tensile strength (Haykal et al., 2012). The non-fibrillar proteins like lamin, tenacin, fibronectin have a structural role in organizing the ECM components and also play a key role in regulating the cell response (Neville et al., 1991).

The ECM also binds to transmembrane protein integrins present on the cell surface. This allows anchorage of cells to the ECM and also other functions like cell migration, intercellular communication, cell division etc. The ECM is connected to the cytoskeleton of the cell via such transmembrane proteins. Thus, ECM plays a major role in regulating the cell response. The ECM is also responsible for sequestration of growth factors required for cell migration, growth and differentiation. The stiffness of ECM has also been found to play an important role in cell morphology, differentiation and proliferation. The basement membrane of the airway consists of lamina lucida, lamina reticular is and lamina densa. At the end of the basement membrane there is a thin layer of collagen which is found only in adults. This layer is thickened in disease conditions like asthma. The basement membrane is made of collagen IV and laminin and the submucosa is made of collagen and elastin secreted by fibroblasts and smooth muscle cells (Puchelle et al., 2006).

## 1.12 Function of the ECM in airway development and repair

During airway development ECM plays a major role. It regulates the proliferation, differentiation, migration of the cells during the development

process via the growth factors sequestered by the ECM, by its stiffness and the ECM components like fibronectin, GAG, laminin, type IV collagen, tenascin C and syndecan. Many of these processes are similar to the repair process, but during injury other players like the inflammatory cells initiate the repair events by secreting peptides that are capable of stimulating the ECM components secretion, thus even though the process of ECM formation is same during development and repair, the cellular signal that initiate the events is different (Ito et al., 2019; Zhou et al., 2018).

## 1.13 Airway physiology

The respiratory system involves the conducting zone and the respiratory zone. The upper respiratory tract and the trachea form the conducting zone, which conducts the air to the lungs. The respiratory zone involves the respiratory bronchioles, alveolar ducts and the alveoli (Hurley and Hensley, 2020).

### 1.13.1 Ventilation

The total gas flow into the lungs per minute is called the total ventilation (VE). The tidal volume (TV) is the total volume of air displaced during normal inhalation and exhalation. The total ventilation is equal to the tidal volume × the respiratory rate. The normal tidal volume of a healthy individual is 500 ml per inspiration. The total ventilation is also expressed as the sum of dead space ventilation and alveolar ventilation. The volume of the airway that does not take part in the gas exchange process is called dead space (Mete and Akbudak, 2018).

### 1.13.2 Air flow/resistance

The air always flows from higher pressure to lower pressure. When we inhale the diaphragm extends downwards, as a result a negative pressure is created in the lungs compared to the atmospheric pressure. As a result, air flows from the outside to the lungs (Kaminsky, 2012).

The air flows in the airway by bulk flow. It can be a turbulent flow or laminar flow depending on the velocity of the air flow. At higher velocities the air can be turbulent and at lower velocities it can be laminar. The formula that predicts it is called Reynold's number,

**Eq. 1,**

$$\text{Velocity (cm/sec)} = \frac{\text{Flow (cm}^3\text{/sec)}}{\text{Cross-sectional area (cm}^2\text{)}}$$

The higher the Renynold's number value, the higher the chances of turbulent flow. The pressure difference required for the gas flow is directly proportional to the friction at the tracheal wall (Resistance).

The Poiseulle's law p= 8Π]lV/4πr, describes the laminar flow characteristics. Where l = length of the airway, r = radius of the airway and Π]= viscosity of the gas. In a normal trachea the resistance ranges from 0.5 to 2cm $H_2O$/L/s, i.e., this much air pressure is required between the mouth and the lungs to achieve an air flow of 1L/s (Cole et al., 1993).

The air resistance depends on the cross-sectional area of the trachea, since the bronchi region has less cross-sectional area. The air resistance in this region is more.

### 1.13.3 Airway collapsibility/compliance

Compliance is the ability of the trachea to expand. This accounts for the ability of trachea to resist mechanical strain. The tracheal compliance is measured by plotting pressure versus the volume curve, the slope of which represents the compliance. When trachea collapses the cartilage bends, decreasing the tracheal diameter and limiting the airflow. Tracheal cartilage has an asymmetric nature and plays a major role in the stiffness of the trachea. The tracheal cartilage has non-uniform stiffness; it is less stiff at the ends and has maximum stiffness at the centre. The tracheal cartilage shows higher strength during compression than extension; hence it is described as a nonlinear material in many of the mathematical modeling studies. Trachea is designed to have lateral semi-rigidity and longitudinal flexibility, these structural features decrease with age as the cartilage calcifies with age (Tiddens et al., 1999).

## 1.14 Neural control of trachea

The parasympathetic and sympathetic neurons control the contraction and relaxation of the smooth muscle and mucous glands functions. The bronchoconstriction (Tiddens et al., 1999) is caused due to the contraction of the smooth muscle; this is controlled by the parasympathetic innervations which come from the vagus nerve. The vagus nerves are also responsible for the secretions of the mucous glands and goblets cells. The tachykinins like neurokinin and substance P mediate these effects on mucous glands and smooth muscles. In a sympathetic nervous system the catecholamines stimulates β2-receptors which results in increase in cAMP and causes bronchodilation and relaxation and bronchoconstriction is caused by α-adrenergic receptors (Pj, 1986).

# CHAPTER 2|

# LITERATURE REVIEW

## 2.1 Pathophysiology

The pathophysiology of the trachea is evaluated by flow volume loop (FVL). It is mainly used for the analysis of lungs, but it can also be used for the evaluation of the trachea. The forced vital capacity (FVC) is the total volume of air exhaled plotted against the flow rate. The FVL analysis can be used to evaluate the presence of any obstruction present in the airway. The obstructions can be of two types; fixed and mobile. In case of fixed airway obstruction, as the airway narrowing increases the expiratory and inspiratory loops demonstrate a uniform level at a faster rate. This trend is first evident in the expiratory loops but only if the diameter is narrowed to 1 cm. The other pulmonary tests which are used for evaluating the tracheal obstructions are the maximum voluntary ventilation and the peak inspiratory flow rate (for inspiratory limitation) and the peak expiratory flow rate (for expiratory limitation). The most common cause of fixed obstructions is postintubation stenosis and other causes are neoplasms and goiters (Al-Qadi et al., 2013).

Mobile obstructions are caused due to lesions which are not circumferentially altering the shape of the lumen and the extraluminal and intraluminal pressures affect the lesion. During inspiration the negative intraluminal pressure causes narrowing of the tracheal diameter and in presence of the variable extrathoracic obstruction the diameter is further narrowed resulting in the obstruction of the airflow. During expiration, the positive intraluminal pressure results in expansion of the airway and maintains the diameter (Santiago-Rosado et al., 2020). These mobile obstructions have a characteristic flattened expiratory loop and normal inspiratory loop and it also causes reduction of peak flow rates. Tracheomalacia and non–circumferential tumors are some of the common examples of mobile obstructions.

## 2.2 Tracheal pathology

### 2.2.1 Congenital

Tracheal atresia or agenesis is a condition where the patient is born without trachea and has normal larynx and lungs, it is fatal by birth. Congenital tracheo

esophageal fistula is another condition where there is a connection between the esophagus and trachea and in some cases tracheal stenosis may also be present. The repair of tracheoesophageal fistula can often lead to tracheomalacia.

Some of the different types of fistulas which are rarely seen are (1) H- type congenital tracheoesophageal fistula, (2) fistula between biliary and respiratory tracts, (3) congenital bronchoesophageal fistula (Varela et al., 2018).

Congenital tracheal stenosis is a condition where the trachea narrows and appears in the shape of a funnel. The stenotic segment is often found to have a complete cartilage ring instead of 'C' shaped cartilage rings (Hofferberth et al., 2015). Congenital tracheomalicia is a rarely occurring condition and does not occur without an extrinsic cause like tracheoesophageal fistula or due to compression of vascular structures. Patients with this condition initially appear normal but start showing symptoms like noisy respiration, cough, apneic spells etc. (Snijders and Barbato, 2015). This is not a fatal condition and often clears with age. In rare cases tracheostomy or stents are used to repair the malacia. Tracheobronchomegaly is a congenital condition but appears only in adult stage and is due the absence of trachealis muscle (Fletcher et al., n.d.)

### 2.2.2 Acquired

The conditions that are caused after birth due to some injury or illness can be divided into tumors, traumatic injury and post-intubation stenosis.

### 2.2.3 Post-intubation stenosis

About 90% of the stenosis is caused due to endotracheal post intubation. Post intubation lesions are the most common cause of stenosis and they often causes laryngeal injuries. Depending on the source of the injury, the obstructive lesions following tracheal intubation can majorly occur in three different regions.

1) The region where the cuff is fixed.
2) The segment between the cuff and the stoma.
3) The region where the tip of the tube touches the tracheal wall.

Lesions occurring at the stromal region are due to the scarring caused due to the incision during tracheostomy, they will be present even after the healing process. This can lead to further complications like granulomas, anterolateral stenosis etc. A major infrastromal lesion that causes stenosis at the cuff level is due to the

pressure necrosis caused by the cuff and results in the erosion of the tracheal wall. In extreme cases, if the pressure is maximum at the anterior region, it causes trachea-innominate artery fistula. And if the erosion penetrates the posterior wall, it causes tracheoesophageal fistula (De and De, 2008). Another major problem arises due to endotracheal intubation is tracheitis, where bacteria colonize at the segment between the stoma and the cuff and can lead to tracheomalacia. The tube size and the duration period have an important role in preventing these conditions (Burton and Silberman, 2020). The more the intubation duration the more the chances of stenosis, if the cuff pressure is more than 25-30 mmHg, the mucosal capillary pressure exceeds and causes mucosal ischemia which is the causative reason for the aforementioned complications. A safe period for the endotracheal intubation is 7-10 days. Even though tracheal stenosis has been reported for shorter periods, their occurrence rate is very less. The occurrence rate of stenosis for 11 days intubation is 12% and the risk increases drastically beyond that (D'Andrilli et al., 2016).

### 2.2.4 Tumors

Primary tumors are very rarely seen in trachea. Adenoid cystic carcinoma is the most commonly seen tracheal tumor. Two third of all the tumors in trachea is due to adenoid cystic carcinoma.

The early detection of these tumors is a challenge making it a difficult condition to treat. Their insidious nature results in a delay in diagnosis making them more difficult to treat. Squamous cell carcinoma is another type of carcinoma that affects the squamous cells and is often distributed to the trachea. It is mostly seen among the smokers and in one third of patients with metastasis at the time of diagnosis. Unlike other tumors adenoid cystic carcinoma progress very slowly, this makes its diagnosis very difficult. It spreads to the perineural and submucosal planes. These types of tumors include both mesenchymal and epithelial histotypes. Secondary tumors formed in trachea are usually migrated from the surrounding tissues like lungs, esophagus, thyroid and larynx. In case of trachea tumors, the patients do not show any early symptoms. It becomes evident only when the diameter of the trachea is narrowed more than 50% (Harris et al., 2018; Madariaga and Gaissert, 2018).

### 2.2.5 Traumatic injury

Injuries affecting trachea can be life threatening. It can be caused by mechanical means or due to burns. Mechanical injuries are very rare and are of two types; blunt or penetrating. Blunt injuries are usually caused by motor vehicle accidents, due to the direct impact of the vehicle's body parts or even from strangulation. Penetrating injuries are usually caused by gunshots, stabbing or other accidents by sharp objects. Burns are usually caused due to the inhalation of toxic substances. Chemicals like isocyanate, ammonia, hydrochloric acid or inhalation of steam are common causes of burns injuries. Laser burns during tracheal interventions are another causative reason for tracheal burns (Santiago-Rosado et al., 2020).

### 2.2.6 Others

The other reasons for lesions affecting the airway can be intrinsic: infections like syphilis, tuberculosis, rhinoscleroma and diphtheria; inflammatory conditions like amyloid, relapsing polychondritis, Wegner'sgranulomatosis and sarcoidosis or idiopathic like cicatriciallaryngotracheal stenosis. Extrinsic lesions like goiters, cysts, tumors can also obstruct the airway by compression.

## 2.3 Diagnosis

Except for some traumatic injuries, all the lesions result in narrowing of trachea and stenosis. The symptoms appear lately, because the airway has large functional reserves and hence the symptoms become evident only when there is 50-70% occlusion (Altinok and Can, 2014).

The laryngotracheal stenosis can be classified in different ways:

1) **Myer-Cotton staging system**-This system classifies the lesions into different grades based on the reduction in its cross-sectional area. It is used for circumferential lesions present in the subglottis.

a. **Grade I -** Less than 50% obstruction in the airway.

b. **Grade II -** 51% to 70% obstruction in the airway.

c. **Grade III -** 71% to 99% obstruction in the airway.

d. **Grade IV** The airway is completely obstructed by the lesion.

2) McCaffrey system-It differentiates the stenosis into four different stages based on the length and the subsites of the stenosis.

a. **Stage I-**The length of the lesion is less than 1 cm and is seen only in the trachea or the subglottis.

b. **Stage II-**Lesions of more than 1cm come under this category and are confined to the subglottis region.

c. **Stage III-**These are lesions seen in only subglottis and tracheal regions not in the glottis.

d. **Stage IV-**The lesions that involve the glottis region.

3) Based on the number of subsites, Lano et al., proposed a system for the classification of the airway obstructions which will predict the prognosis and decannulation.

a. **Stage I -** the lesion is present only in one subsite.

b. **Stage II -** the lesion is present in two subsites.

c. **Stage III -** the lesion is present in three subsites.

These classification systems help to evaluate the lesions and in its prognosis and management (Zhao et al., 2017).

## 2.4 Surgical treatment

### 2.4.1 Short segments

#### 2.4.1.1 Tracheal resection and end to end anastomosis

For tracheal stenosis, tracheal resection is rarely done. Clearing the stenotic region, either for short term or long term is done immediately. Tracheal resection is done only after thorough examination of the defect. For lesions of more than 1cm size, there could be potential damage of the surrounding tissues. In such cases resection of the defective region is recommended. Tracheal resection and end to end anastomosis is the most commonly used surgical method to repair the

defective airway. Due to the elastic nature, half the length of the adult trachea and one by third of the child tracheas can be resected out and the ends can be extended and joined to remove the defective part. This method cannot be used for defects that require resection of more than half of the adult trachea. In such cases a donor trachea is recommended (Elsayed et al., 2016). The steps that involve the mobilization of the trachea include:

1) Dissection of the right hilar region and separation of the right pulmonary ligament.

2) Separation of left main bronchus.

3) Separation of the pulmonary vessels from the pericardium.

There is a difference in the position of the trachea with the age. In youngsters, the lateral projection of the trachea is much more vertical. And on extension more than half comes to the neck region and on flexion a major portion goes back to the thoracic region. However, in older people due to kyphosis, the position of the trachea does not change much with cervical extension or flexion. Hence longer length of the trachea can be removed in youngsters than in older people (Nandakumar et al., 2011).

Even after the resection of the defective part and end to end anastomosis, there are chances of restenosis. Restenosis after end-to-end anastomosis has been seen in 6-9% of all the cases.

### 2.4.2 Long segments

#### 2.4.2.1 Slide tracheoplastyand patch tracheoplasty

These are the surgical techniques used when the defective part is too long to resect out. In such cases patch tracheoplasty to slide tracheoplasty is used. Patch tracheoplasty uses pericardial grafts or the costal cartilage to keep the trachea patent after the resection of the defective segment. Compared to the patch tracheoplasty, slide tracheoplasty is safer and has shown results. Unlike patch tracheoplasty, the defective part is not removed in slide tracheoplasty (Elliott et al., 2009). The midpoint of the stenotic region is horizontally divided and a vertical incision, one posteriorly and other one anteriorly is made on the upper and the lower segment of the stenotic region. The two segments are then slide to

each other and sutured. By slide tracheoplasty the cross-sectional area of the trachea is quadrupled and its circumference is doubled (Grillo, 1994).

## 2.5 Tracheal replacements

There are cases of tracheal lesions where tracheal resection and end to end anastomosis or slide tracheoplasty is not possible. The maximum limit for the tracheal resection and end to end anastomosis is half of the total length of the trachea. Lengthy lesions which cannot be treated by resection and reconstruction are using managed by stents or T-tubes. But these are temporary cure which has long term affects and other complications like multiple infections are quite often among these patients. An efficient and safe tracheal replacement is highly required for the treatment of such conditions (Delaere and Van Raemdonck, 2016).

## 2.6 Requirements

Based on the lessons from the in vivo studies, Neville proposed a set of requirements for a successful tracheal replacement (Neville et al., 1991).

1) Longitudinally flexible but laterally rigid.

2) It should have ciliated epithelium in the lumen or should facilitate cell migration and epithelialization.

3) The material should be non-immunogenic, non-carcinogenic and biocompatible.

4) The replacement should not erode, distort or dislocate over time.

5) Should prevent accumulation of secretions in the lumen.

6) It should have anti-bacterial activity.

## 2.7 Approaches

There have been many approaches for the development of a tracheal replacement. It includes synthetic prostheses, stents, scaffolds, autologous tissue reinforced with synthetic material, non-viable tissue, vascularized and non-vascularized grafts. These are discussed in detail below.

### 2.7.1 Stents

#### 2.7.1.1 Silicone tube

One of the early stents used for the treatment of the subglottic stenosis is the Montgomery T-tube made of silicon. Since then, many different types have been used which includes silastic T-tube, dynamic stent, Dumon stent with was designed for preventing migration. The main advantages of such stents are: it can be removed, minimal granulation, bio-inert and its adjustability. A major disadvantage of silicon-based stents is the lack of re-epithelialization which leads to the obstruction of the lumen. They are difficult to place and also have a tendency to migrate and distort over time (Liu et al., 2002).

#### 2.7.1.2 Expandable metallic stents

The advantages of metallic stents over silicon stents is it is easy to place and can be performed under local anesthesia. Compared to the silicon stents they have less chance of migration and obstruction. But they are more of a permanent structure, once placed tissue grow over it and are difficult to adjust or remove. They include first generation, second generation and third generation stents. The first generation is made of uncovered balloon expandable metallic stents. The second generation involves uncovered or partially covered self-expandable metallic stents and the third generation was designed to solve the problem of stent removal. It involves completely covered self-expanding metallic stents (Li et al., 2020; Serrano et al., 2016).

#### 2.7.1.3 Bioresorbable

Bioresorbable polymers like polylatic acid, polyglycolic acid, poly D, L-lactide-co-glycolideetc are designed to degrade into bioresorbable nontoxic products over time. Hence the painful process of stent removal can be avoided for such stents. At the same time, they provide the required structural support and facilitate epithelialization. However, their long-term effects of such stents are still under study (Zhu et al., 2011).

## 2.7.2 Tracheal prostheses and scaffolds

### 2.7.2.1 Solid

Several attempts using different materials like Vitallium, Teflon, Glass, Lucite, Polyethylene, Ivalon, Silicon tube with Dacron cover, Polyvinyl chloride etc. have been made in animal models. There were many clinical studies using Tantalum, Teflon, Lucite, Stainless steel, Silicon and Hydroxyapatite. In many of the cases, the patients suffered from stent migration, obstruction of lumen due to granulation tissue and vascular erosion (Folch and Keyes, 2018).

### 2.7.2.2 Porous

To address the problems associated with the solid prosthesis, porous structures were designed which using different materials which is expected to facilitate epithelial cell migration and allows tissue in growth. There were many studies which used materials like Titanium metal, Polytetrafluoroethylene, Steel wire, Marlex, Polyurethane and so on. They were also studies were omentum, pericardium, fascia was used to wrap the implant to seal the pores and for better tissue integration. The porous structure allowed tissue in-growth but it let to its overgrowth and formation of scar tissue which resulted in obstruction of the lumen and stenosis (Grillo, 2002).

The longer tracheal replacements had subtle tissue in-growth and subsequently failed due to bacterial infection.

### 2.7.2.3 Non-viable tissue

Trachea and other tissues from the cadaver haven used in different forms; frozen, crosslinked, lyophilized and have been tested both in animal models and in humans. Although there was not immune rejection, they let to the formation of granulation and scar tissue (Grillo, 2002).

## 2.7.3 Autologous tissues combined with synthetic material

Apart from the non-viable tissues many other tissues alone or in combination with synthetic materials have been tried for the tracheal replacement. These include perichondrium, diced cartilage, jejunal patch, dermal grafts, omentum, buccal mucosa reinforced with auricular cartilage. The use of autologous tissues reinforced with synthetic materials or other tissues was an interesting approach for the development of tracheal replacement. But many of the met with limited

success, the bladder mucosa resulted in edema formation and subsequent obstruction. When perichondrium was used along with the facial flaps, it differentiated to form the cartilage and also facilitated re-epithelialization. But the graft lacked enough mechanical strength and failed due to stenosis. In a patch graft tracheoplasty, costal cartilage along with pericardium was used for the treatment of congenital stenosis. Even though the graft survived for a while and showed some encouraging results. Over time the pericardium was replaced with scar tissue and the cartilage was resorbed. In some of the other studies involving similar patch tracheoplasty approach, the graft remained patent over a period of two years (Haykal et al., 2014).

### 2.7.4 Vascularized flaps

The integration and survival of the graft after *in vivo* implantation is a major challenge. Pedicled grafts were used expecting the vasculature will help in better survival of the graft in vivo; pedicled intercostal muscle, proplast with conchal cartilage and skin flap, buccal mucosa along with the periosteum where some of the attempts for testing this approach. But most of them had limited success and no follow up (Kim et al., 2017; Liu and Zhang, 2017).

### 2.7.5 Tube reconstruction

The previous attempts were aimed at treating window defects. A whole pedicled tubular graft was also tested in animal models and in humans (Goh et al., 2018). The graft composed of skin graft reinforced with costal cartilage designed in the shape of trachea was implanted. The other autologous tubular shaped tissues like esophagus, aorta was also tested clinically for the replacement of trachea. All these attempts involved complicated surgical procedures and were also associated with many complications like bacterial infections and lack of healing etc. (Kim et al., 2017).

### 2.7.6 Autografts

Even in studies where the animal's own trachea was re-implanted immediately were often unsuccessful because of lack of angiogenesis. The success of such graft depends on the length of the graft. The short segments are easy to re-vascularize and had greater chances of survival. The long-segmented grafts failed to re-vascularize and failed due to stenosis, obstruction etc. Even though the

shorter segments were successful, its cartilage over time got resorbed and was replaced with scar tissue. Hence a major reason for the failure of most of the implants was lack for vasculature and nourishment of the tissue (Haykal et al., 2014).

### 2.7.7 Allografts

In most of the studies that involved implantation of allografts without immunosuppression failed due to immunerejection. In another study, the graft rejected even in presents of immunosuppression due to lack of revascularization. Histology results showed the graft had liquefaction necrosis and failed due to stenosis. The mucosal layer of trachea plays a major role in immune rejection. They carry some critical antigenic factors that plays important role in initiating immune response, when the great epithelium was replaced with the recipient epithelium, it mitigated the immune response. The above-mentioned studies show that revascularization is very important for the successful implantation of tracheal replacement. Since initiating angiogenesis efficiently is still under research, many attempts were made to revascularize the graft indirectly by wrapping the graft in pedicled tissues like omentum, musclofacial flaps etc. (Etienne et al., 2018).

The following tissues were used to revascularize the tracheal autograft: intercostal muscle, omentum, chondromuscular flap and deltopectoral flaps. Such flaps were effective only to certain length; omental flap of more than 4cm length became ischemic and led to stenosis. A different procedure was the graft is first implanted in a primary site like omentum in peritoneal cavity or in the forearm and later transferred in to the secondary site i.e.; the replacement site has shown to be more effective (Azorin et al., 2006; Ershadi et al., 2018).

Studies involving tracheal replacement using allografts showed severe immune rejection, the removal of graft epithelium mitigated the immune reaction and the vasculature kept the chondrocytes viable but eventually led to chronic immune reaction and failed due to vascular occlusion (Lenot et al., 1993). The methods involving removal of epithelium using detergents washes and revascularization emerged as a promising strategy for improving the graft viability, but its inability to re-epithelialize the graft remained a challenge. However, other studies involving heterotopic implantation for vascularization and later implant in

orthotopically in the defect site showed some promising results. In some of the studies, allograft of aorta when implanted showed no graft rejecting without immunosuppression but it required stenting to prevent collapse of the graft. The first study to show some promising results involving allograft transplant was reported in 1979. A donor trachea implanted under sternocleidomastoid muscle heterotopically for revascularization and later orthotopically implanted as a pedicled graft in the defective trachea showed some initial success. No immunosuppressive drugs were given in this case; hence the strategy remains to be a promising one for tracheal replacement. In other studies, involving omental wrap for revascularization led to tissue necrosis and eventually stenosis even after immunosuppression which further required stenting (Ershadi et al., 2018).

### 2.7.8 Direct revascularization

While taking about indirect vasculature, it is also important to mention about the studies involving direct revascularization. These studies involved microsurgical techniques to reestablish the vasculature of the tracheal graft. In one of the studies involving a thyrotracheal graft where the thyroid artery was surgically joined to the carotid artery (Nakanishi, 2007). Some studies also show that the venous vasculature is also important for the prevention of tissue necrosis. The role of vasculature is expanding after each study. Many pedicled tissues like corticoperiostal tissue, forearm, and anterolateral thigh tissue have been used for this study. In a study involved replacement of larynx due to edema. An allograft with matching leukocyte antigen was used. The allograft also had a portion of trachea with five rings. The major feat of this study was they were successful in re-establishing the arterial and venous vasculature and also the anostomosis of the neural network. Despite of some initial immune reaction, under immunosuppression the patient regained normal deglutition and vocal cord function. From the lessons gained from the aforementioned studies, it is important for a graft to have normal vasculature, epithelium and non-immunogenicity for its survival (Nakanishi, 2007).

### 2.7.8 Tracheal tissue-engineering

Even though the above-mentioned tissue graft-based studies showed some promising results, they all required a donor tissue, which may not be possible in

all the cases. For a clinically viable technology, it is important to have easy supply of the grafts. The idea of tissue engineering aims to artificially create a tissue construct for long segmental tracheal replacement, which has functional epithelium and cartilage. The construct is then vascularized and then transplanted into the defect. And they are expected integrate well with the neighboring tissues and survive without any immunosuppression (Law et al., 2016; (Dhasmana et al., 2020).

The term tissue engineering involves three components: cells, scaffold and bioreactors. The idea mainly combines the concepts of regeneration and material science. It involves culturing of cells in vitro and seeding them on to the scaffolds, which are then used for implantation. The cells are expected to regenerate the missing tissue and the scaffold is expected to support the growth and function of the cells (Kojima and Vacanti, 2014).

#### 2.7.8.1 Cells

##### 2.7.8.1.1 Epithelial cells and tracheal adult stem/progenitor cells

In adult trachea, progenitor cells are limited in number compared to the fetus stage. The epithelial cells are present in niches in the basal layer of trachea. These cells can be isolated and expanded and differentiated in vitro and then can be engrafted in *in vivo* models. This *in vitro* culture of epithelial cells is not easy, its morphology changes with culture conditions and passage number. Ciliated epithelium can only be maintained in air liquid interface or, some studies have used notch knockdown cells for the generation of ciliated cells (Firth et al., 2014). These cells can be made into cells sheet on seed into the graft for implantation (Chistiakov, 2010; Seguin et al., 2013).

##### 2.7.8.1.2 Non-tracheal adult stem/progenitor cells

Since culturing of primary airway epithelial cells for the re-epithelialization of grafts is not a feasible option other stem cells of different origins were tested. It includes mesenchymal stem cells, induced pluripotent stem cells, embryonic stem cells, stem cells derived from umbilical cord blood and amniotic fluid stem cells. The ESC has great pluripotency and has been successfully used for the generation of airway epithelium. However, using them for clinical experiments is unethical due to its potential tumor risk (Khazraee et al., 2018).

Mesenchymal stem cells isolated from the blood generated two populations of cells. One of them showed the characteristic epithelial marker cytokeratin (ESC), but was also positive for hematopoietic marker CD45. The other population was positive for the characteristic KRT5 and CXCR4 and moreover FGF7 administration mobilized these cells to the epithelial injury site. The umbilical cord derived stem cells showed similar potency as that of the bone marrow stem cells. The stem cells derived for the amniotic fluid were pluripotent capable of generating all the three-germ layers without any tumor risk. However, its capability to regenerate the airway epithelium is less studied. Induced pluripotent stem cells generated from reprogramming the somatic cells is a promising candidate for the regeneration airway epithelium, due to it pluripotency and easily available cell source. Some recent studies showed generation of functional ciliated epithelium using iPSC by knocking down the Notch gene (Elliott et al., 2012).

#### 2.7.8.1.3 Chondrocytes

Autologous chondrocytes are usually harvested form rib cartilage, nose cartilage and ear cartilage. These are comparatively safe sites from where the tissue can be harvested without much morbidity. The cells are then expanded *in vitro* and then implanted in to the defect site of in the scaffold. These cells secrete collagen II and other ECM components. Different scaffold has been used along with growth factors for better cell response. Autologous chondrocytes from ear cartilage seeded on a three layer tubular scaffold comprising of polyglycolic acid mesh, gelatin sponge with fibroblast growth factor, and collagen sheet (Kojima et al., 2003). The construct was used for the repair of short segment tracheal defect. The study showed presence of FGF improved chondrogenesis to heal the defect. For better biocompatibility a scaffold free construct by cultivating autologous chondrocytes in bioreactor was used. The study was successful in generating well vascularized graft, but the construct lacked mechanical strength. Even though chondrocytes showed ability to regenerate and repair the cartilage defect. They have less capacity to proliferate. Hence other cells like progenitor cells and stem cells have been studied for its ability to differentiate and regenerate into functional chondrocytes (Maughan et al., 2017).

#### 2.7.8.1.4 Mesenchymal stem cells

Mesenchymal stem cells were first identified by Friedenstein from bone marrow. They have characteristic trilineage differentiation potential giving rise to chondrocytes, adipocytes and osteocytes. Apart from its differentiation into the cells of mesodermal origin, they have also shown transdifferential potential to generate cells of other germline, such as those of endodermal or ectodermal origin like hepatocytes or neurons. This property of the mesenchymal stromal cells made some authors to consider them as stem cells (Seguin et al., 2013). The mesenchymal stromal cells are a heterogenous population containing mesodermal progenitor cells. This population also contains a sub endothelial population of cells expressing CD146. Hence all fibroblast like cells having plastic adherence, regardless of their organ can be considered as mesenchymal stromal cells. These mesenchymal stromal cells are capable of secreting it's on ECM and has potential for multi lineage differentiation (Kim et al., 2020; Shin et al., 2014).

### 2.7.8.2 Scaffolds

Scaffolds are biomaterial-based structures designed to have a desired cell response for the formation or repair of a functional tissue. The physicochemical and biological properties of the scaffold have a great impact on the tissue formation (O'Brien, 2011). A scaffold is made with an appropriate biomaterial and into order to make it into a desired structure a suitable fabrication method is used. The commonly used biomaterials and fabrication techniques are discussed in the following section.

#### 2.7.8.2.1 Biomaterials

The use of synthetic materials for the fabrication of scaffolds allows tailoring its mechanical properties like porosity, shape, dimensions, microstructure and degradation rate, to get a desirable effect. However, they lack cell adhesion molecules and surface topology as that of the natural scaffolds. There are many materials that have the potential to be used as an efficient biomaterial; Degrapol PLA, PGA, PCL, and co-polymers of them like PLGA, PLCL etc. When these materials have excellent mechanical properties, the natural biomaterial like collagen, gelatin, alginate, silk lack mechanical properties as that of the synthetic materials but have remarkable cell attachment and cell response (O'Brien, 2011).

Recently, a composite of polyhedral oligomericsilesquioxane (POSS) and poly (carbonate-urea) urethane (POSS-PCU) was tested clinically to transplant a whole airway including the carina and main bronchi. Casted porous foam in the shape of a ring was used for the cartilage part and coagulated foam was used for the annular ligament part that connects the cartilages. The study showed that the scaffold supported the recipient autologous progenitor cells. However, its long-term outcome is unknown (Dhandayuthapani et al., 2011).

Based on the source the biomaterials can be classified into two groups: natural biomaterials and synthetic biomaterials. The synthetic biomaterials like polylactic acid, polycaprolactone, polyglycolic acid and polyurethane have very impressive mechanical properties but also have disadvantages, for example, their biocompatibility and ability to remodel is very less compared to the natural biomaterials. Hence the scientists are focusing more on the naturally derived biomaterials. The naturally derived biomaterial scaffolds could be protein based or polysaccharide based. The protein based includes collagen, gelatin, silk etc. and polysaccharide based includes chitosan, agarose, chitin, cellulose etc. (Pina et al., 2019).

**2.7.8.2.1.1 Silk**

Silk is a natural protein that is spun in to fibers by insects like silkworm, mites, scorpion and spider. Silk proteins are secreted by epithelial cells lining the glands of these organisms. The insects use these silk cocoons for egg protection, web formation, and nest formation. Among these the silk worm silk is most extensively used for the biomaterial application. The core protein of the silk fiber silk fibroin and this has an outer coating of a sticky protein called sericin that glues the silk fibers together (Li et al., 2013). The silk fibroin consists of a heavy chain (390 kDa), light chain (26 kDa) and a glycoprotein chain called P25. The heavy chain and the light chain are present in the equal ratio and are joined by a single disulfide bond between Cys-c20 of heavy chain and Cys-172 of light chain. The P25 glycoprotein is non-covalently linked to these proteins. The heavy chain is responsible for the mechanical properties of the silk fibroin and the light chain is for the secretion of the silk from the silk gland. The sericin is a hydrophilic protein of 20-310 kDa size; this allows the fibers to stick together and for different structures like the cocoon. Among the other natural biomaterial silk

fibroin is a promising candidate due to its biocompatibility, mechanical strength, biodegradability and its availability. Fibroin protein consists of 40% Glycine and 25% Alanine, and the remaining amino acids are mostly glutamine, proline, tyrosine, arginine, serine, leucine, valine. Even though spider silk has superior mechanical properties compared to the silk worm. They are not much used for both commercial and biomaterial applications due to lack of domestication and low productivity (Bandyopadhyay et al., 2019).

#### 2.7.8.2.1.2 Chitosan

Chitin is a hard, white exoskeleton component of invertebrates. Chitin is hydrophobic and comprises of 1-4-β-acetyl-D-glucosamine units. For the sake of chemical modification, the acetyl group of the chitin is removed. Chitosan is one such derivative of chitin where it is partially deacetylated. Hence chitosan is a mixture of N-acetyl-D-glucosamine and D-glucosamine. Chitosan is insoluble in neutral and basic pH but soluble in acidic pH. It has been used in many *in vivo* studies, and found to have nontoxic degradation products (Croisier and Jérôme, 2013). Special attention has been given to chitosan for the repair of cartilage tissue. Because of the avascular nature the cartilage is vulnerable to many diseases and trauma. And once damaged its capacity to repair its own is very less. Different strategies have been attempts to repair the damaged cartilage, had very limited success in regenerating the hyaline cartilage. Since the cartilage ECM has proteoglycan as one of its studies involving chitosan and glycosaminoglycan composite found to be promising strategy (Venkatesan et al., 2015). The anti-bacterial and hemostatic properties of the chitosan are another added advantage of chitosan. The polycataionic nature of chitosan interact with the microorganisms results in its growth bacterial and its killing. On the basis of these results several chitosan based wound dressing materials, injectable system for articular cartilage repair have been developed (Rodríguez-Vázquez et al., 2015).

#### 2.7.8.2.1.3 Polycaprolactone

Polycaprolactone is widely used polyester for the biomedical application. It is semi crystalline and has a Tg value of -60°C and a Tm of 60°C. Like the other polyesters the physical and mechanical properties of the PCL depends on its

crystallinity and molecular weight. The polymer is insoluble in alcohol and water and soluble in most of the chlorinated or fluorinated organic solvents. It has a tensile strength of 16-500 MPa and young's modulus of about 400 MPa and has a long degradation period of 2 to 4 years depending upon its molecular weight and crystallinity. It can be easily copolymerized with other polymers to give polymers of desirable characteristics (Janmohammadi and Nourbakhsh, 2018).

#### 2.7.8.2.1.4 Polylactic acid

Polylactic acid is polyester mainly used for making sutures and other biomedical applications. PLLA is semi crystalline polymer having a melting temperature 180° C and Tg value of 60-65° C. They are hydrophobic in nature and usually soluble in most of the fluorinated or chlorinated organic solvents and are in soluble in water and alcohol. It has a high tensile modulus of 3 GPa and tensile strength of about 50-70 MPa. They are brittle in nature and not much preferred for load bearing application. However, it shows impressive mechanical properties on increasing its molecular weight. Compared to polycaprolactone it has a shorter degradation period of one month to one year. The D-lactide isomer of the lactic acid is amorphous and adding D-lactide while polymerization increases its degradation rate. The degradation rate is also dependent on its molecular weight. Lower molecular weight has higher degradation rate. The degradation occurs by hydrolysis of ester bonds. Even though the degradation product is acidic lactic acid, it is bioresorbable and easily metabolized by the body. However, many studies have reported to have inflammatory response due to acidic degradation product caused due to bulk degradation of PDLLA (Lopes et al., 2012; Singhvi et al., 2019).

#### 2.7.8.2.1.5 Polyurethane

Polyurethanes (PUs) are well studied and much preferred synthetic polymers for tissue engineering applications because of their mechanical flexibility, biocompatibility and diverse compositions. The material has been widely used for catheters, shape memory materials, biosensors etc. The efficacy of this material for drug delivery, bone, cartilage, muscle tissue repair and regeneration is also well studied.

However, certain medical grade polyurethanes like Pellethane, Mitrathane, Biomer and Estane contain aromatic isocyanate like diphenylmethanediisocyanate (MDI), which can form carcinogenic methylenedianiline upon sterilization, degradation and processing which can cause serious problems. Hence new polyurethane with aliphatic isocyanate and non-cytotoxic polyol and chain extender is highly desirable.

### 2.7.8.3 Fabrication methods

#### 2.7.8.3.1 Electrospinning

Electrospinning is a versatile manufacturing technique which has been widely used for the fabrication of nanofibrous tissue engineering scaffolds. Since electrospinning generates nanofibrous architecture which is similar to the native extracellular matrix (ECM), the technique is much preferred in the field of tissue engineering. It is a facile and robust technique which can be used to fabricate tubular, nanofibrous scaffolds with fiber diameter of varying size from nanometer size to micrometer size with great efficiency.

Electrospun nanofibrous scaffolds can provide a functional environment for the cells to regenerate. The electrospinning technique is relatively new in the field of tissue engineering; it was introduced into the field as a fabrication technique in the early 1990s. Since then, the technique has shown promising results in terms of scaffold fabrication and cell response. Electrospinning has garnered much interest within a short period due to its low cost of production, customizability and simple and easy to use set up. It provides the flexibility to choose various parameters like polymer of interest, its concentration, flow rate, needle to collector distance etc. These parameters can be used to tweak the characteristics of the nanofiber produced.

#### 2.7.8.3.2 3D printing

3D printing is a form of additive manufacturing technology where a design of desired size and shape is fed to the 3D printer which precisely fabricates the structure as per the design. The technique has great potential in fabrication of tissue constructs or devices for biomedical application. A scaffold seeded with cells is used to facilitate tissue repair or regeneration. The scaffold needs to be designed in such a way it supports the growth of the seeded cells. This depends

on the materials used and the geometrical features like the pore size and internal structures. Another important feature is the mechanical property of the printed structure should be comparable with the native tissue (Gao et al., 2017).

Being an additive manufacturing technique, 3D printing builds the structure in a layer-by-layer fashion. The term 3D printing was first used by a group in MIT in 1993 where the standard inkjet printer was modified to make 3D structures. Over the last three decades several modified forms of the technology have been developed. Based on the printing method they can be categorized into inkjet based, FDM based, powder based and polymerization-based 3D printing. But all of them come under the general term additive manufacturing, which involves building of structure in a layer by layer fashion (Frejo and Grande, 2019).

A general protocol of additive manufacturing involves modeling of the structure using computer aided design (CAD) softwares like ProE, Solidworks, autodesk etc. The model file in .stl format involving movement instructions for the printing device is then exported to the printing device. Compared to early printing devices, 3D printing now has become a very flexible technique that allows direct manufacturing of very complex structures with high precision. The technology also allows designing of the medical prosthesis based on the size and shape of the defect from its scanned image. The technology has provided scientists and doctors ample tools for the development of scaffolds with desirable characteristics. The technique allows designing and fabrication of tissue constructs having desirable shape and dimensions and microenvironment favorable for the cells to proliferate and differentiate to form a functional tissue. There are mainly two modes of 3D printing that has been used for tissue engineering application. The one which uses a bioink were the cells are mixed in anaqueous based polymer which gels as soon as it is deposited by the printer. The second mode is called fused deposition modeling (FDM) where a solid polymer is used to fabricate the scaffold without cells and the cells are seeded on it after the printing and is further used for its *in vitro* or *in vivo* application (Xia et al., 2019).

Over the last four decades many biodegradable polymers with impressive properties have been developed. This includes both synthetic and natural biomaterials. The advantage of synthetic polymers over the natural polymers is

its mechanical properties can be easily tuned and they are easily available. Polyesters like polycaprolactone, poly lactic acid, polyglycolic acid or their copolymers like poly(glycolic acid-co-lactide), poly(lactide-co-caprolactone) are commonly used for tissue replacement and they can also be used for 3D printing (Ahn et al., 2019).

To use 3D printing in the area of tissue engineering, it is important to have a detailed knowledge of the biomaterials used. The material selection and its mechanical properties are some of the key requisites that have to be noted before the 3D printing. Apart from the aforementioned features, the internal structure and the scaffold architecture is also crucial for development of a successful tissue reconstruction.

Structures with interconnected pores allow transfer of oxygen and other nutrients and allow improved vascularization and proliferation which improves the cell survival and cell response, an ideal pore size and porosity for the scaffold ranges from 200-500 nm and 60 to 90% respectively (Hsieh et al., 2018).

## 2.8 Aims

The overall aim of the study is to generate a tissue engineered tracheal construct having comparable mechanical properties as that of the native trachea.

## 2.9 Hypothesis

A 3D elastomeric biphasic tracheal scaffold which can support cells and have adequate mechanical strength is expected to bring both mechanical property and cytocompatibility in one system.

## 2.10 Objectives

1. Synthesis of elastomeric biomaterial for tracheal tissue engineering.

Part I: Synthesis of polyurethane urea (PUU).

Part II: Synthesis of poly (lactide-co-caprolactone) (PLCL).

2. Fabrication of the synthesized elastomeric biomaterial into a 3D scaffold system for tracheal tissue engineering.

3. Development of a biphasic design having elastomeric framework and a hydrogel system having appropriate mechanical properties and cytocompatibility.

## 2.11 Significance

Tracheal stenosis, traumatic injury and malignancy require tracheal resection and end to end anastomosis. If the defect is less than 50% of total length of adult trachea and one third in children, tracheal resection and end to end anastomosis is affordable. For defects involving longer lesions there is no effective treatment strategy available currently and leads to tracheostomy and palliative care. It is highly imperative to develop novel strategies for the treatment of long segment tracheal defects.

Even though some of the studies involving implantation of decellularized tracheal graft showed some promising results, they dependent on the donor organ and is not a feasible strategy for the clinical requirement. Results from the past studies showed that and tracheal replacement should be longitudinally flexible and laterally rigid tube, the lumen should have ciliated epithelium, the material should be biocompatible and should integrate well with the surrounding tissue. Tracheal replacement with decellularized allograft found to have vascularization and re-epithelization but many of them lacked mechanical strength and had to use stents to keep the graft patent. A major effort focused on the development of a synthetic tracheal replacement has been directed. But a major setback of synthetic tracheal graft is lack of epithelization and vascularization. Recently strategies involving heterotopic implantation, where the graft is implanted in a primary site like forearm or in the peritoneal cavity for vascularization and later implanted to the defect site improved the re-epithelization and tissue integration due to improved vascularization.

With the advent of 3D printing the field of tissue engineering has advanced remarkably. A broad range of tissues having different mechanical and functional properties have been designed and 3D printed so far. Many of them have been tested clinically and have shown promising results. Even though there have been many attempts to 3D print a tracheal replacement, most of them lack mechanical properties comparable with the native trachea, which may result in mechanical mismatch with native tissue and might lead to the graft failure. To address these issues, an elastic material having desirable degradation property and excellent 3D printability has been synthesized and tested its capability to be used as a material for 3D printed tracheal graft. To use cells in 3D printing, the bioink has to be an

aqueous system, so far there has been no bioink developed which has mechanical strength and at the same time support cell growth without any compromise. And when 3D printing of solid polymers by FDM is concerned, it gives very good mechanical strength but cells cannot be used because it involves melting of the polymer. This study proposes a biphasic design where the cells can be simultaneously seeded while printing and the FDM based 3D printed elastic framework provides the required mechanical. This helps in the successful development of 3D printed tracheal substitutes.

# CHAPTER 3 |
# MATERIALS & METHODS

## 3.1 Objective 1: Synthesis of elastomeric biomaterial for tracheal tissue engineering

**Part I: Synthesis of Polyurethane urea (PUU)**

**Part 2: Synthesis of Poly(lactide-co-caprolactone)**

### 3.1.1 Synthesis of polyurethane urea

The PUU was synthesized by a two-pot or pre-polymer method. Toluene (Spectrochem) was used as solvent for the polymerization. PCL diol of molecular weight 2000 (Sigma) was used as the polyol. The synthesis was done using hexamethylenediisocyanate (TCI) as isocyanate and 1,4-Diamino butane (Sigma) as chain extender. A molar ratio of 1:2:1 for PCL diol:HDI:BDA was used for the synthesis. In the two-pot synthesis method the first step involves preparation of isocyanate end capped PCL diol. The synthesis was carried out in a three neck round bottom flask, the PCL diol was dried at 60$^{o}$ C under vacuum for 24 hrs and the toluene was dried over calcium hydride and distilled at 40$^{o}$ C. HDI diluted with dry toluene was added drop wise to the dry PCL diol with constant stirring. After the addition the temperature was raised to 80$^{o}$ C and the reaction was continued for 18 hrs without any catalyst.

Once the pre-polymer is formed, the temperature was reduced to 37$^{o}$ C and the chain extender BDA diluted in dry toluene was added drop wise to the pre-polymer. All these reactions were done in inert atmosphere with constant supply of nitrogen. After the addition of the chain extender the temperature was increased to 80$^{o}$ C and continued the reaction for 18 hrs. The reaction temperature is reduced to 37$^{o}$ C and the polymer solution was precipitated in hexane solution. The precipitate was dried at room temperature and dissolved in chloroform and again precipitated in hexane, this was repeated until it gave a constant weight.

### 3.1.2 Synthesis of poly(lactide-co-caprolactone)

Predetermined amount of L-lactide and ε-caprolactone were added to a clean round bottom flask. The flask was purged with nitrogen for 30 min. Stannous octoate was added at a comonomer:catalyst ratio of 2000:1. The reaction was done at 140° C for 24 hrs. The product was dissolved in chloroform and precipitated in excess methanol to remove the unreacted reactants. The product is then dried at 45° C.

## 3.1.3 Physico-chemical characterization of the synthesized polymers

### 3.1.3.1 Fourier ransform infrared spectroscopy (FTIR)

The IR spectra were obtained using (Bruker) spectrometer in attenuated total reflection (ATR) mode at room temperature. Solvent casted films were used as the samples for PUU, PLCL and lyophilized chitosan-hyaluronic acid dialdehyde (CH-HDA) gels were used for the gel samples. The spectra were measured in the range of 3500 to 1000 $cm^{-1}$.

### 3.1.3.2 Proton nuclear magnetic resonance ($^1$H-NMR)

$^1$HNMR spectra of the synthesized PUU and PLCL were recorded using a $^1$HNMR spectrometer (Bruker). The samples were dissolved in deuterated chloroform ($CDCl_3$) and tetramethylsilane (TMS) as internal standard. The molar ratio of the copolymer was calculated by using the following formula,

**Eq. 2,**

$$\text{Mole \% of caprolactone} = \frac{\text{relative moles of caprolacone}}{\text{relative moles of caprolactone+relative moles of lactide}} \times 100$$

### 3.1.3.3 Gel permeation chromatography

The molecular weight distribution of the synthesized PUU and PLCL were measured using Shimadzu GPC instrument with IR and UV detectors. THF (HPLC grade) was used as the mobile phase and Agilent column (Pgel-Mixed C) was used and the flow rate was maintained at 1 ml/min. The samples were dissolved in the same solvent at a concentration of 5 mg/ml. Polystyrene standards were used to generate the calibration curve and the molecular weight distribution was measured using the RI detector.

### 3.1.3.4 Analysis of thermal properties

Thermal analysis was performed using a Perkin Elmer DSC instrument, calibrated with indium standards. Standards of 5-10 mg were cooled at 90$^o$ C and heated to 250$^o$ C at a heating rate of 10$^o$ C/min under nitrogen atmosphere. The heat stability of the hydrogel was analyzed by thermogravimetric analysis (TGA). The TGA was performed using TGA analyzer (TA instruments), 5-10 mg of samples was heated from room temperature to 700$^o$ C at a heating rate of 10$^o$ C min in nitrogen atmosphere.

### 3.1.3.5 Water contact angle measurement

The hydrophobicity of the materials was evaluated by water contact angle measurement by sessile drop method using a goniometer (Dataphysics). Polymer solution prepared in chloroform was used to dip coat glass slides and was air dried for 48 hr. This thin uniform polymer film was used for the water contact angle measurement.

### 3.1.3.6 Mechanical testing

The tensile testing of the samples was done as per ASTM standard D882. Solvent casted films of PUU and PLCL having dimensions of 12 mm width, 60 mm length and 0.02 mm thickness were used. The tensile strength of the samples were measured using an instron UTM (Universal testing machine) and the experiment was conducted at room temperature with crosshead speed of 5 mm/min and a load cell of 10 N was used.

### 3.1.3.7 Cell viability studies: Live/dead staining

Rabbit articular chondrocytes of passage 2 was trypsinized and seeded on to the PUU and PLCL electrospun scaffold and was given an incubation time of 1.30 hr for the cells to attach on to the scaffold. Chondrogenic media was added and cultured for three days. After three days the scaffold was retrieved and washed in PBS and stained for 20 min with Calcein/ Etbr (Thermofisher) stain prepared in PBS as per the manufacture's protocol. After the staining, the samples were washed in PBS and observed under the confocal microscope (Zeiss).

### 3.1.3.8 MTT assay

The test was done as per the ISO standards ISO10993-5. Nine milligram of samples was incubated in 2 ml cell culture media for 1,7 and 14 days. After the incubation period, 100 µl of the media was added to the L929 cells plated on 96 well plate. The cells were cultured for 24 hrs and then MTT prepared in PBS was added and incubated for 3 hrs. The colour formed was then dissolved using 100 µl DMSO and the O.D values were measured at 590 nm.

## 3.2 Objective 2: Fabrication of the synthesized elastomeric biomaterial into a 3D scaffold system for tracheal tissue engineering.

### 3.2.1 Fabrication of tubular scaffold by electrospinning

A horizontally placed electrospinning unit was used here. 10 ml of PLCL or PUU solution in chloroform:methanol in 70:30 ratio was used for this study. The solution was loaded in a plastic syringe and placed in a syringe pump (KD scientific). A blunt end metallic needle of 21 gauge was used and an electric potential of 15 Kv was applied on to the needle. The fibers were collected onto the rotating mandrel of 6 mm diameter. The experiment was run for 2 hrs at a flow rate of 1 ml/hr and a mandrel speed of 1000 rpm. Once the tubular scaffold was formed 30% PCL solution in chloroform was extruded through a syringe onto the electrospun tube to make 'C' shaped rings. The scaffold was incubated at 37$^{o}$ C for 24 hrs for solvent evaporation of the 'C' rings.

### 3.2.2 Scaffold design and 3D printing

The printing was done using a 20 gauge nozzle at a temperature of 140° C, 120 psi pressure and speed of 30 mm/sec in a biobot 3D printer. The samples were sterilized using 70% ethanol.

The scaffold was designed using 123D CAD software and sliced using slic3r in .stl format. The design was similar to the native rabbit trachea, having 5 mm internal diameter and 3.5 cm length. The printing was done using a 21 gauge nozzle at a temperature of 140° C, 120 psi pressure and speed of 30 mm/sec. The samples were sterilized using 70% ethanol.

## 3.3 Objective 3: Development of a biphasic design having an elastomeric framework and a hydrogel system having appropriate mechanical properties and cytocompatibility

For 3D printing the biphasic structure, a hydrogel system is required for delivering the cells. A chitosan and hyaluronic acid dialdehyde based system having a Schiff's base crosslinking chemistry was chosen for this purpose. The preparation of the hydrogel and its characterization techniques is explained in detail in the following session.

### 3.3.1 Preparation of hyaluronic acid dialdehyde

Hyaluronic acid was oxidized to make hyaluronic acid dialdehyde. One gram of hyaluronic acid was dissolved in 100 ml distilled water and required amount of periodate was added to make 50% oxidized hyaluronic acid dialdehyde. The content was stirred in the dark for 6 hrs at 25º C. The content was then dialyzed against distilled water for 3-4 days and the water is changed at every 6 hrs, the dialysis was continued until the dialysate was free of periodate. The presence of periodate was analyzed by adding 250 µl of dialysate to 250 µl of 1% silver nitrate and checked for presence of any precipitate. The silver nitrate reacts with the sodium metaperiodate to form silver metaperiodate which precipitates in water. The dialysate was then lyophilized and stored at -20º C.

For preparing the hydrogel, 1.2% of chitosan was dissolved in 1% acetic acid and then neutralized with 0.2 M HEPES, 0.3 M sodium bicarbonate and 0.05 M sodium hydroxide buffer solution and brought the final chitosan concentration to 1%. The HDA was prepared in PBS, 5% of HDA was neutralized with the same buffer. The gel was prepared by mixing the 1% neutralized chitosan and HDA in three different ratios of the crosslinker (Table 1).

**Table 1. Compositions of the chitosan-HDA hydrogel**

| Sample | Composition | Chitosan (µl) | HDA (µl) |
|---|---|---|---|
| 1 | 10:1 | 50 | 5 |
| 2 | 10:3 | 50 | 15 |
| 3 | 10:5 | 50 | 25 |

### 3.3.2 Characterization of chitosan-HDA hydrogel

#### 3.3.2.1 Degree of cross linking

The degree of crosslinking of the hydrogel was determined by ninhydrin assay. The amount of free amine groups in the three different ratios of the hydrogel was determined and was compared to the amount of free amino groups in uncrosslinked chitosan. Ninhydrin was freshly prepared in acetone and 10 mg of

the lyophilised chitosan-HDA hydrogel samples were boiled with freshly prepared ninhydrin reagent at 100º C for 1 hr. After boiling, 1 ml ethanol was added to it to stabilize the color formed. The absorbance was measured at 590 nm with a spectrophotometer (Cary). The amount of the free amino groups present in the hydrogel was calculated using glycine at various concentrations as standards. The samples were used in triplicates for the determination of the amount of free amino groups. The degree of crosslinking was calculated by the following equation,

**Eq. 3,**

Percentage degree of crosslinking = $C_i - C_f C_i \times 100$

Where, $C_i$ is the optical absorbance of uncrosslinked chitosan.

$C_f$ is the optical absorbance of chitosan-HDA hydrogel.

**3.3.2.2 Determination of gelling time**

The gelling time of the chitosan-HDA hydrogel was determined by measuring its change in viscosity with time when the two components are mixed together. The viscosity was measured using a viscometer (Brookfield) with spindle SLV-64 and sample adaptor (5 ml) at 150 rev/min at 25° C.

**3.3.2.3 Determination of percentage of gel fraction**

To determine the percentage of gel fraction lyophilized chitosan-HDA hydrogel samples of 2 mm thickness and 5mm diameter was immersed in milliQ water for 16 hrs at room temperature and the sample was again lyophilized and the insoluble part was weighed. The percentage of gel fraction was the calculated using the following formula,

**Eq. 4,**

Percentage gel fraction $= \frac{Wd}{Wi} \times 100$

Where, Wi is the initial weight of the lyophilized sample, and Wd is the weight of the lyophilized sample after incubation in water. The samples were used in triplicates for this study.

**3.3.2.4 Determination of degree of swelling**

The degree of swelling of the hydrogel was determined to study the water holding capacity and the stability of the hydrogel in aqueous condition. The lyophilized

hydrogel samples of 2 mm thickness and 5 mm diameter were weighed and incubated in PBS buffer. The samples were retrieved and at regular intervals and its wet weights were measured until uniform weight was attained. The swelling ratio was calculated by the following formula,

**Eq. 5,**

$$\text{Percentage degree of swelling} = \frac{\text{Final weight} - \text{initial weight}}{\text{Final weight}} \times 100$$

**3.3.2.5 Characterization of stiffness by AFM**

The stiffness of the hydrogels of different ratios was measured using Atomic Force Microscopy (Agilent). A silicon nitride cantilever having a spring constant of 0.025 N/m and a resonant frequency of 25 kHz and a tip radius of 2 nm was used to measure the force indentation curves. The Young's modulus was calculated from the force curves using SPIP software using Hertz's contact model.

The following equation was used to calculate the Young's modulus,

**Eq. 6,**

$$F = \frac{4}{3} \times \frac{Es}{1 - \nu s^2} \times \sqrt{r} \times \delta \frac{3}{2}$$

Where,

Es- Sample modulus

νs – Poisson's ratio

r- Tip radius of the curvature

δ- Opening angle

**3.3.3 Isolation of rabbit chondrocytes**

Chondrocytes isolated from the rabbit articular cartilage were used for the *in vitro* studies of the hydrogel. (SCT/IAEC-130/August/2014/85) The rabbit knee joint was cut open aseptically and the cartilage was scrapped off. The isolated cartilage pieces were taken inside the laminar air flow, washed with sterile PBS and was cut to small pieces of about 0.5 mm thickness and 2-3 $mm^2$ size. The cartilage

pieces were then digested with 0.3% collagenase type II digestion media prepared in DMEM containing 1% ABAM (Gibco) for 4hrs at 37° C**.** After the digestion, the enzyme was inactivated using DMEM containing 10% FBS and centrifuged at 1500 rpm at 4° C for 10 min. The pellet containing chondrocytes were collected and the supernatant was discarded. The pellet was resuspended in chondrogenic media containing 10 ng TGFβ, 10 ng dexamethasone, 1% ascorbic acid, 1% proline and DMEM containing 10% FBS, and seeded on tissue culture plate and allowed to become confluent in an incubator at 37° C and 5% $CO_2$. After the cells have become confluent, the cells were trypsinized using 0.25% trypsin-EDTA solution, and cells of passage 3-4 were used for the study.

**3.3.3.1 Encapsulation of chondrocytes in hydrogel**

Passage 3-4 of the isolated chondrocytes were trypsinized and neutralized HDA at a density of 5000/µl. Different volumes of neutralized HDA 5 µl, 15 µl and 25 µl were used and was mixed with 50 µl of neutralized chitosan to encapsulate the cells in the hydrogel of different crosslinking ratio. The gels were then transferred into chondrogenic media and cultured for 7, 14 and 28 days. The media was changed every 2 days and after the culture period the samples were retrieved and used for live/dead staining, collagen I. Collagen II immunostaining, alcian blue and Sirius red staining and for estimation of glycosaminoglycan by DMMB assay.

**3.3.3.2 Viability testing of the encapsulated cells by live/dead staining**

The viability of cells after encapsulation was tested using calcein-AM/EtBr live/ dead staining (Invitrogen). After the retrieval the samples were washed in PBS and stained with a mixture of 4 mM calcein-AM and 2 mM ethidium bromide homodimer for 20 min. The calcein-AM stains the live cells and the EtBr stains the dead cells. The samples were then washed with PBS thrice for 5 mins each using a dancing shaker. The images were taken using a confocal microscope (Zeiss).

**3.3.3.3 Estimation of total glycosaminoglycan**

After culturing for 7, 14 and 28 days the samples were retrieved and washed with PBS. The samples were then digested with proteinase K (Sigma) at 55$^0$ C for about 12-16 hrs until the samples are dissolved completely. The total GAG content was estimated using 1,9-dimethylmethylene (DMMB) assay using

different concentrations of chondroitin 4-sulfate as standards (Rodriguez et al., 2011). The values were normalized to the amount of DNA content of each sample. The samples were taken in triplicates to calculate the standard deviation.

**3.3.3.4 Immunostaining of chondrocyte encapsulated hydrogel**

The samples cultured for 7, 14 and 28 days were retrieved and washed with PBS. The samples were fixed using 4% paraformaldehyde for 15 min.The samples were then washed thrice (5 mins each wash) in PBS to remove the paraformaldehyde. The samples were blocked with 3% bovine serum albumin (BSA) for 1hr at room temperature and were incubated in primary antibody for collagen type II (sc-52658 in 1:200 dilution) and collagen I (abcam, ab6308, at 1:200 dilution) overnight at 4 °C. The samples were then washed thrice with PBS, the collagen II samples were incubated with goat anti-mouse Alexa fluor488 (abcam- ab150113) secondary antibody and for collagen I PE conjugated anti mouse secondary antibody (Santacruz, sc-3761) at room temperature for 1 hr. The samples were then washed thrice with phosphate buffer saline (PBS) and the nucleus was stained with DAPI (Thermofisher, D1306) for 20 min and washed thrice with PBS. The imaging was done using a confocal microscope (NIKON).

**3.3.3.5 Histological analysis**

After each time points the cultured samples were retrieved, sectioned and histology analysis was done. The samples were washed in PBS and fixed in 4% paraformaldehyde for 20 min. The samples were then washed and embedded in a tissue freezing medium (Leica, 14020108926). The samples were frozen at -20° C and sections of 0.7 μm were taken using cryostat (Leica) and the sections were stored at 4º C. To remove the tissue freezing medium, the samples were gently washed in distilled water and were stained used hematoxylin. The sections were also stained with alcian blue and Sirius red to evaluate the secretion of glycosaminoglycans and collagen respectively.

**3.3.3.6 Statistical analysis**

All the error bars are represented as standard deviation. One way/two-way ANOVA was used to statistically compare the groups followed by the post hoc Tuckey test. A difference of $p < 0.05$ was considered statistically significant.

# CHAPTER 4 | RESULTS

### 4.1.1 Synthesis of polyurethane urea

The mechanical properties of the scaffold play a major role while designing a tissue engineered construct. Tissues like trachea are elastomeric in nature hence the biomaterial used is also expected to have mechanical properties similar to the native tissue. Towards this goal we have synthesized two elastomeric polymers polyurethane urea and poly(lactide-co-caprolactone) and its physicochemical characterization was done. In the second objective the feasibility of these two polymers to fabricate into a tracheal construct having three-dimensional cell organisation is tested. The third objective comprises fabricating a 3D tracheal construct based on the material and selected material and fabrication technique.

Since polyurethanes are known for its mechanical properties, we decided to start with synthesising elastomeric polyurethane. Since we are using diamine as a chain extender the polyurethane formed is polyurethane urea. The polyol used is PCL-diol is expected to make the resulting polymer biodegradable. The synthesis was performed without using any catalyst, which makes the material more biocompatible (Park et al., 2013). A two-pot synthesis method is adopted to get more control over the synthesis (Fig. 4.1).

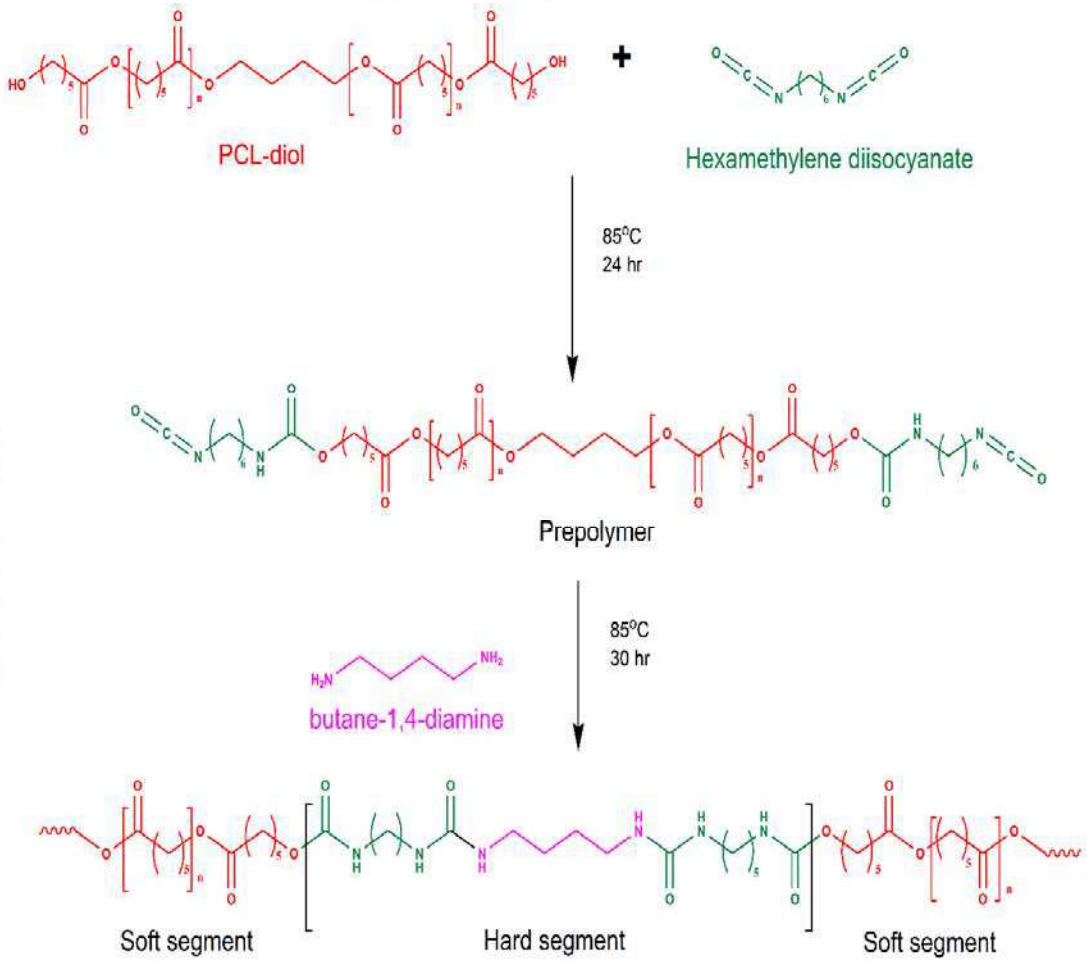


**Figure 4.1. Two-pot synthesis of polyurethane urea.**

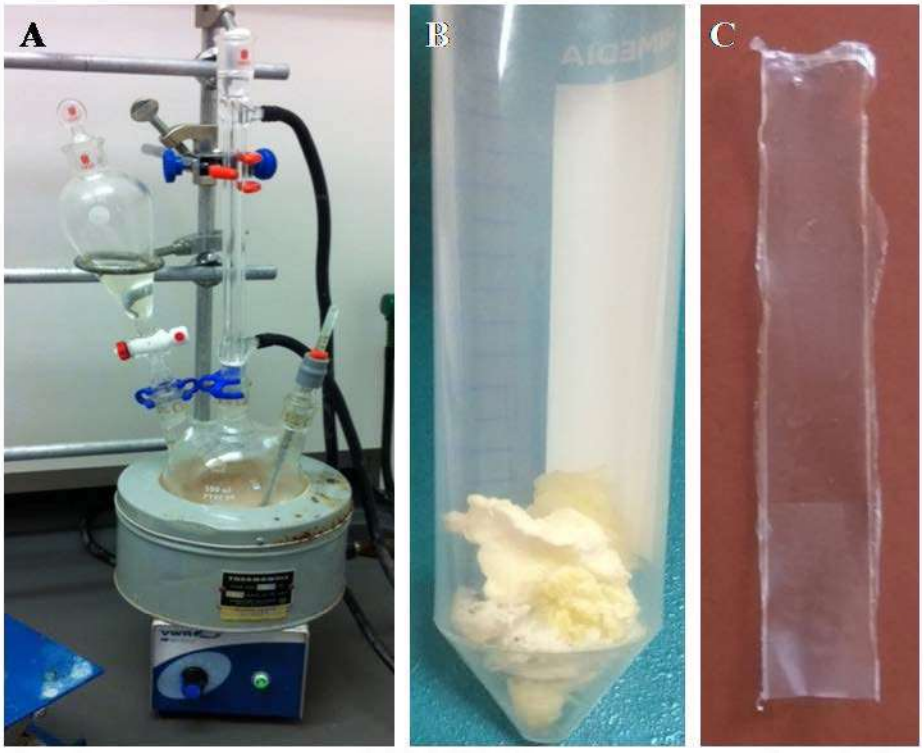


**Figure 4.2. (A) Synthesis set up of polyurethane urea. (B) After synthesis the PUU is precipitated in hexane and air dried. (C) The PUU is dissolved in chloroform and solvent casted into films.**

### 4.1.2 FTIR analysis of the synthesized polyurethane urea

The interest of segmented polyurethanes is increasing in the medical field due to its attractive mechanical properties and its possibility in using it as an artificial extracellular matrix for tissue engineering. The molar ratio of its hard and soft segments influences the biological and physical properties required for the application. PUU was synthesized using HDI as the isocyanate, PCL diol having 2000 g/mol molecular weight as the polyol and 1,4-diaminobutane as the chain extender.

The chemical structure of the synthesized PUU was characterised by FTIR spectroscopy (Fig. 4.3). In the amine region, the broad peak at 3329 $cm^{-1}$ was observed which corresponds to the N-H vibrations of urea and urethane groups. Bands corresponding to symmetric and asymmetric methylene were observed at 2860 $cm^{-1}$ and 2925 $cm^{-1}$ respectively. Further a highly intense peak at 1725 $cm^{-1}$ which corresponds to the C=O of the ester bond of PCL was observed. The

complete conversion of the monomer isocyanate to its polymer polyurethane was confirmed by the absence of isocyanate peak at 2250-2280 $cm^{-1}$ and presence of amine and carbonyl peaks. The peaks observed at 1461 $cm^{-1}$, 1364 $cm^{-1}$, 1237 $cm^{-1}$ are attributed to the $CH_2$ bending. The band at 1047 $cm^{-1}$corresponds to the C-O-C bond present in the urethane and peaks present at 1159 $cm^{-1}$, 1094 $cm^{-1}$ corresponds to the ester bond of the PCL. The polyurethanes have two types of carbonyl groups: carbonyl groups that take part in hydrogen bonding and carbonyl groups which are free and are not involved in the hydrogen bonding. The peak at 1725 $cm^{-1}$ corresponds to the free carbonyl group present in PCL while the carbonyl group of the urethane is involved in the hydrogen bonding was observed at 1683 $cm^{-1}$. Due to the presence of urea groups the hydrogen bonded carbonyl groups were also present in the urea. The peak at 1621 $cm^{-1}$ corresponds to the amide I (C-N stretching) of the hydrogen bonded carbonyl urea and peaks at 1573 $cm^{-1}$attributes to the amide II (N-H bending) of the urea.

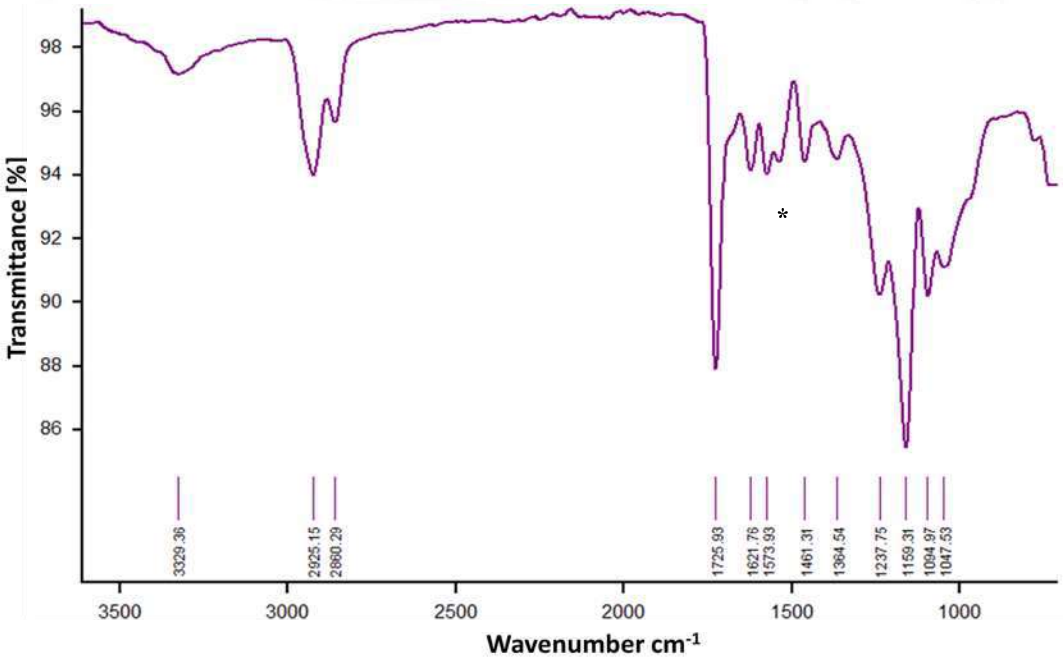


**Figure 4.3. FTIR spectrum showing NH stretching at 3329 $cm^{-1}$. Urea and urethane bond formation were confirmed by peaks at 1621 $cm^{-1}$and 1573 $cm^{1}$ respectively. Absence of isocyanate peak at 2250-2280 $cm^{-1}$ and presence of carbonyl and amide peaks shows conversion of monomers into polymers.**

### 4.1.3 NMR analysis of the synthesized PUU

The chemical structure of the PCL based polyurethane urea was confirmed by NMR spectrometer by detecting the $^{1}H$ (Fig. 4.4). The resonances at 1.4 ppm ($\delta^{a}_{H}$: CH2-CH2-CH2-), 1.67 ppm ($\delta^{b}_{H}$: -$CH_2$-$CH_2$-O), 2.3 ppm ($\delta^{c}_{H}$: $CH_2COO$) and 4.09 ppm ($\delta^{d}_{H}$: $CH_2OCO$) corresponds to methylene protons of PCL. In addition to the characteristic PCL peaks, peaks at 3.1ppm ($\delta^{e}_{H}$, $CH_2NHCO$) and 4.75ppm ($\delta^{f}_{H}$, NHCO) are observed which confirmed the formation of urea and urethane bonds in the polymer chain.

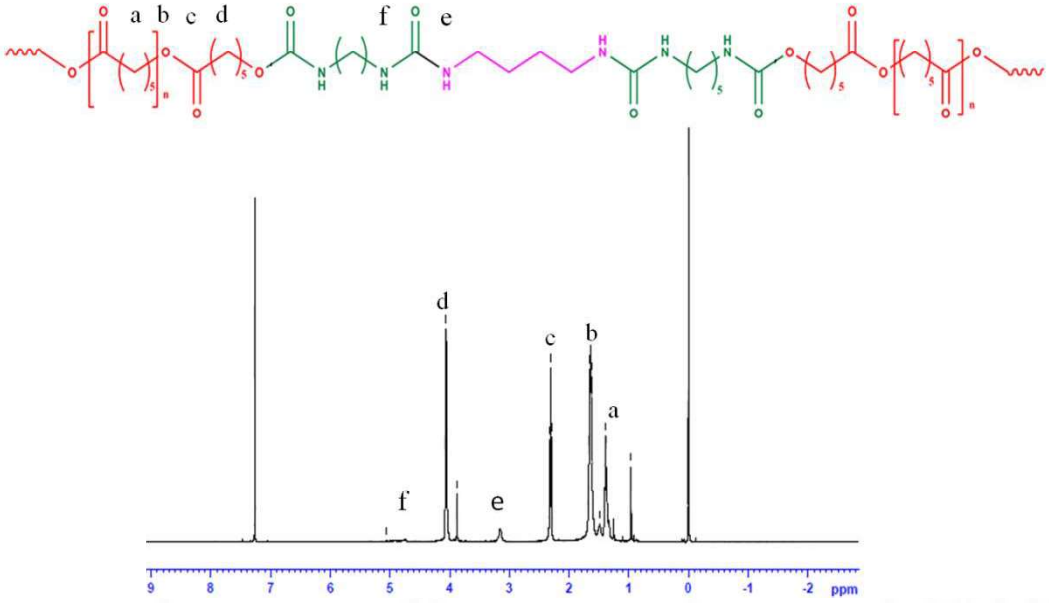


**Figure 4.4. NMR spectrum of PCL-HDI-BDA based polyurethane urea.**

### 4.1.4 Determination of molecular weight distribution by GPC

The molecular weight distribution of the synthesized PUU was determined by GPC. HPLC grade THF was used as the mobile phase, the same solvent was used to dissolve the sample at a concentration of 5 mg/ml.

The synthesized PUU gave a unimodal curve having a weight average molecular weight of 73000 g/mol and a polydispersity index of 1.6 (Fig. 4.5).

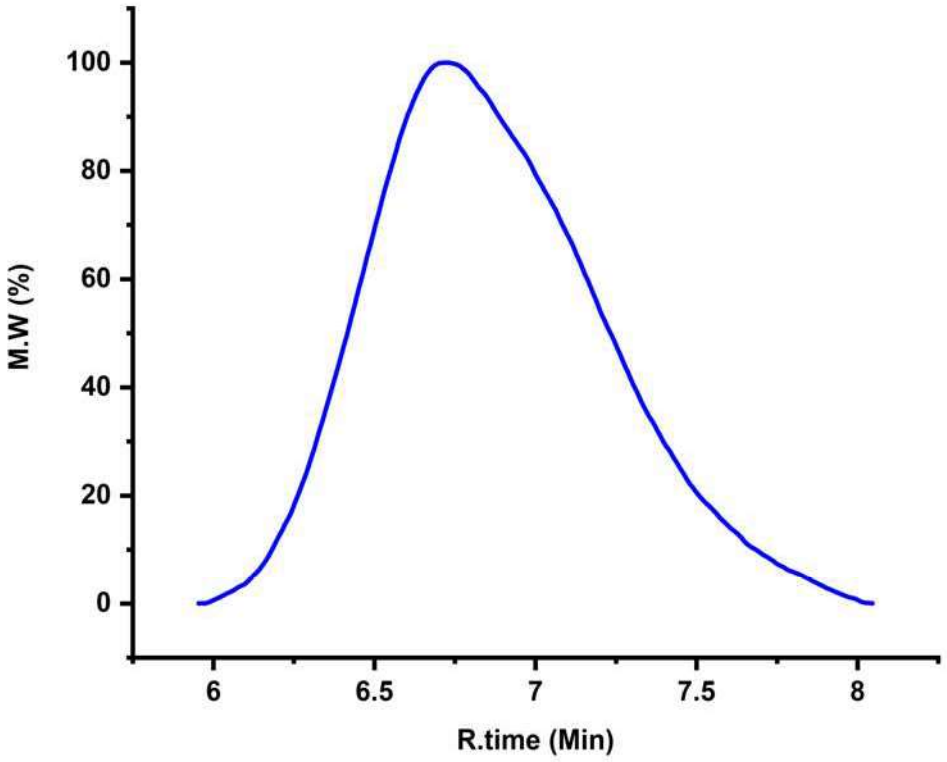


**Figure 4.5. GPC curve showing the molecular weight distribution of the synthesized PUU.**

**Table 2. Molecular weight distribution of PUU**

| Mn | Mw (g/mol) | Mw/Mn |
|---|---|---|
| 44426 | 73763 | 1.66038 |

### 4.1.5 Differential scanning calorimetry

The DSC was used to study thermal changes like glass transitions (Tg), enthalpy changes occurring during phase separation, crystallization. The DSC scan (Fig. 4.6) showed a Tg at -56° C which corresponds to the soft segment. This also indicates that the polymer is elastic at room temperature. It should also be noted that the Tg of the synthesized PUU is higher than the pure PCL which has a Tg of -60, this indicates the mixing of the soft segment and hard segment of the PUU. The material also showed two melting points at 25° C and 335° C, indicating the presence of phase separated hard and soft segments. The sharp peak at 335° C is attributed to the hard segment and that at 25° C corresponds to the soft segment. The endothermic peak at 375° C attributes to the degradation of the material immediately after the melting point.

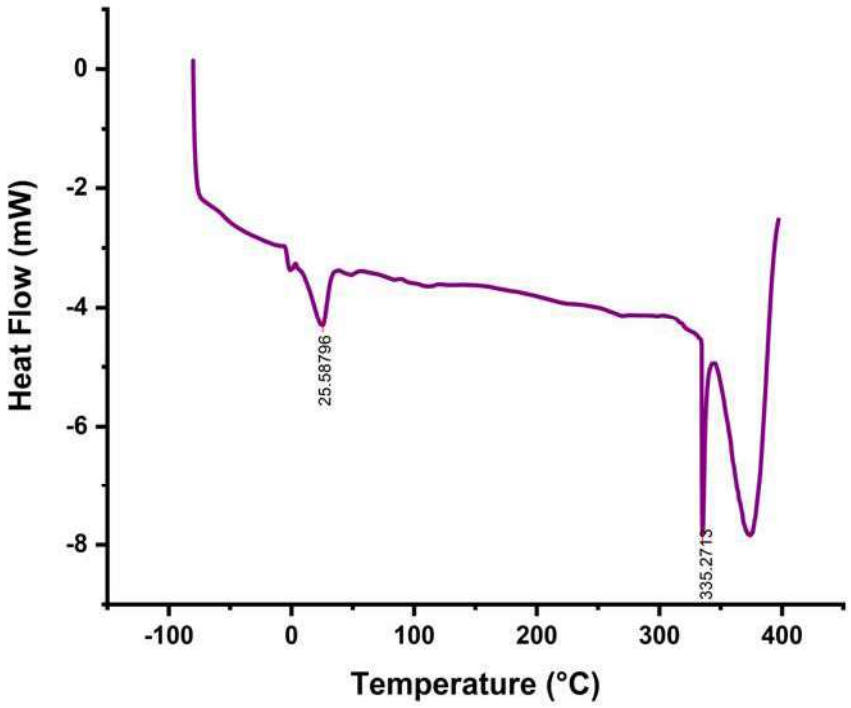


**Figure 4.6. DSC curve showing thermal behaviour of the synthesized PUU.**

### 4.1.6 Water contact angle measurement of PUU

Hydrophobicity is an important factor responsible for the cell adhesion and immune reaction of the biomaterial *in vivo*. A water contact angle of about 60$^{o}$ is preferred for biomaterials (Rahul M Visalakshan et al., 2019). The

hydrophobicity of the synthesized PUU films was measured by water contact angle and was found to be 78$^{o}$ (Fig. 4.7).

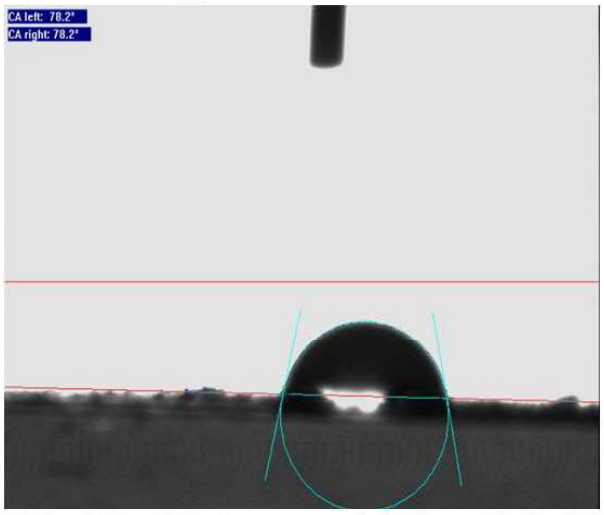


**Figure 4.7. Water contact angle measurement of PUU films.**

### 4.1.7 Mechanical properties of the synthesized PUU

The stress-strain curve of the synthesized PUU films is shown in Fig. 4.8. The result shows, after the yield point the material is having strain-hardening without any necking being observed during the stretch. The Young's modulus of the material was found to be 3.79±0.95 MPa and tensile strength 10±1.3 MPa. The material showed an elongation at break of 770.5±6.2%.

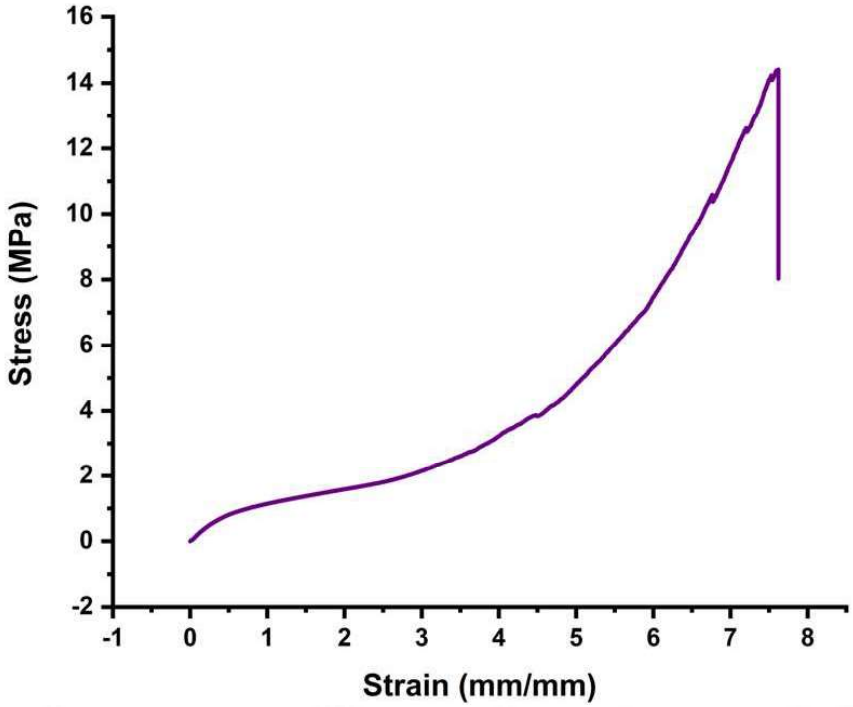


**Figure 4.8. Stress-strain curve of PUU showing typical elastomeric nature**

### 4.1.8 Evaluation of cytotoxicity of PUU by MTT assay and live/ dead staining

The cytotoxicity of the material was tested using MTT assay and live/dead staining. The results (Fig. 4.9) showed comparable cell viability as that of the tissue culture plate after 48 hrs of culture of L929 cells. Further the live dead assay using chondrocytes showed no or negligible dead cells and had comparable cell viability as that of the tissue culture plate. The cytotoxicity was also tested by direct contact method, where the material was placed over the cell culture for 48 hrs and no morphological changes were observed compared to the negative control.

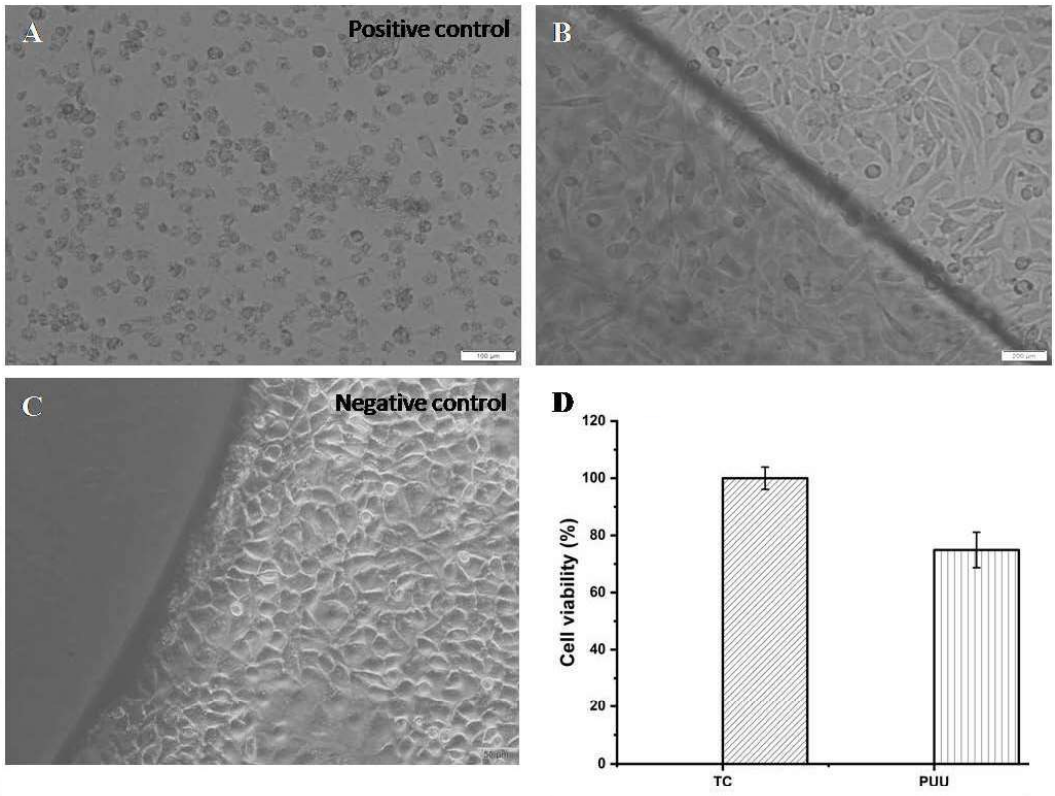


**Figure 4.9. (A) Positive control showing L929 cells cultured on treated PVC were found to be dead. (B) Direct contact test showing PUU incubated over L929 cells showing no morphological changes compared to the negative control (C) HMWPE. (D) MTT assay of PUU extract showing comparable cell viability as that of the tissue culture flask.**

### 4.1.9 Chondrocytes cultured on PUU showing chondrogenesis

Confocal images of chondrocytes cultured on PUU showed expression of collagen II after 7 days culture in chondrogenic media. The live/dead staining showed typical round morphology of the chondrocytes and had no dead cells (Fig. 4.10A). After 7 days the cells stained positive for collagen II, a marker for hyaline cartilage. In absence of the blue filter, it showed typical hallow like cartilage morphology having an unstained region in the centre (Fig. 4.10B). A merged image of DAPI and collagen II staining showed collagen II deposited around the chondrocytes (Fig. 4.10C). The results indicate the material can support cartilage formation with no cytotoxic effect.

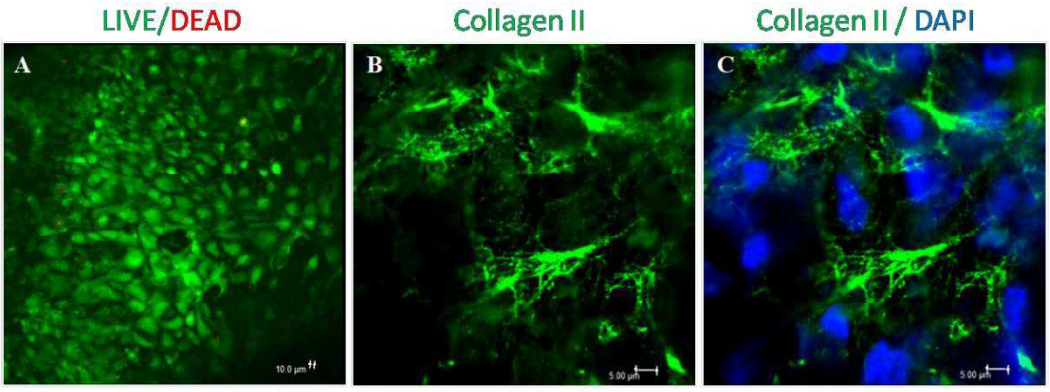


**Figure 4.10. (A) Chondrocytes seeded on PUU and cultured for 7 days showing live/dead staining. (B) Chondrocytes seeded on PUU and cultured for 7 days showing collagen II immune staining. (C) Chondrocytes seeded on PUU and cultured for 7 days showing collagen II immune staining with DAPI stained nucleus.**

### 4.1.10 Synthesis and characterization of poly(lactide-co-caprolactone)

The PLCL copolymers were synthesized by ring opening polymerization at 140° C (Fig.4.11). Copolymer was synthesized at four different ratios of caprolactone and lactide. The feed monomer ratios of PLCL were 65:35, 70:30, 80:20 and 90:10. Other ratios with increased caprolactone content (60:40) were also tried and were found to be tacky and not suitable for our application. The ratio with higher lactide content (95:5) was very brittle; hence we selected the aforementioned four ratios for our further studies. The reaction was performed in a nitrogen atmosphere using stannous octoate as catalyst for 24 hrs. Previous studies have shown highest molecular weight and yield was obtained at 140° C using a comonomer: catalyst ratio of 2000:1 (Fernandez et al., 2012). It has also been reported that with increase in time of reaction the lactide content changes. Hence, a change in material property is also expected. Since the desired mechanical property was achieved at the above conditions, we performed the synthesis at these conditions.

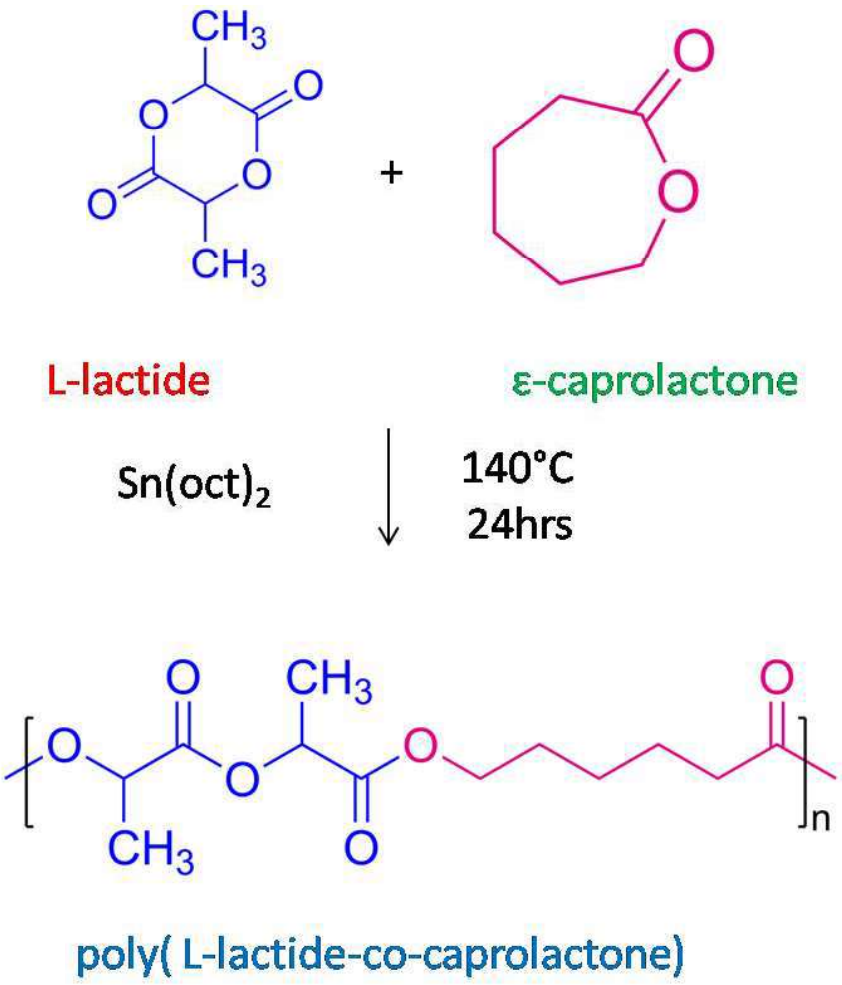


**Figure 4.11. Synthesis of poly(lactide-co-caprolactone) by ring opening polymerization.**

### 4.1.11 FTIR characterization of synthesized poly(lactide-co-caprolactone)

The absorption spectra of different carbon compounds present in the synthesized PLCL were analyzed with different wavelengths. The peak at 1738 $cm^{-1}$ corresponds to the carbonyl stretching of the PLA and PCL (Fig. 4.12). The band in the region 1000 $cm^{-1}$-1300 $cm^{-1}$ corresponds to the ester group and band at 1182 $cm^{-1}$ confirms the long alkyl chain ester present in the polymer. Bands present at 2990 $cm^{-1}$, 2942 $cm^{-1}$, 2860 $cm^{-1}$are responsible for the alkyl groups of the PLCL copolymer and absence of the band at 2990 $cm^{-1}$ in PCL confirms the presence of characteristic CH stretching of PLA, present in the PLCL copolymer. The formation of PLCL is further confirmed by the NMR studies.

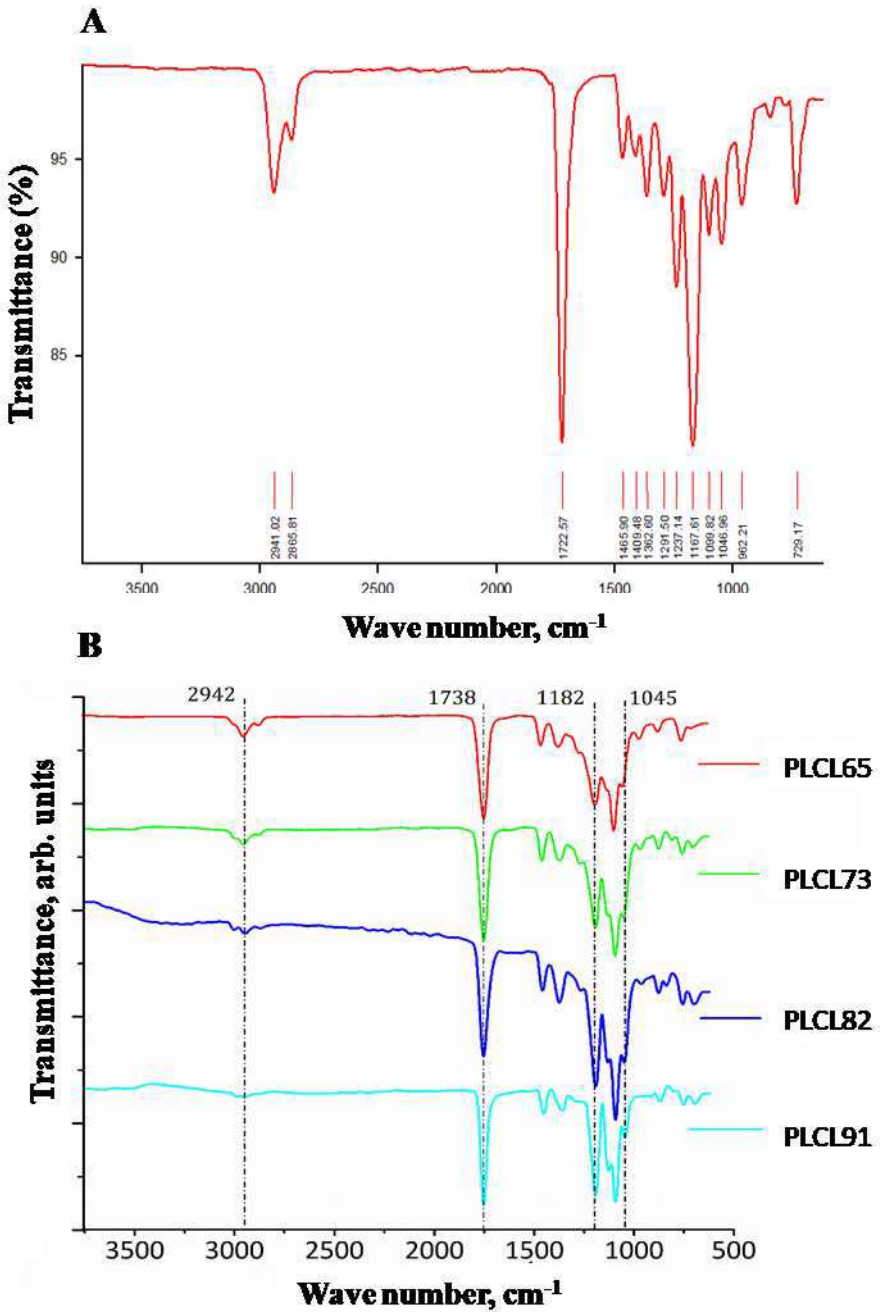


**Figure 4.12. FTIR spectra of the synthesized PLCL showing characteristic peaks. (A) FT-IR spectra of PCL showing the characteristic peak of carbonyl stretching at 1738 $cm^{-1}$. (B) FTIR spectra of synthesized samples in different ratios of caprolactone and lactide - 65:35, 70:30, 80:20, 90:10. Peak at 2942 $cm^{-1}$ corresponds to alkyl chain of PLCL. Peak at 1738 $cm^{-1}$ corresponds to carbonyl stretching of the PLCL. Peak at 1182 $cm^{-1}$ represents the long alkyl chain present in the polymer.**

### 4.1.12 Confirmation of chemical structure of the synthesized poly (caprolactone-co-lactide) by NMR

The structure of the synthesized copolymer was confirmed by proton nuclear magnetic resonance spectra (Fig.4.13). The PLCL spectrum showed signals at 1.57 ppm and 5.1 ppm which corresponds to the $CH_3$ and CH of the PLLA. The signal at 1.35 ppm-1.67 ppm corresponds to the alkyl groups of the PCL. The signals around 2.3 ppm and 4.03 ppm correspond to the α and ε methylenes of caprolactone (CL). The signals at 2.4 ppm, 4.1 ppm, 5.0 ppm confirmed the presence of CL-LA linkage and were present in all the ratios. The peaks of lactide (LA) protons were prominent in the PLCL91 spectrum. With the increase in the caprolactone ratio, the caprolactone peaks started appearing at 2.3 ppm and 4.03 ppm.The monomer ratio of CL/LA present in the PLCL copolymer was calculated by the ratio of integral values of the peaks at 5.1 ppm for LA unit and 4.00 ppm for CL unit and is found to be similar to the feed molar ratio (Table-6).

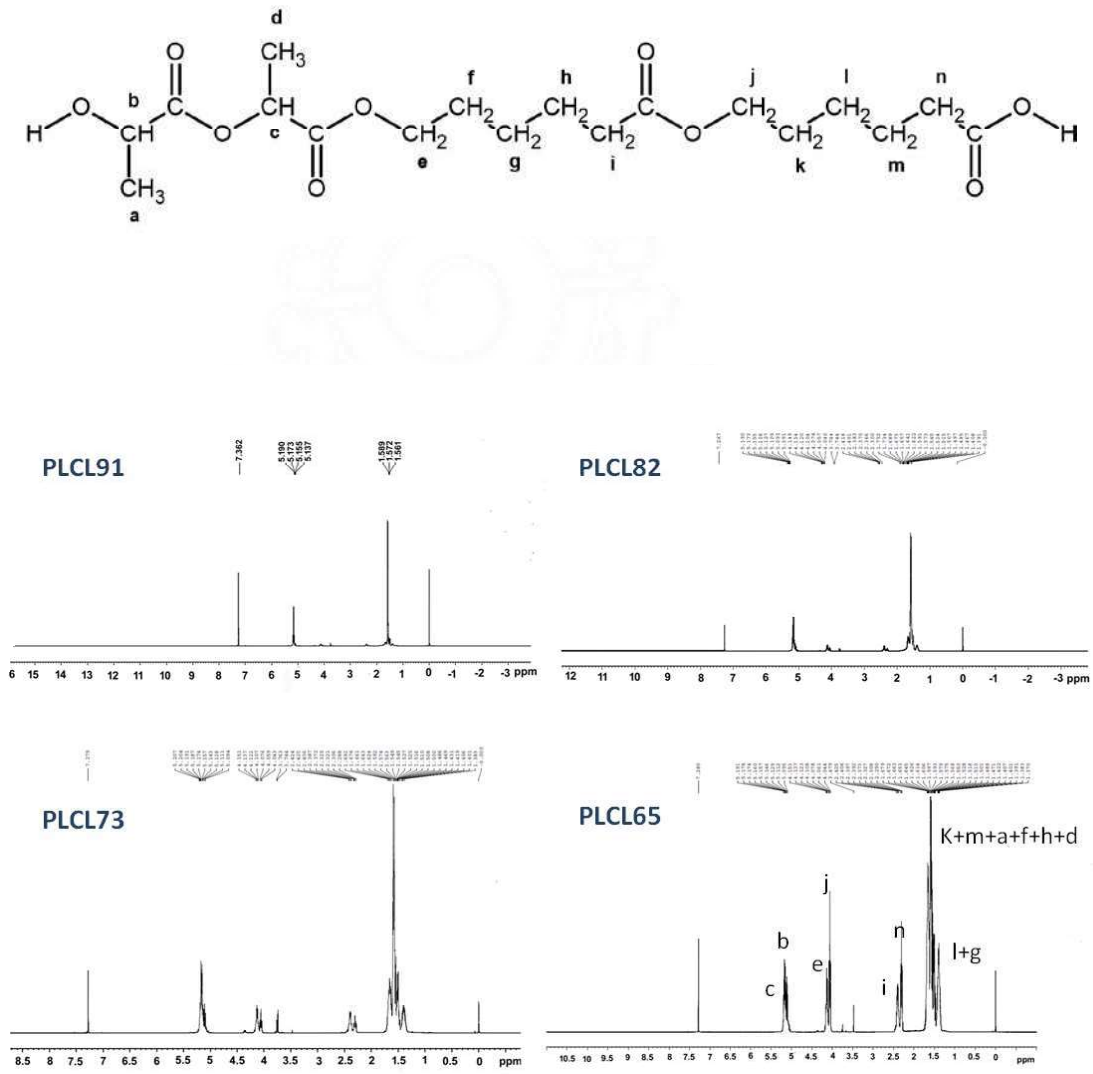


**Figure 4.13. NMR spectrum showing the characteristic peaks of PLCL; 1.57 ppm ($CH_3$); 5.1 ppm (CH); 1.3-1.6 ppm ($CH_2CH_2$ $CH_2$); 2.3 ppm- ($CH_2$ CO); 4.03 ppm ($CH_2$ O); LA-CL junction-2.4 ppm, 4.1 ppm, 5 ppm.**

### 4.1.13 Determination of molecular weight of the synthesized PLCL by GPC

The molecular weight distribution of the synthesized PLCL was determined by GPC. HPLC grade THF was used as the mobile phase, the same solvent was used to dissolve the sample at a concentration of 5 mg/ml.The molecular weight of the PLCL was found to be increasing with increase in the lactide content (Fig. 4.14). PLCL65 was found to have the lowest molecular weight of 34335 g/mol and PLCL91 gave the highest molecular weight value of 158329 g/mol.

**Table 3. Molecular weight distribution of PLCL**

| No. | Title | Mn | Mw (g/mol) | Mw/Mn |
|---|---|---|---|---|
| **1** | **PLCL65** | 23427 | 34335 | 1.46561 |
| **2** | **PLCL73** | 36419 | 80835 | 2.21956 |
| **3** | **PLCL82** | 49320 | 96022 | 1.94694 |
| **4** | **PLCL91** | 75775 | 158329 | 2.08947 |

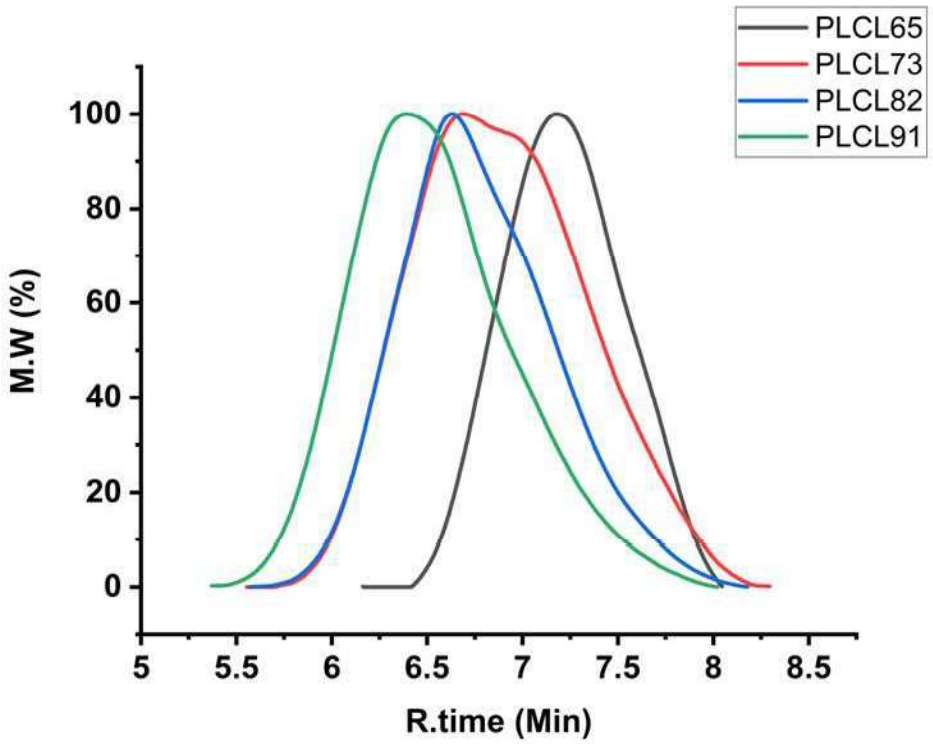


**Figure 4.14. GPC analysis of the synthesized PLCL indicates molecular weight (Mw) of PLCL increases with increase in the lactide ratio.**

### 4.1.14 Analysis of thermal properties of PLCL by differential scanning calorimetry

The melting points of all the ratios of the synthesized PLCL were in between the melting points of PLA (180º C) and PCL (60º C). Since all the synthesized copolymers have a single melting peak, it confirms the copolymer formed is a random copolymer. The splitting of the melting peak attributes to the existence of PLLA crystals in different perfection. It corresponds to the melting of α form and η form stereocomplex crystals of polylactic acid, which subsequently merge to form a single peak with increasing the lactide content. Tg values of the lowest ratios PLCL65 and PLCL73 were around 18º C, whereas that of the higher ratios PLCL82 and PLCL91 had a Tg value of 41º C and 46º C respectively (Fig. 4.15). This indicates that the lower ratios are elastic in nature and the ratios with higher lactide content are brittle. All the ratios showed a crystallization peak at around

80$^{0}$ C which shows the crystallization of the lactide content on melting. The melting point of the PLCL was also found to be increasing with increase in the lactide content. The intensity of the curve also increased with increase in the lactide content. The percentage of crystallization calculated from the DSC curve also showed an increasing trend in percentage of crystallization with increase in the lactide content (Eq-7, Table-3).

**Eq-7,**

$$X_c\% = \frac{\Delta H_{m1} + \Delta H_{m2} - \Delta H_c}{\Delta H_m^0} \times 100$$

$X_c$ = Degree of crystallization

$\Delta H_{m1}$ = Enthalphy of melting

$\Delta H_m^0$=Enthalpy of melting of pure material

$\Delta H_c$ = Enthalpy of crystallization

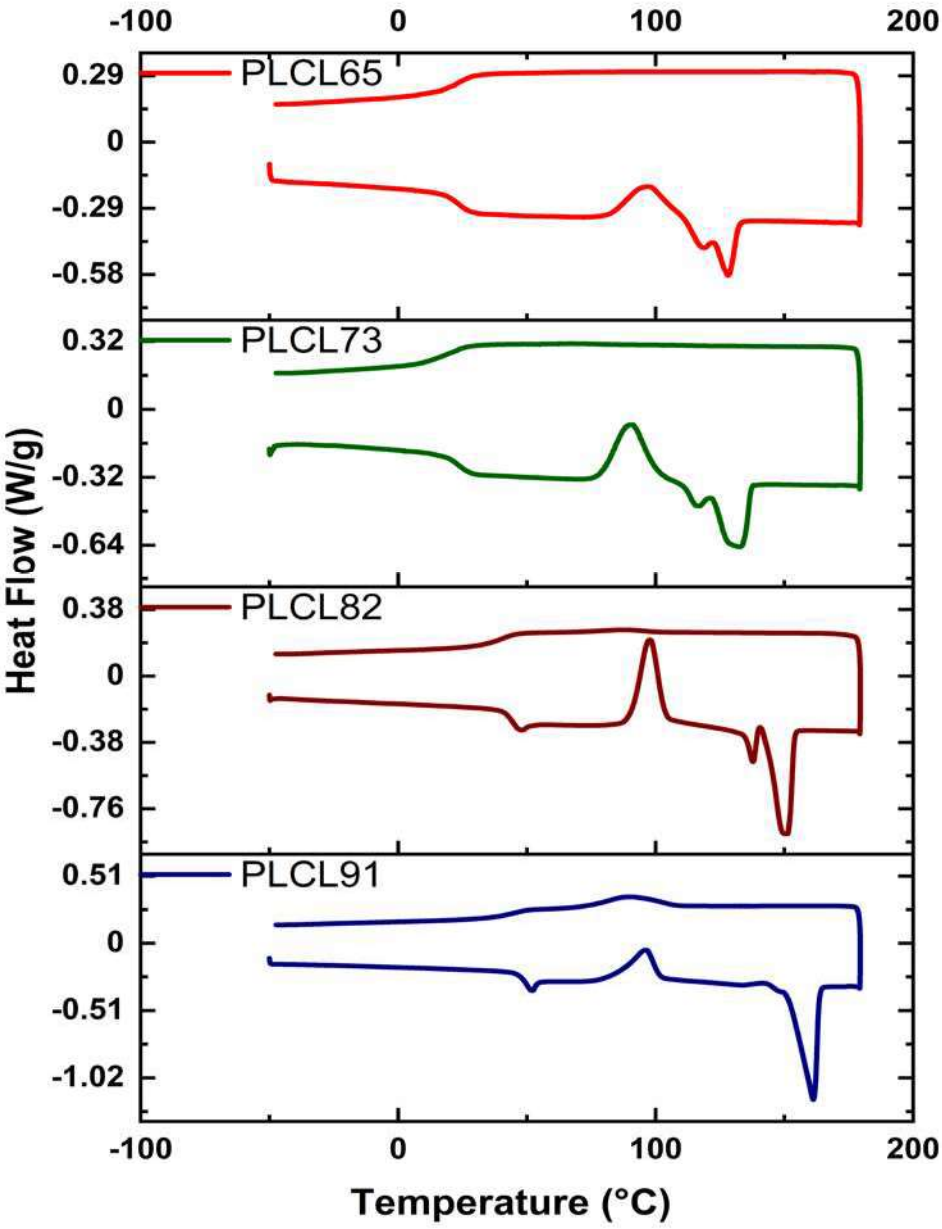


**Figure 4.15. Differential scanning calorimetry of all four ratios of the synthesized PLCL.**

**Table 4. DSC peaks of the PLCL**

| Sample | $\Delta H_{m1}$ (J/g) | $\Delta H_{m2}$ (J/g) | $\Delta H_c$ (J/g) | Xc % | Tm (°C) | Tg (°C) |
|---|---|---|---|---|---|---|
| **PLCL65** | 5.5 | 3.1 | 13.11 | 20.4 | 128 | 18 |
| **PLCL73** | 15.91 | 4.3 | 21.43 | 39.28 | 133 | 18 |
| **PLCL82** | 26.43 | 5.3 | 23.14 | 51.3 | 150 | 41 |
| **PLCL91** | 37.81 | 1.2 | 16.18 | 52.06 | 161 | 46 |

### 4.1.15 Thermal stability of PLCL measured by TGA analysis

Since FDM (Fused deposition modeling) based 3D printing involves melting of the polymer, the thermal stability of the synthesized polymer is an important factor to study. (Fig. 4.16) Shows the TGA curves of four different ratios of the synthesized PLCL, there is an evident increase in the degradation temperature with increase in the caprolactone content (Table-5). The temperature at which 50% of weight loss observed was taken as the degradation temperature (Td). Hence addition of caprolactone is increasing the heat stability of the material (Fig. 4.16).

**Table 5. Degradation temperatures of PLCL**

| Sample | Td (°C) |
|---|---|
| **PLCL91** | 339 |
| **PLCL82** | 346 |
| **PLCL73** | 342 |
| **PLCL65** | 351 |

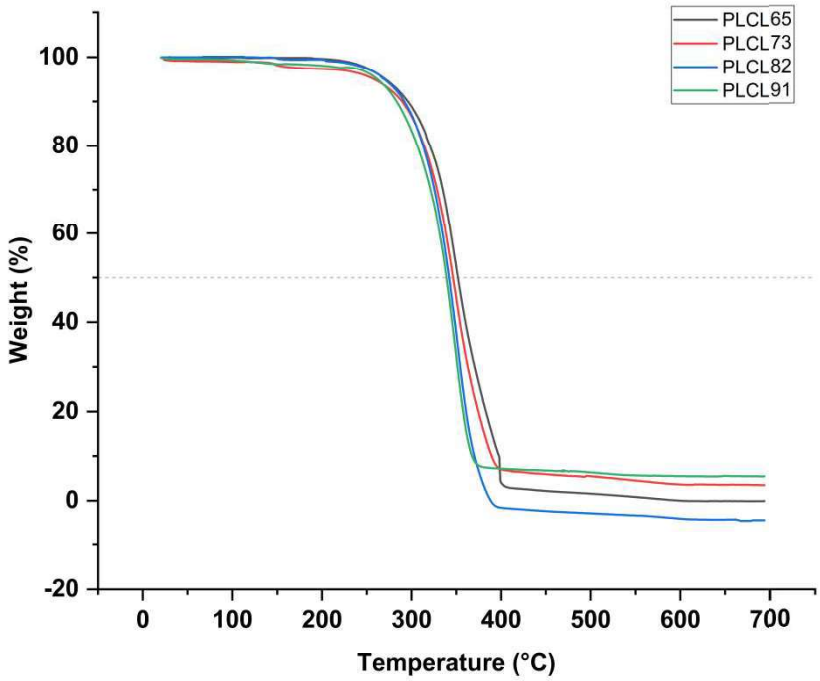


**Figure 4.16. Thermogravimetric analysis (TGA) of all four ratios of the synthesized PLCL.**

### 4.1.16 Evaluation of mechanical properties of the synthesized PLCL by UTM

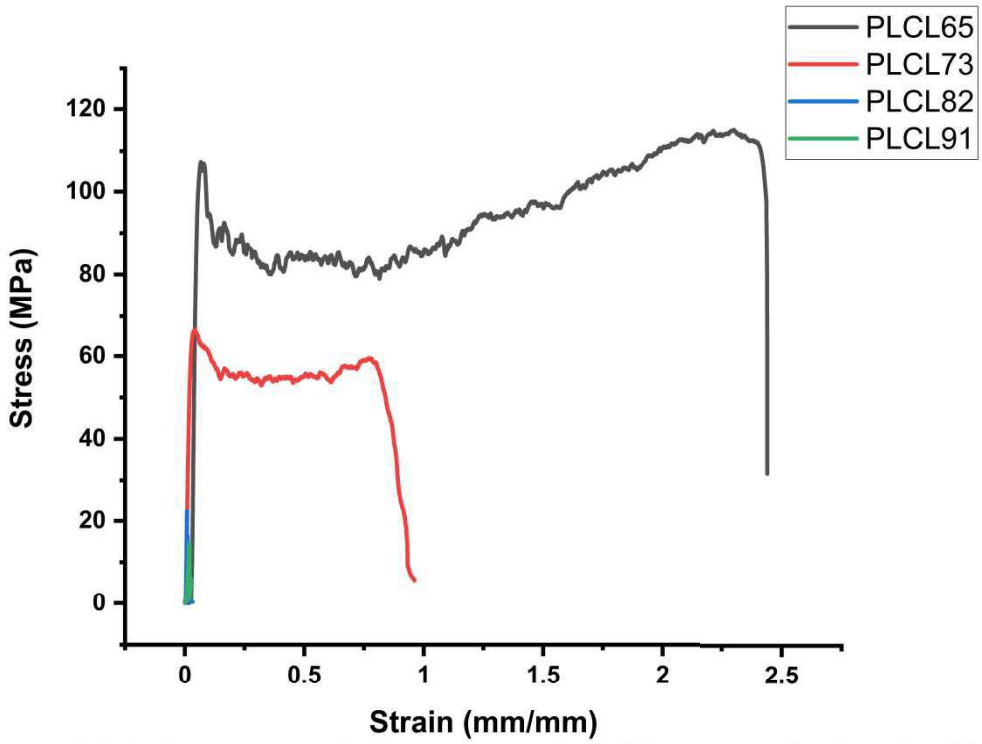


**Figure 4.17. The stress-strain curves of four different ratios of PLCL.**

The mechanical properties of the synthesized PLCL were confirmed by mechanical testing using universal testing machine (UTM). The results showed the ratios with high caprolactone content is highly elastic in nature whereas the ratios with higher lactide content (PLCL82 & PLCL91) totally lacked the plastic region and were found to be brittle (Fig. 4.17). The tensile test clearly demonstrates the ability of the PLCL65 and PLCL73 ratios to withstand high strain. The ratios PLCL65 and PLCL73 showed an elongation at break of 200±9% and 99±2% respectively, whereas higher lactide containing ratios PLCL82 and PLCL91 break at 7±0.2% and 5±0.9% respectively just after its yield point. The tensile strength showed a decreasing trend with increasing the lactide content. The tensile strength of PLCL65 and PLCL73 were 112.5±7 MPa and 63.4±3 MPa respectively, whereas the PLCL82 and PLCL91 showed a tensile strength of 18.7±3 and 15.6±2 respectively. Out of the four ratios, PLCL65 and PLCL73 were found to be elastic and are expected to be suitable for our application (Fig. 4.18).

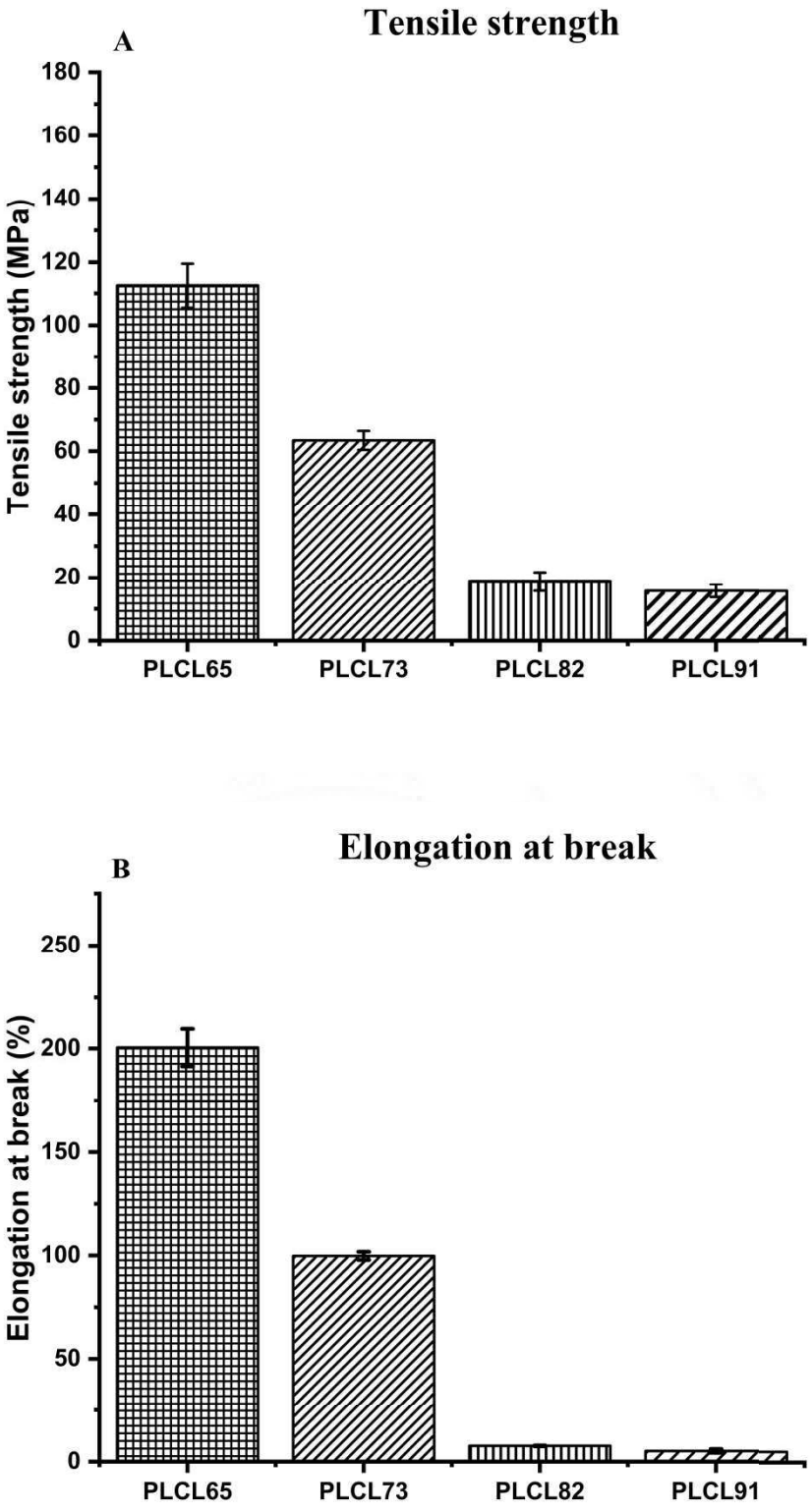


**Figure 4.18. (A) Tensile strength of all four ratios of the PLCL. (B) Showing percentage of elongation of all the four ratios of PLCL.**

### 4.1.17 Water contact angle of the PLCL shows increase in hydrophilicity with corresponding increase in lactide content

Since there are more hydroxyl groups in lactide than the caprolactone the copolymers with more lactide groups are expected to be more hydrophilic than the copolymers of lower lactide ratio. This is confirmed by water contact angle measurement of the copolymer films. The copolymer PLCL65 showed a water contact angle of 98.1°, PLCL73 showed a contact angle of 89.1°, PLCL82 showed a contact angle of 78.3° and PLCL91 showed a contact angle of 75.6° (Fig. 4.19).

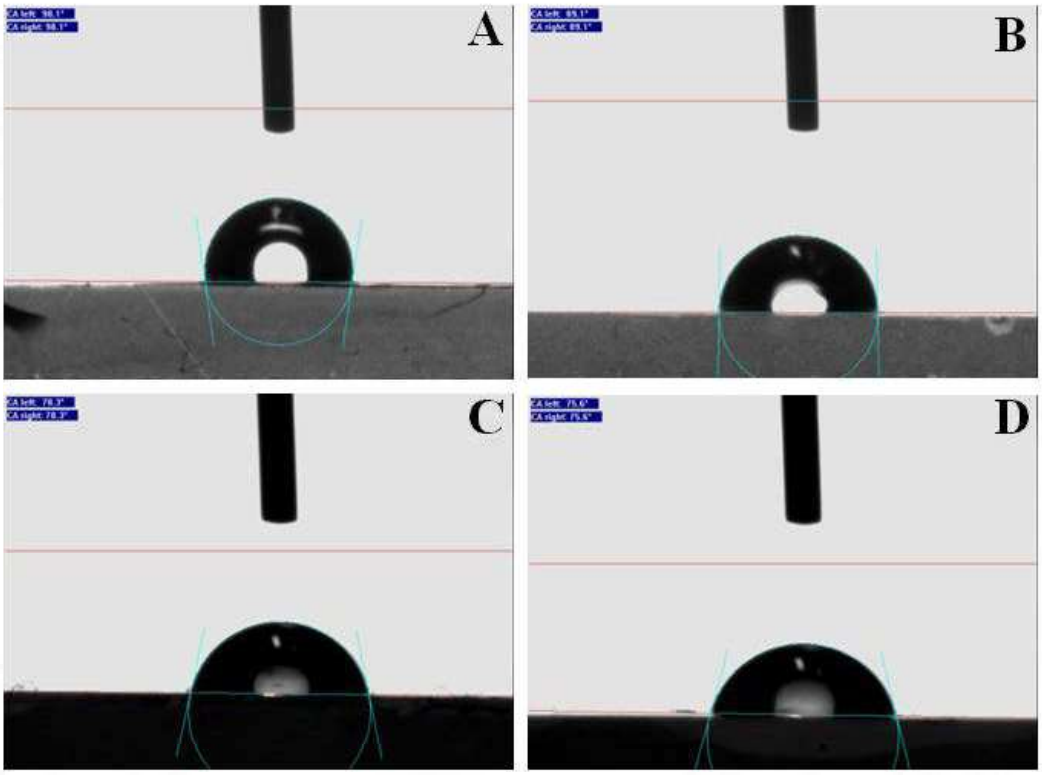


**Figure 4.19. Water contact angle showing the hydrophilicity of the synthesized copolymer (A) PLCL65, (B) PLCL73, (C) PLCL82, (D) PLCL91.**

**Table 6. Water contact angle values of PLCL**

| Sample | Contact angle |
|---|---|
| **PLCL65** | 98±4° |
| **PLCL73** | 89±3° |
| **PLCL82** | 78±6° |
| **PLCL91** | 75±4° |

**Table 7. Summary of physicochemical characterization of PLCL**

| Sample | Feed mol. ratio | | Copolymer composition | | Tm (°C) | Tg (°C) | Xc (%) | Tensile Strength (MPa) | Elongation at break (%) | M.W (g/mol) |
|---|---|---|---|---|---|---|---|---|---|---|
| | % LA | % CL | % LA | % CL | | | | | | |
| **PLCL 91** | 90 | 10 | 89 | 11 | 154.8 | 46 | 52.06 | 15.6±2 | 5.15±0.9 | 158329 |
| **PLCL 82** | 80 | 20 | 76.1 | 23.9 | 123.4 | 46 | 51.3 | 18.7±3 | 7.6±0.2 | 96022 |
| **PLCL 73** | 70 | 30 | 67 | 33 | 142.5 | 18 | 39.28 | 63.4±3 | 99.8±2 | 80835 |
| **PLCL 65** | 65 | 35 | 47.8 | 52.2 | 155.2 | 18 | 20.4 | 112.5±7 | 200.47±9 | 34335 |

### 4.1.18 Evaluation of cytotoxicity by live /dead staining

Live/dead staining was used to evaluate the proportion of live and dead cells on the PLCL L929 cells. As shown in the Fig. 4.20, all the four ratios of PLCL showed no or negligible dead cells after culturing up to two days. The live cells stained with calcein appeared green and the dead cells stained with ethidium bromide (Etbr) appeared red. The ratios with higher caprolactone content PLCL65 and PLCL73 were hydrophobic in nature and the cells appeared in spherical morphology. Whereas the ratios PLCL82 and PLCL91 where less hydrophobic and the cells cultured on it had more fibroblastic morphology.

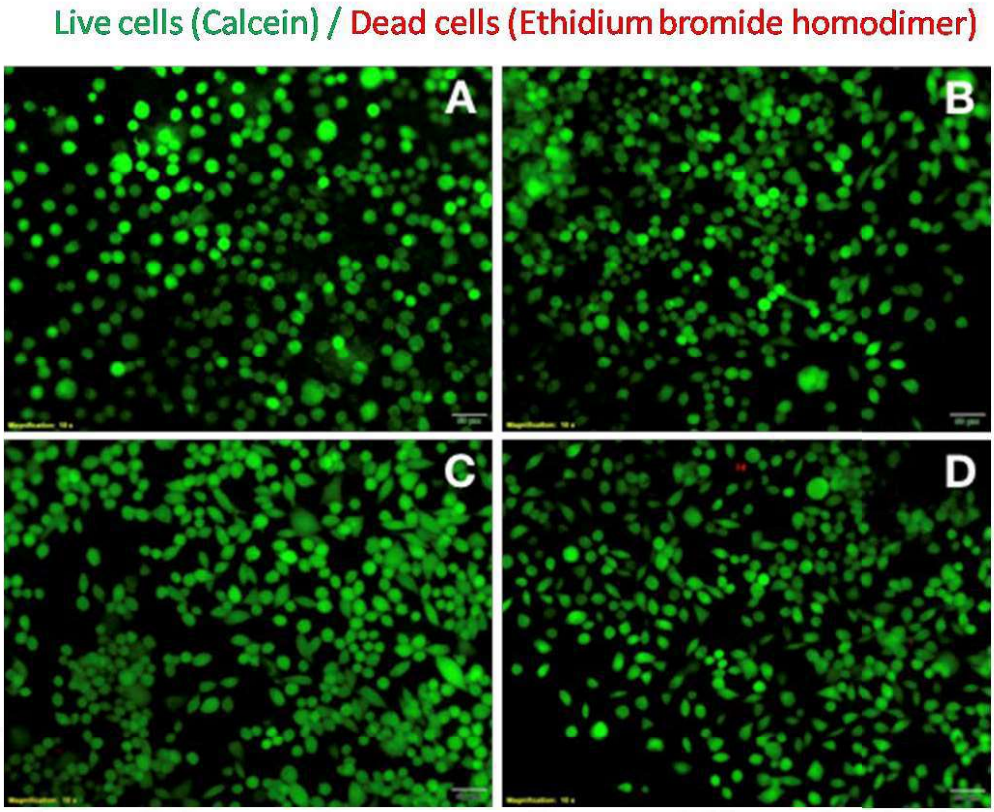


**Figure 4.20. Live/dead staining of L929 cells on (A) PLCL65, (B) PLCL73, (C) PLCL82, (D) PLCL91 showed cells are viable on the material.**

### 4.1.19 Evaluation of cytotoxicity by MTT assay and direct contact test

The proliferation of L929 cells on all the ratios of PLCL material extract samples collected after two weeks of incubation was evaluated by MTT assay and was compared with the cells cultured on the tissue culture dish. Fig. 4.21 shows the viability of the L929 cells were comparable to that of the tissue culture dish. The percentage cell viability of PLCL91, PLCL82, PLCL73 and PLCL65 of day one extract were 93±7%, 97±4%, 93±3%, 92± 5% respectively and that of seven days were 89±5%, 94±4%, 90±3%, 84±3%. The fourteen days extract showed more than 80% viability for all the groups compared to the tissue culture plates. And showed no significant difference ($p>0.05$). Evaluation of cytotoxicity by direct contact test also showed no change in the cell morphology compared to the negative control (Fig.4.22). Hence, the *in vitro* cytotoxic studies showed that all the ratios of PLCL do not have any cytotoxic effects and are capable of supporting the growth of the cells.

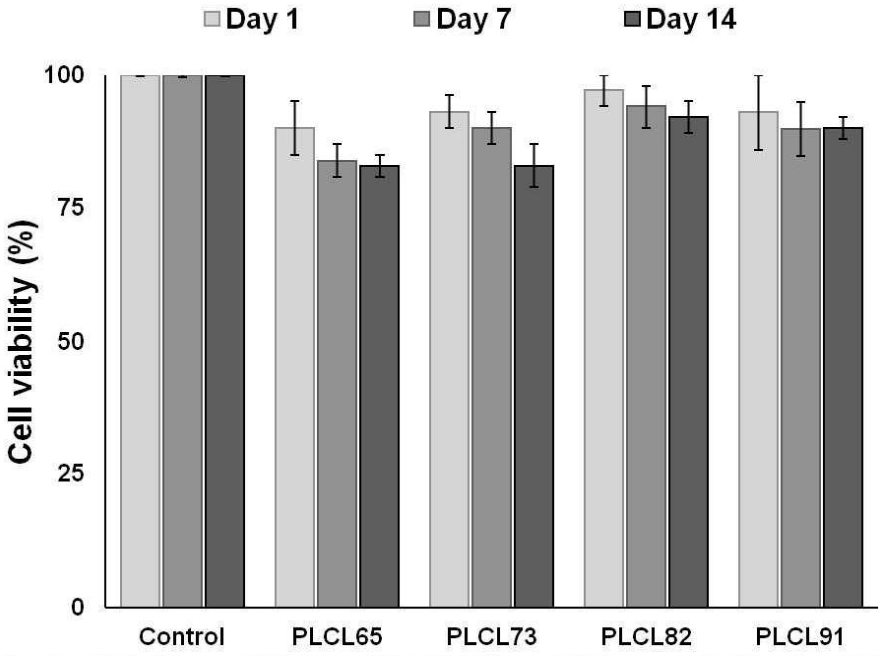


**Figure 4.21. MTT assay of the four different ratios of PLCL extract showed comparable cell viability as that of the tissue culture flask ($p>0.05$).**

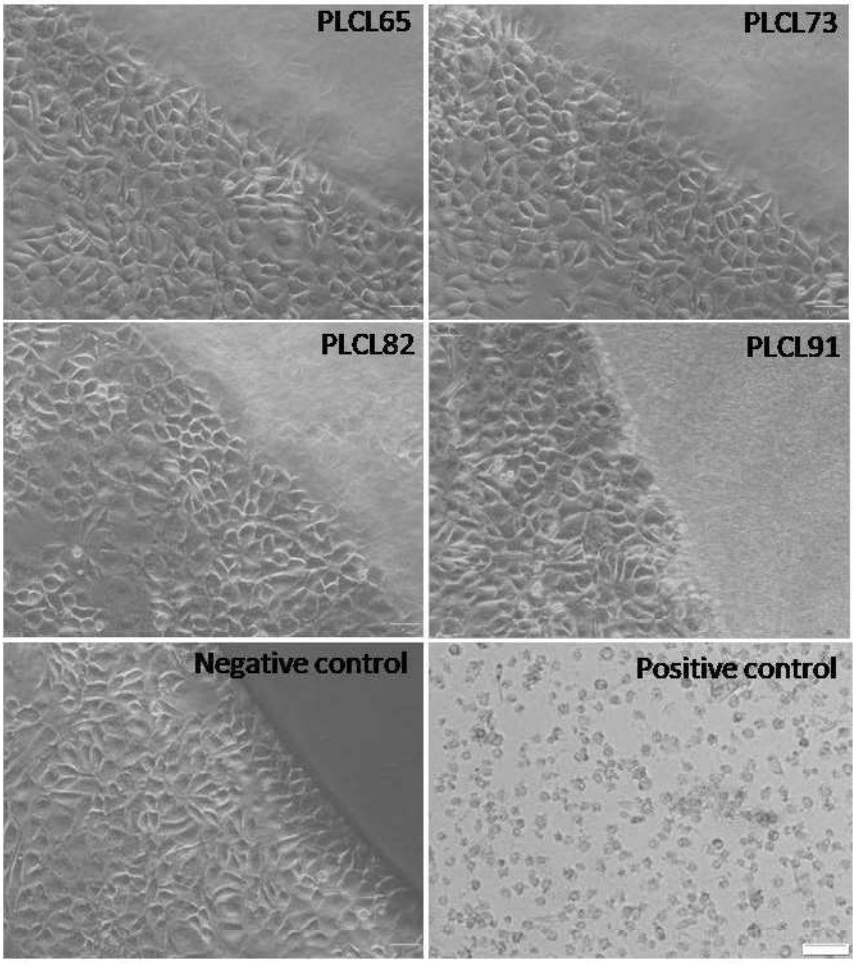


**Figure 4.22. Direct contact test showing no change in cell morphology compared to the negative control.**

### 4.2.1 Fabrication of synthesized PUU into an electrospun tracheal scaffold

Electrospinning has been used for the fabrication of fibrous scaffold for several decades. The fibrous morphology and the interconnected pores of the electrospun scaffold resemble the native extracellular matrix (ECM) and facilitate the regeneration process. A tubular nanofibrous tracheal scaffold was fabricated by electrospinning and alternate 'C' shaped rings were made using PCL over the electrospun tubular structure. Ten percent of PUU solution in chloroform/methanol (7:3) was electrospun into a rotating mandrel having 6 mm diameter.

Since the airway has to withstand constant pressure variations, 'C' shaped rings are made by solvent evaporation using 30% PCL solution in chloroform. The 'C' shaped PCL rings act as a substitute for the cartilage rings and hence prevent the electrospun tubular structure from collapsing. Table-8 describes the parameters followed for the electrospinning of the material. PUU solution of concentration 10% was taken in a 15 ml syringe having a 21 gauge nozzle and loaded on to the pump. The electrospinning was carried out at a flow rate of 1 ml/hr; a rotating mandrel having a diameter of the native rabbit trachea was used as the collector. The incoming nanofibers were collected onto the collector placed at a distance 12 cm away from the nozzle tip, rotating at a speed of 1000 rpm. The fibers start forming at 10 kV and a stable taylor cone was observed at 15 kV, hence the electrospinning was done at 15 kV.

The electrospinning was continued for 2 hrs to get a tubular scaffold of 0.4 mm thickness. In order to make the 'C' shaped rings, 30% PCL solution in chloroform were manually extruded over the electrospun tube into a 'C' shaped ring leaving a gap in the dorsal side. The rings are placed alternatively leaving a 3 mm gap between two rings. The 'C' shaped ring is attached to the electrospun tube by means of solvent welding. Since the PCL solution is highly concentrated, the chloroform did not incite any visible damage to the electrospun tube, as evidenced by the SEM images (Fig.4.25C).

Fig. 4.23 shows the animated image of the electrospun scaffold having 'C' shaped rings, the structure was fabricated by electrospinning and solvent

evaporation method, photographic images of which are shown in Fig. 4.23. It clearly shows the electrospun tubular scaffold having alternatively arranged 'C' shaped PCL rings.

**Figure 4.23. Animated design of electrospun tubular scaffold with alternate 'C' rings.**

**Table 8. Electrospinning conditions of PUU**

| Solution | Collector used | Flow rate | Tip to collector distance (cm) | Voltage (kV) |
|---|---|---|---|---|
| Solvent- Chloroform:methanol 7 : 3 10% PUU- 73000 M.W | 6 mm dia. Rotating mandrel | 1 ml/hr | 18 | 15 |

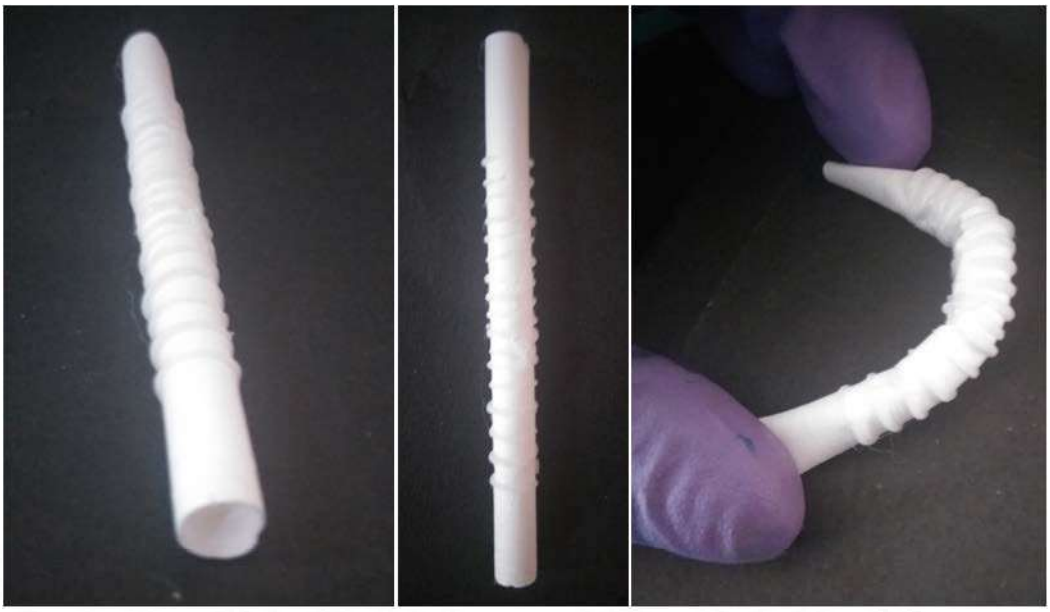

**Figure 4.24. Showing electrospun PUU scaffold with solvent casted 'C' shaped PCL rings.**

## 4.2.2 SEM analysis of electrospun PUU scaffold

The synthesized PUU were fabricated into a tubular scaffold by electrospinning. The nanofibrous morphology of the PUU is observed by SEM analysis (Fig. 4.25A). The electrospun fibers were deposited in a random orientation without any visible beads. The fibers had a diameter of 0.468±0.357 μm and inter-fiber distance of 11.60±7 μm. (Fig. 4.25B) The cross section of the 'C' ring showed the ring is adhered well on to the tubular part and the ring is complete with a gap connected by the fibrous part. A zoomed image of the interface between the solvent casted 'C' ring and the fibrous layer showed no visible damage to the fibrous layer (Fig.4.25C).

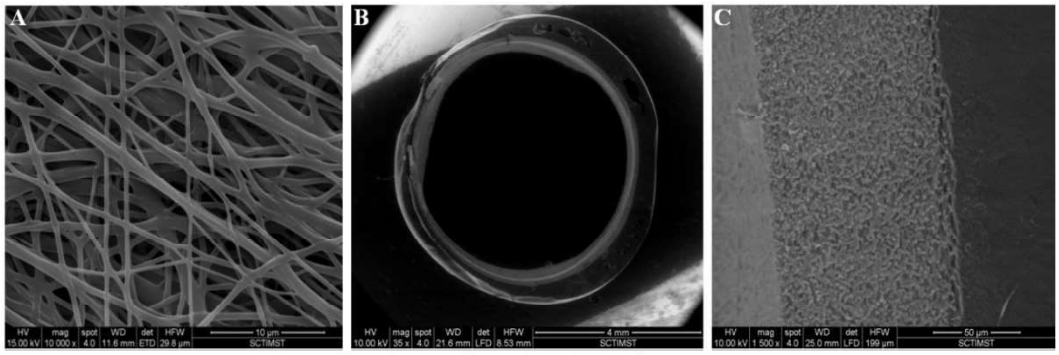


**Figure 4.25. (A) SEM images of electrospun PUU scaffold showing fibrous morphology. Distribution of fibre diameter ranges from 0.468±0.357 µm. Distribution of pore size ranges from 11.60±7 µm. (B) Cross section of the solid PCL ring over fibrous PUU tube. (C) Interface between the solvent casted PCL rings over the electrospun tube showing intact structure.**

### 4.2.3 Evaluation of cell penetration on the electrospun PUU scaffold by confocal microscopy

Fig.4.26 shows confocal images of chondrocytes seeded on the electrospun PUU scaffold and cultured for 3 days. The images clearly show there is a lack of cell penetration in the scaffold, due to the highly dense fibers. The cells were found to penetrate only up to 30 µm depth.

The electrospun scaffolds have a close resemblance to the extracellular matrix due to its nanofibrous morphology. This porous morphology helps in diffusion of nutrients and other metabolites essential for the proper functioning of the cells. The nanofibrous morphology mimics the fibrous morphology of the collagen and helps in better cell adhesion. However, the conventional process of electrospinning produces densely packed fibrous structures with very less interfiber distance, moreover while seeding the cells on the scaffold, the hydrophobicity of the material makes the penetration of the cells through the interfiber space difficult. Hence, cells seeded on such scaffold system experience a 2D pattern of cell growth with minimal cell penetration rather than a 3D cell organization. This poor cell infiltration into the scaffold continues to be a major drawback of the electrospun scaffold system. Cell penetration is essential for the

development of a functional 3D culture system which will eventually promote tissue regeneration. There are many advanced techniques being developed that can facilitate better 3D cell distribution.

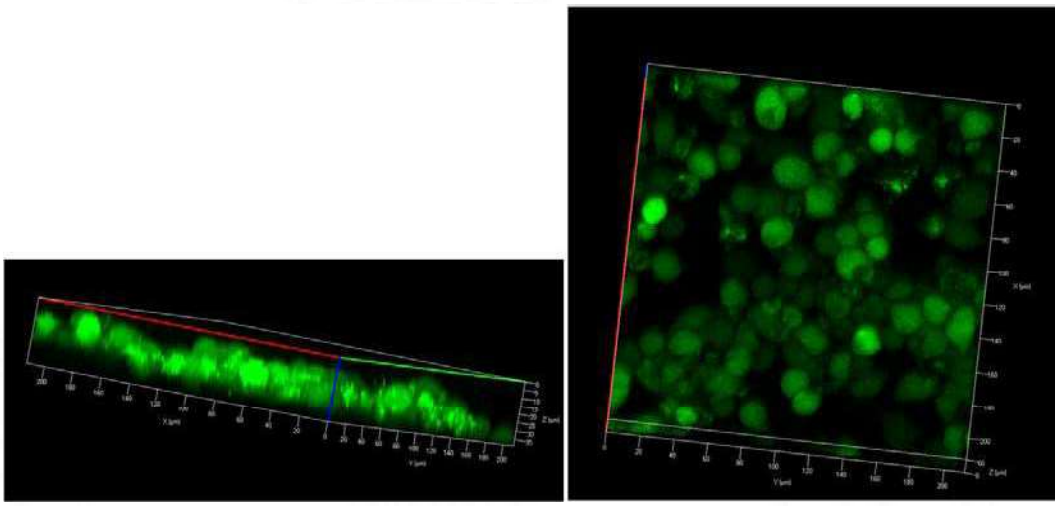

**Figure 4.26. Confocal images of chondrocytes seeded on PUU electrospun scaffold showing cell penetration only upto 30 µm depth.**

### 4.2.4 Fabrication of synthesized PLCL into an electrospun tracheal scaffold

The synthesized PLCL was fabricated into electrospun tubular scaffold and alternate 'C' shaped rings were made using 30% PCL as per the previously described design (Fig. 4.23). All the four ratios of the PLCL were tested for its feasibility to electrospin. The electrospinning was carried out using 20% PLCL prepared in chloroform:methanol mixture at 15 kV voltage and 1hr/ml flow rate (Table-9). Even though all the four ratios of the synthesized PLCL were able to electrospin, the higher ratios PLCL91 and PLCL82 produced fibers of diameter ranging 0.26±0.24 µm and 0.28±0.22 µm respectively, but the structures were brittle as seen in the mechanical test results. The lower ratios PLCL73 and PLCL65 were found to be elastic in nature corroborating the mechanical test results. Both of these ratios were forming fibers during the electrospinning process. However, on SEM analysis the fibers were found to be fused and had lost its fibrous morphology (Fig. 4.28C& D). Since only the brittle ratios of the

PLCL formed proper fibrous morphology, for the tracheal tissue engineering application electrospun PUU which is elastomeric and electrospinnable is a better candidate.

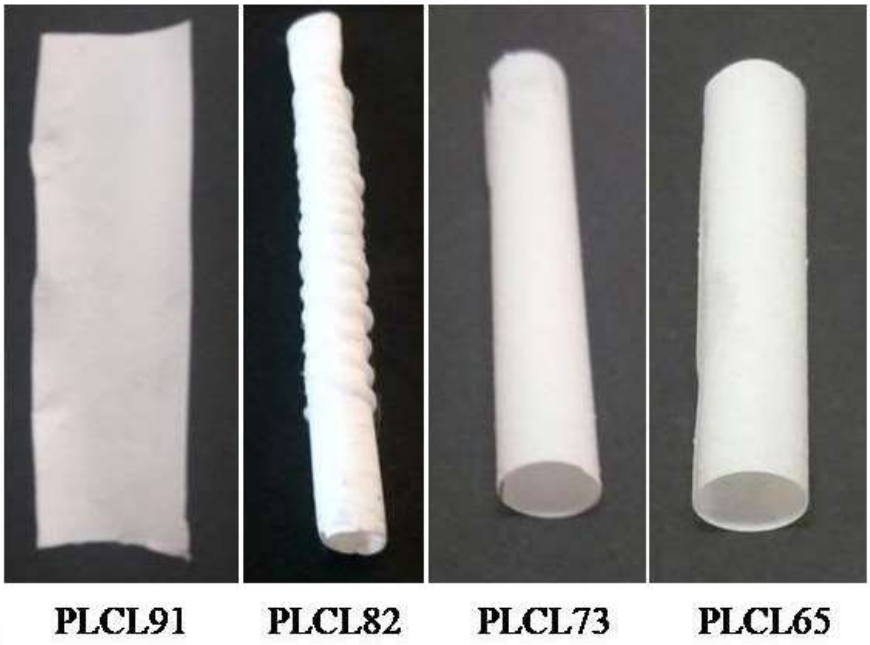


**Figure 4.27. Showing the electrospun PLCL scaffolds of all the four ratios.**

**Table 9. Electrospinning conditions of PLCL**

| **Solution** | **Collector used** | **Flow rate (ml/hr)** | **Tip to collector distance (cm)** | **Voltage (kV)** |
|---|---|---|---|---|
| Solvent- Chloroform: methanol 70 : 30 20% PLCL-30000-150000 M.W | 6 mm dia. Rotating mandrel | 1 | 18 | 15 |

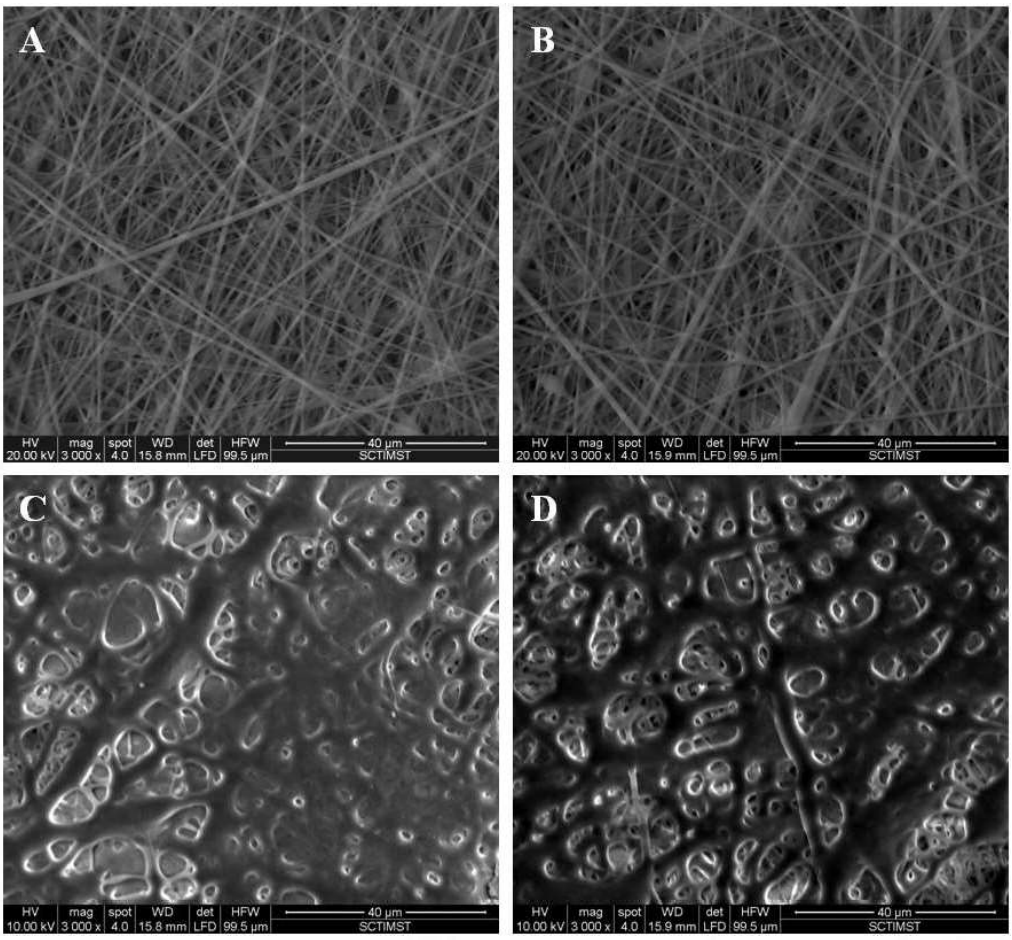


**Figure 4.28. SEM images of electrospun (A) PLCL91 and (B) PLCL82 scaffold showing fibrous morphology with an average fiber diameter of 0.26±0.24 µm and 0.28±0.22 µm respectively. (C&D) Fused fibers of PLCL65 and PLCL73 respectively.**

### 4.2.5 Evaluation of cell penetration on the electrospun PLCL82 scaffold by confocal microscopy

Since the PLCL91 was too brittle and PLCL73 and PLCL65 failed to form the fibrous morphology, among the four ratios PLCL82 was found to be suitable for the tracheal scaffold application. Hence, we decided to test the ability of cells to penetrate through the nanofibrous scaffold, so that it can form three dimensionally organized tissues. For this, chondrocytes were seeded on the electrospun PLCL65 scaffold and cultured for three days. (Fig.4.29) Confocal

images of the calcein/Etbr stained samples showed cell penetration only up to 30 µm same as that of the electrospun PUU scaffold.

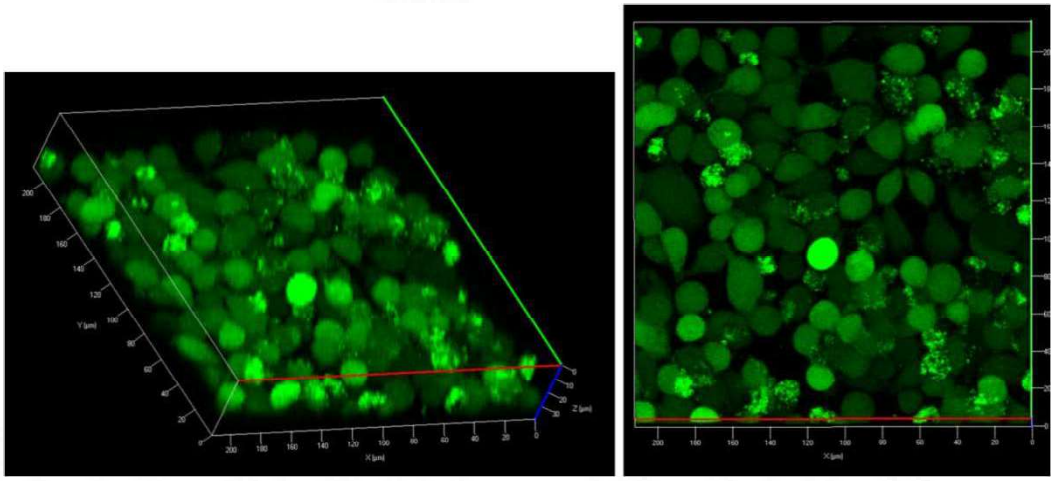

**Figure 4.29. Confocal images of chondrocytes seeded on PLCL82 electrospun scaffold showing cell penetration only upto 30 µm depth.**

### 4.2.6 Fabrication of 3D printed PLCL tubular scaffold

Since both the PUU and PLCL82 electrospun scaffolds had subtle cell penetration, the electrospun scaffold system cannot provide a 3D culture system. Hence other fabrication strategies were explored. Because of its ability to deposit the bioink and make structure as per the desired design in a very precise way, the feasibility of the synthesized biomaterials to 3D print was evaluated.

Our efforts to 3D PUU failed due to its high melting point and a degradation point immediately after the melting point (Fig. 4.6). Hence the synthesized PCL based polyurethane urea could be a potential material for the generation of electrospun elastomeric scaffold system. However, it cannot be used for applications involving melting of the material. Further, the ability of the PLCL system as a 3D printing material was evaluated.

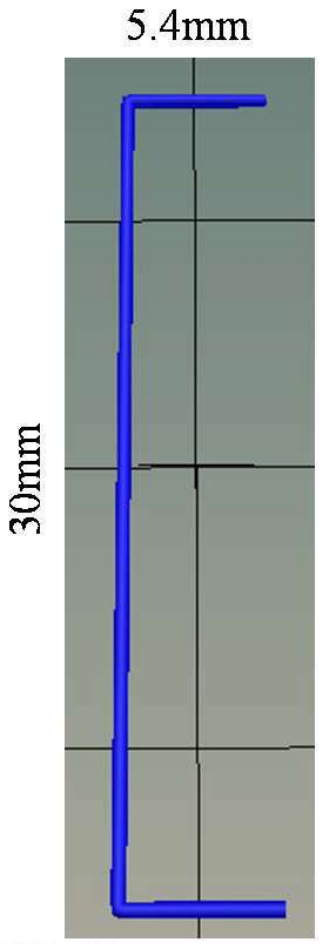


**Figure 4.30. CAD design of line for the standardization of 3D printing speed, pressure and temperature.**

### 4.2.7 Characterization of printability of PLCL65 and PLCL73

3D printing was introduced in the field of tissue engineering to fabricate scaffolds. Even though there are many materials like PCL, PLA etc. which have proven their 3D printability, a dual component material having caprolactone and L-lactide as monomers is expected to provide the desired mechanical properties and 3D printability required for the tracheal scaffold. The 3D printed PLCL may offer an efficient method to improve the elasticity of the PCL or PLA scaffolds, thus it may help to extend the role of polyester scaffolds in soft tissue engineering.

In order to standardize the 3D printing parameters of the synthesized PLCL, a line drawing method was used. The printing speed, pressure and temperature of the PLCL65 and PLCL73 ratios were standardized by this method. For this a line

was drawn using CAD software 123D having 30 mm length and 5.4 mm long side line at both the ends (Fig. 4.30). The design was then printed using the PLCL65 and PLCL73 ratios using a 20 gauge nozzle. The dimensions of the printed structure were compared with the design and were standardized for the best printing conditions.

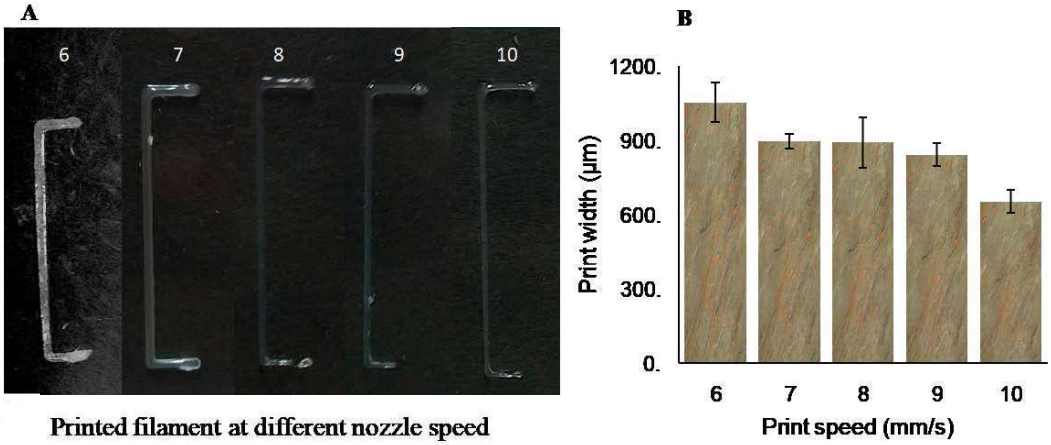


**Figure 4.31. (A) Shows the printed lines of PLCL65 at different speeds. (B) A speed of 9 mm/s gave similar width as that of the nozzle diameter.**

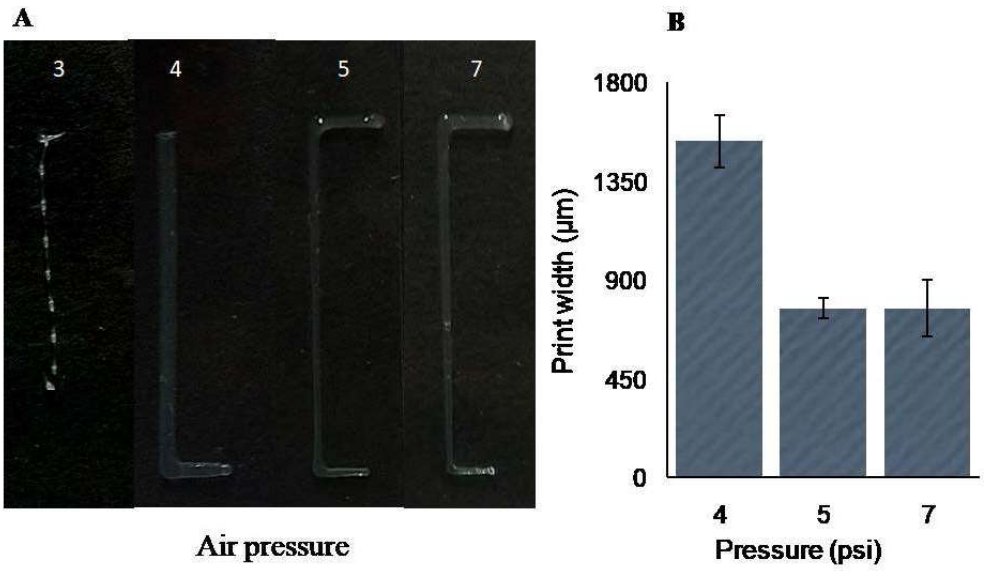


**Figure 4.32. (A) Shows the printed lines of PLCL65 at different pressure. (B) Air pressure of 5 psi gave similar width as that of the nozzle diameter.**

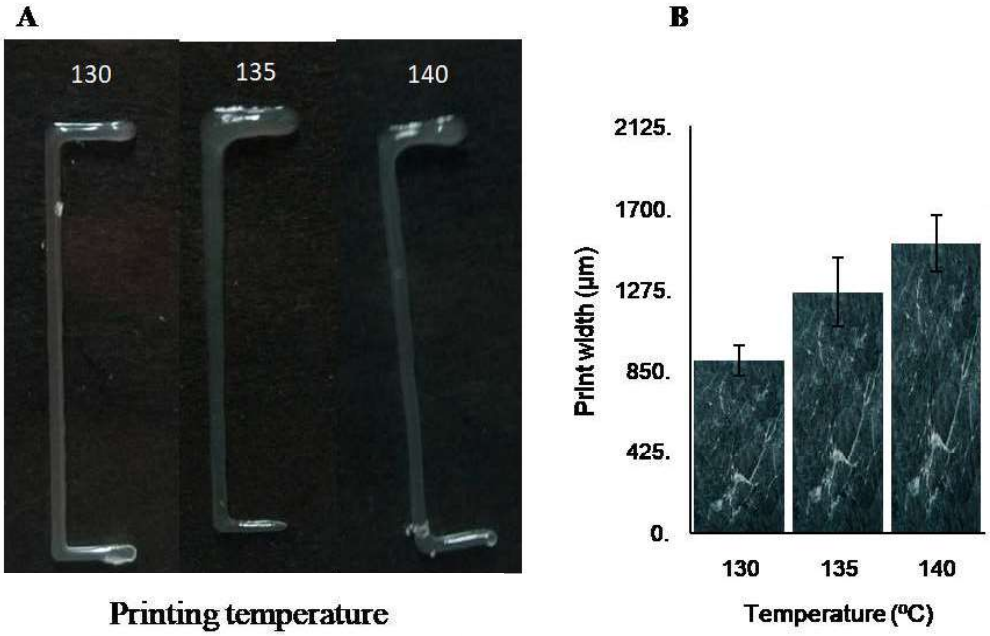


**Figure 4.33. (A) Shows the printed lines of PLCL65 at different temperature. (B) A temperature of 130° C gave similar width as that of the nozzle diameter.**

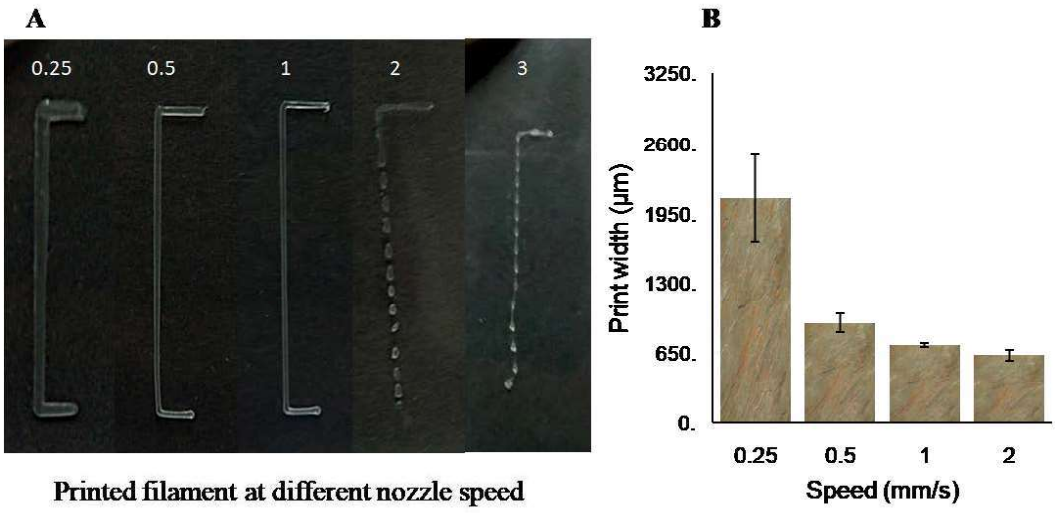


**Figure 4.34. (A) Shows the printed lines of PLCL73 at different speeds. (B) A speed of 0.5 mm/s gave similar width as that of the nozzle diameter.**

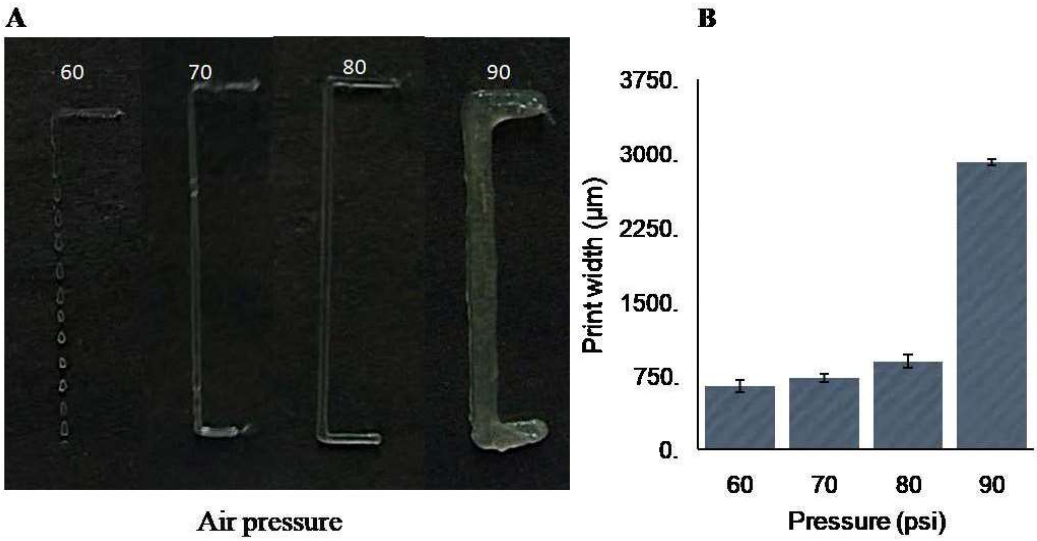


**Figure 4.35. (A) Shows the printed lines of PLCL73 at different pressure. (B) A pressure of 80 psi gave similar width as that of the nozzle diameter.**

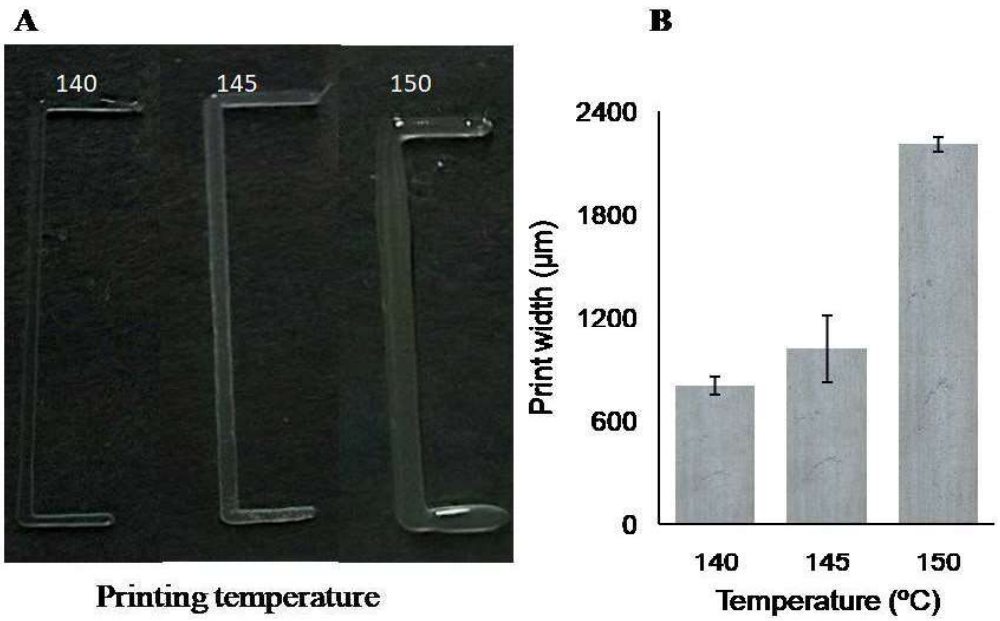


**Figure 4.36. (A) Shows the printed lines of PLCL73 at different temperature. (B) A temperature of 140° C gave similar width as that of the nozzle diameter.**

Since the PLCL65 has lower molecular weight and viscosity and melting point compared to the PLCL73, comparatively lower values of 5 psi and 130° C were observed for pressure and temperature respectively for printing PLCL65 (Fig. 4.32 & 4.33). Hence the printing of PLCL65 was done at a high speed of 9 mm/s to maintain the line width (Fig. 4.31). Whereas in PLCL73, the material has comparatively higher molecular weight, viscosity and melting point compared to its counterpart PLCL65. This difference was reflected in the printability and printing parameters of these two materials. A high pressure of 80 psi was observed for PLCL73 and a temperature of 140° C gave a line width similar to the nozzle diameter (Fig. 4.35& 4.36). Because of its high viscosity at 140° C temperature and 80 psi pressure, the rate of extrusion was very slow; hence it required a very slow speed of 0.5 mm/s in order to print a line of width similar to the nozzle diameter (Fig. 4.34).

### 4.2.8 Evaluation of Printability of PLCL

When the material being printed takes more time to solidify and has some fluidity, the printed structure would fuse at the cross site which makes the material not suitable for 3D printing. When a material that solidifies quickly after the extrusion is used for printing, it gives very precise grids with sharp edges and distinguished layers. And its dimensions and shapes will be very much similar to the given design. Here the printability of the PLCL65 and PLCL73 is evaluated by calculating the printability characteristic (Pr) using the equation (8). When the 3D printed material gives a Pr value within the range of 0.9-1.1, it indicates sound 3D printing capability of the material (Ouyang et al., 2016).

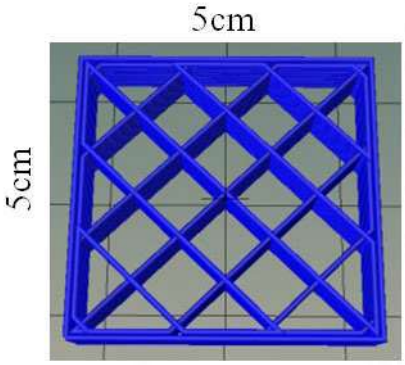


**Eq. 8,**

$$Pr = \frac{\pi}{4} \times \frac{1}{C} = \frac{L^2}{16A}$$

Pr- Printability
C- Circularity
L- Perimeter
A-Area

**Figure 4.37. Evaluation of 3D printability by grid method.**

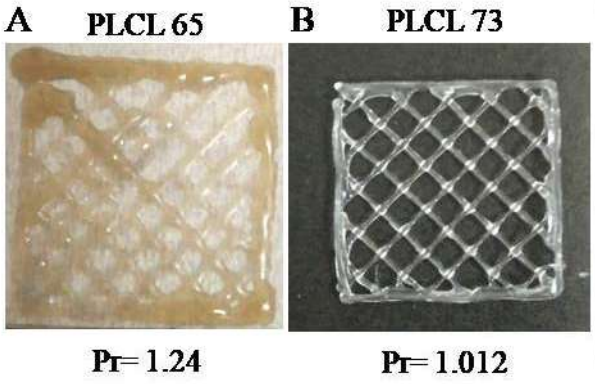


**Figure 4.38. (A) 3D printed grids using PLCL65. (B) 3D printed grids using PLCL73.**

When PLCL65 was used for 3D printing, due to its long curing time, it gave irregular structures. Fig. 4.38A shows irregular structures at certain regions and due to spreading of the polymer the grid area was less when compared to the PLCL73,this resulted in a high Pr value of 1.24 for PLCL65. Whereas PLCL73 has a short curing time compared to the PLCL65 and after extrusion it solidified quickly than the PLCL65.As a result, more precise and continuous structures were formed when compared to the PLCL65 (Fig. 38B). It gave a Pr value close to 1 which indicates its sound 3D printing capabilities.

### 4.2.9 Filament collapse test of PLCL65 and PLCL73

The bridging capability and shape fidelity is a very important factor to 3D printing complex and simple structures. The bridging capability and shape fidelity of the material can be measured by printing the material across gaps of increasing distances. A simple device was made for this and the bridging capability of both the PLCL65 and PLCL73 was measured by printing over the gap and measuring the area under the filament. Materials with high print fidelity would not deflect at the gap and form a straight line, whereas materials with low print fidelity are expected to sag across the gap and would give less area under the filament. When PLCL65 was used to print across the gaps of 5 mm, 10 mm, 15 mm and 20 mm distance, the filament started hanging from 10mm distance and it completely collapsed at 20 mm distance (Fig. 4.39A), whereas PLCL73 formed almost a straight line across all the distances and hence gave a higher collapse area factor compared to the PLCL65 (Fig.4.39B).

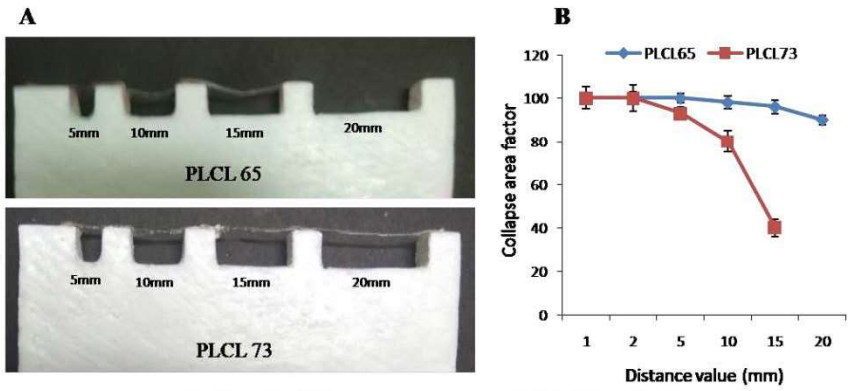


**Figure 4.39. (A) Showing filament collapse test of PLCL65 and PLCL73. (B) PLCL73 showed better stability and bridging capacity than PLCL65.**

### 4.2.10 Evaluation of Print fidelity of PLCL

Even though the print fidelity of a material can be measured by filament collapse test, it is further confirmed by printing a cylinder of 5 mm, the height of the cylinder was normalized with the original height of the design and its percentage is taken. PLCL65 had only 30% height of the original height whereas the PLCL73 showed 100% height which further confirms the previous results.

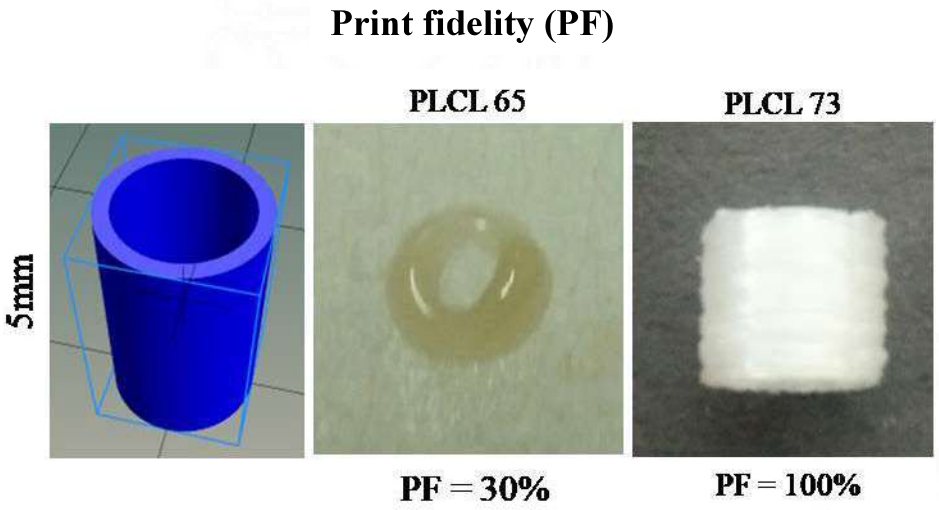


**Figure 4.40. Assessment of print fidelity of PLCL65 and PLCL73 by height maintenance method.**

### 4.2.11 3D printing of PLCL

Since PLCL65 was found to have less print fidelity (Fig.4.39 & 4.40) and higher Pr value (Fig.4.38), PLCL73 was selected for further 3D printing application. A cylinder of 35 mm height was designed (Fig.4.41A) and 3D printed as per the standardized printing parameters. A temperature of 140$^{o}$ C, pressure 80 psi and speed 0.5 mm/s was used for 3D printing. The structure was successfully 3D printed into a cylinder of 35 mm height (Fig.4.41B). However, due to lack of pores it is a completely impermeable structure with no cell penetration. Hence, to have three dimensionally organized cells and better nutrient diffusion a modified design with porous structure is required for further studies.


**Figure 4.41. (A) CAD image of cylindrical structure. (B) 3D printed PLCL73 cylinder.**

## 4.3 Biphasic design for better three-dimensional organization of cells

The biphasic system involves a double walled cylindrical lattice structure having alternate 'C' shaped solid rings along the length. The lattice structure forms its skeletal framework and is 3D printed using the elastomeric polymer. At both the ends of the scaffold, there are long solid rings for suturing the structure to the native tissue. (Fig. 4.42) The lattice structure is filled with the hydrogel mixed with cells which can regenerate the cartilage. The lattice framework imparts mechanical strength and the hydrogel helps in cell growth, making it an open system for free diffusion of the nutrients and other metabolites.

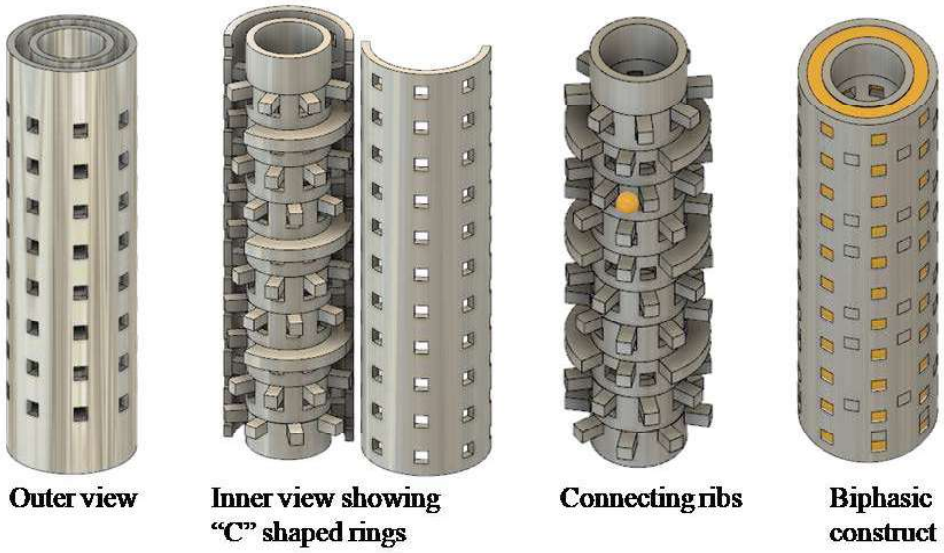


**Figure 4.42. Shows the lattice frame work and the biphasic structure of the design.**

**Table 10. Dimensions of biphasic design of tracheal scaffold**

| Components | Dimensions (mm) |
|---|---|
| Inner Dia. | 5 |
| Wall thickness | 0.6 |
| Hole size | 1 |
| Connecting ribs | 1 |

Fig.4.43A shows the 3D printed framework structure using PLCL73. The printing parameters used were the same as the values standardized by the line drawing method (Table-10). The dimensions of the printed structure were then measured and were found to be similar to the theoretical values. PCL being a commonly used material for 3D printing was taken as a positive control and the dimensions were compared to the 3D printed PLCL (Table-12). The theoretical values of the pore size, wall thickness and the gap distance were 1 mm, 0.8 mm and 1 mm respectively. The size of the pores printed using PLCL73 was 0.2 mm smaller compared to the theoretical pore size of the design. Whereas the pores of the PCL structure was only 0.1 mm smaller, the PCL produced structures with wall

thickness and gap distance exactly same as the theoretical value of 0.8 mm and 1 mm repectively. Whereas the PLCL produced 0.1 mm thicker walls and 0.24 mm smaller gaps. Even though the PCL produced more precise and accurate dimension values than the PLCL, both the materials could not produce the exact dimensions of the design. The slight variation in the accuracy and the precision of the PLCL and PCL can be improved by using advanced 3D printing nozzles.

**Figure 4.43. 3D printed PLCL73.**

**Table 11. 3D printing parameters of PLCL**

| PLCL | Printing parameters |
|---|---|
| **Print speed** | 5 mm/s |
| **Layer height** | 0.8 mm |
| **Temperature** | 140$^{o}$ C |
| **Pressure** | 80 psi |

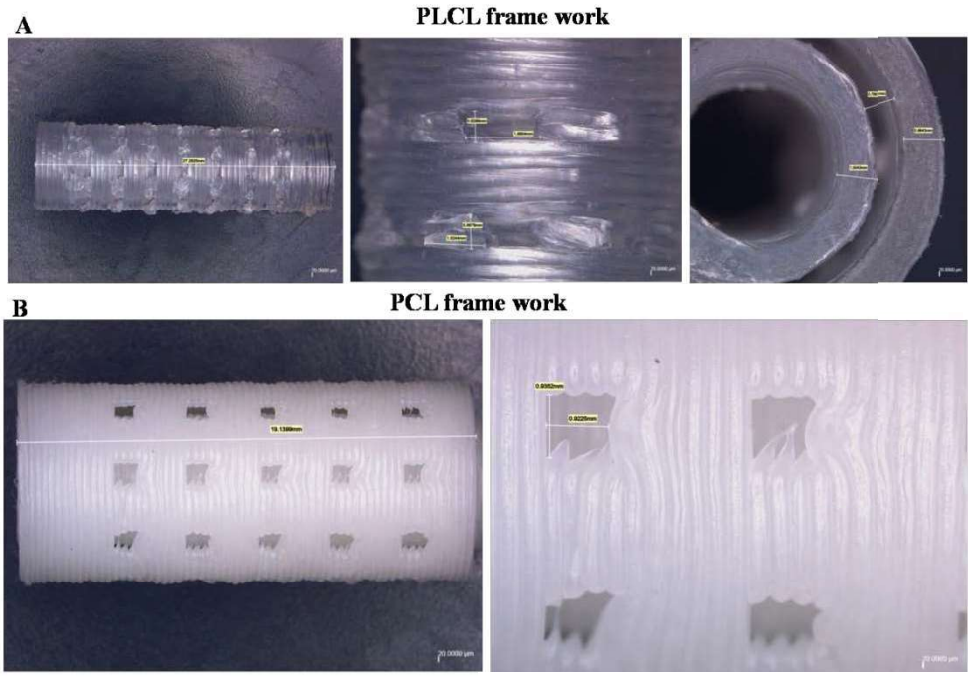


**Figure 4.44. 3D printed (A) PLCL73 and (B) PCL structures.**

**Table 12. Dimensions of 3D printed PCL and PLCL structures**

| Features | Theoretical value (mm) | PLCL (mm) | PCL (mm) |
|---|---|---|---|
| **Pore size** | 1 | 0.8 | 0.9 |
| **Wall thickness** | 0.8 | 0.9 | 0.8 |
| **Gap distance** | 1 | 0.76 | 1 |

### 4.3.2 Preparation of chitosan-hyaluronic acid dialdehyde hydrogel system for 3D printing biphasic construct

The interaction between cells and the extracellular matrix plays a very important role in the cell response and its regenerative capability. It has been noticed in many studies, culturing of cells on 2D culture wares changes the cell response and leads to loss of many desirable characteristics and functionalities of the cells. This is mainly due to the stiffness and absence of signaling molecules and growth factors present in the native system.

Recently the scientific efforts have been focused on generation of 3D printable hydrogel systems for therapeutic purposes which can be used for making organ

substitutes, drug testing and other studies. There is a huge requirement of such hydrogel systems for the 3D printing industry. The chondrocytes are resuspended in the hydrogel and 3D printed as per the designed model. The hydrogel apart from playing the role of a carrier for delivery of the cells also plays the role of extracellular matrix, and hence it is important to consider the physical characteristics of the hydrogel and design it similar to the native cartilage ECM.

To evaluate the effect of the hydrogel stiffness on the cell response we prepared chitosan-HDA hydrogel in three different compositions (Table-11). The reaction involves formation of Schiff's base linkage between the aldehyde groups of the hyaluronic acid dialdehyde and amino groups of the chitosan (Fig.4.45). The formation of Schiff's base linkage between the amino group and the aldehyde group was confirmed by the FTIR-ATR. The presence of peak at 1630 $cm^{-1}$ corresponds to CN bond of Schiff's base linkage and the peak at 1365 $cm^{-1}$ corresponds to the CN stretching of the Schiff's base linkage. The presence of NH peak at 3286 $cm^{-1}$, CH stretch at 2920 $cm^{-1}$ and NH bending at 1555 $cm^{-1}$ has confirmed the reaction. The degree of cross linking varied with different crosslinker ratio, this change in the crosslinking pattern was also evident in the FTIR. The intensity of the NH peak decreased and the peak at 1630 $cm^{-1}$ which corresponds to CN bond showed increase in its intensity with increase in the crosslinker amount (Fig. 4.46).

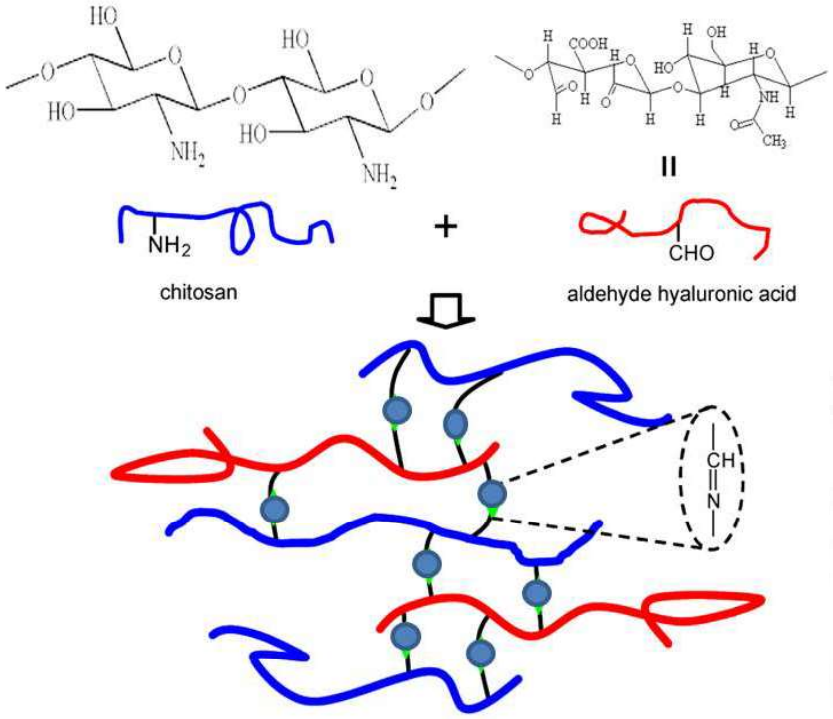


**Figure 4.45. Schiff's base linkages are formed between free amino groups of the chitosan and the aldehyde groups of the HDA leading to the crosslinked structure.**

**Table 13. Compositions of CH-HDA hydrogel**

| Compositions used | | | |
|---|---|---|---|
| **Sample** | **Composition** | **Chitosan (µl)** | **HDA (µl)** |
| **A** | 10:1 CH-HDA | 10 | 1 |
| **B** | 10:3 CH-HDA | 10 | 3 |
| **C** | 10:5 CH-HDA | 10 | 5 |

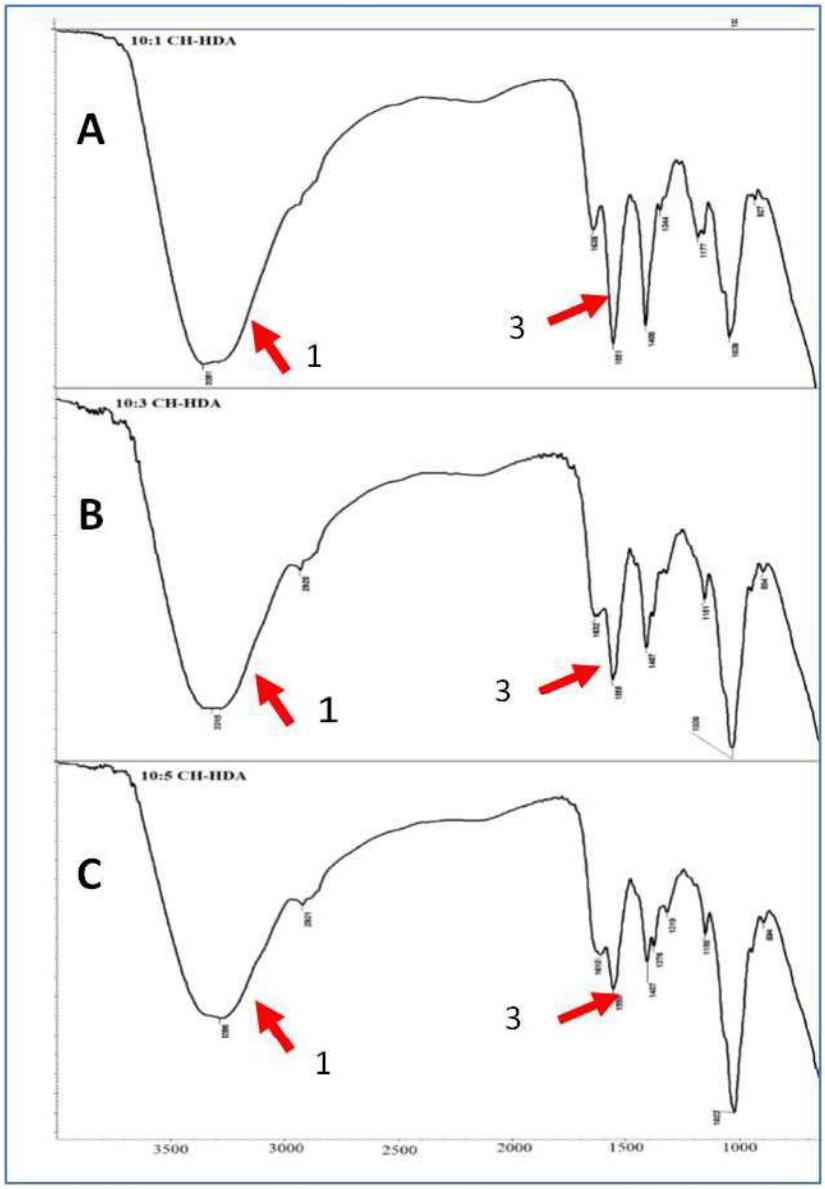


**Figure 4.46. FTIR plot of three gel formulations of chitosan-HDA (A) 10:1CH-HDA, (B) 10:3 CH-HDA and (C) 10:5 CH-HDA.**

**Table 14. FTIR peaks of CH-HDA hydrogel**

| Peak label | Peak assignment | Peak ($cm^{-1}$) |
|---|---|---|
| **1** | N-H stretch | 3286 |
| **2** | C-H stretch | 2921 |
| **3** | N-H bending | 1555 |
| **4** | C-N stretch | 1365 |

Hydrogel of varying stiffness was developed to test its effect on the chondrocyte response. The stiffness of the hydrogel was varied by varying the crosslinking density. The percentage degree of crosslinking of hydrogel with varying the crosslinker ratio was determined by estimation of the amount of free amine groups in the hydrogel after the gelling reaction. As the amino group takes part the Schiff's base linkage with the aldehyde group present in the HDA, increase in the amount of HDA allows more aldehyde groups to react with the amino groups, hence the amount of free amino group decreases with the increase in the amount of HDA. The free amino group after the gelling reaction was measured by ninhydrin assay. It was found that the percentage degree of crosslinking of 10:1 CH-HDA gel is 79.35±1.82 % and it increased to 88.50±2.12 % for CH-HDA of 10:5 ratio (Fig.4.46).

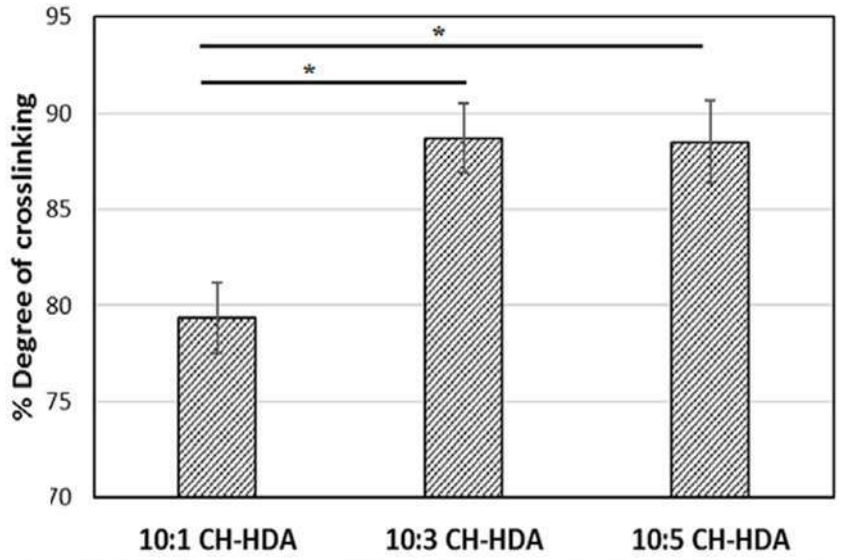


**Figure 4.47. Degree of cross linking of CH-HDA hydrogel increased with increase in HDA ratio.**

The results showed there is no significant difference between the 10:3 and 10:5 ratios of the CH-HDA hydrogel. But there was a significant difference in the percentage crosslinking degree between the 10:1 and the stiffer ratios 10:3 and 10:5 of the CH-HDA hydrogel. This pattern was also followed in the percentage gel fraction results of the hydrogel. The percentage gel fraction of the 10:5 and 10:3 ratios of the hydrogel showed significant difference as that of the 10:1 ratio. The percentage gel fraction of the 10:1 ratio was 31.13±2.28% and as the crosslinker ratio increased to 10:3 and 10:5, the percentage gel fraction ratio also increased to 39.42±2.21% and 41.33±1.62% respectively. When the percentage gel fraction of the two higher crosslinker ratio 10:3 and 10:5 is compared there was no significant difference.

When it comes to 3D printable hydrogel gel systems, the gelling time plays a major role in delivering the gel *in vivo*. The gelling time of this system changed with changing the crosslinker ratio. It was observed that the CH-HDA gels of higher crosslinker ratio gelled fast compared to the gel of lower crosslinker ratio. The gelling time was measured by measuring the change in viscosity with time. The CH-HDA gel of 10:1 ratio showed a gelling time of 60±3 sec whereas, the higher crosslinker ratio of 10:3 and 10:5 gelled at a faster rate of 27±5 sec and

25±2 sec respectively (Fig. 4.49). The decrease in the degree of crosslinking of the 10:1 hydrogel compared to the higher crosslinker ratio is indicative of lesser crosslinked structures and hence larger pore size which is expected to favor easy diffusion of nutrients and other metabolites. The crosslinking density did not have any variation between the 10:3 and 10:5 ratios (Fig. 4.48). This is probably because the hydrogel has attained maximum crosslinking capacity and hence further increase in the crosslinker ratio does not bring any change.

It is important to study the swelling behavior of the hydrogel to understand the ability of the hydrogel to hold water and other nutrients. The swelling studies were carried out in PBS and as expected the results showed that the degree of swelling decreased with increase in the crosslinker ratio. As the ratio of the crosslinker increases there will be more crosslinked structures which restrict the swelling of the hydrogel (Fig. 4.49).

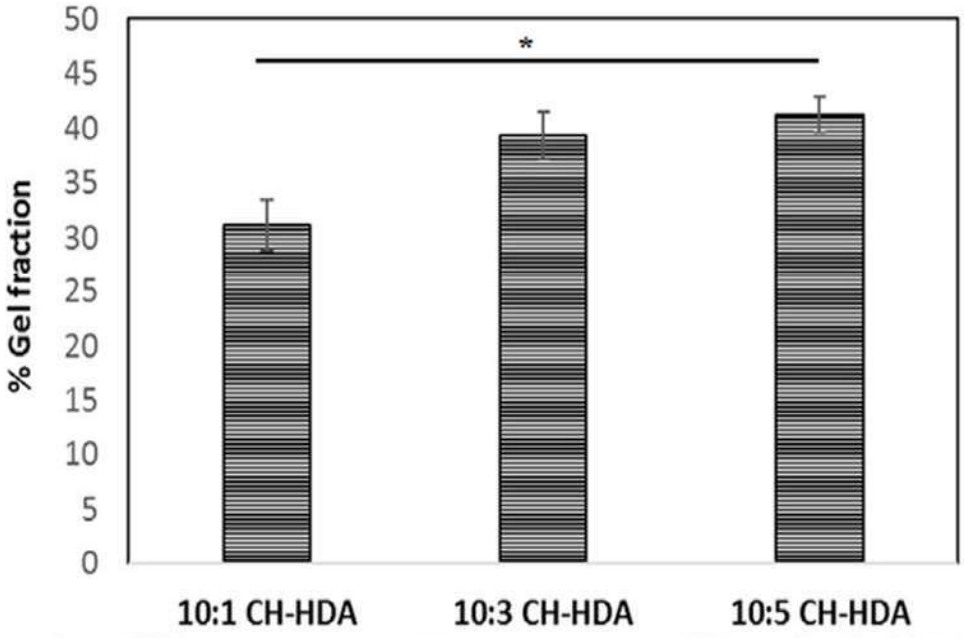


**Figure 4.48. Percentage gel fraction of the crosslinked CH-HDA gel. Data were presented as mean ± standard deviation (SD) (n = 3) (* p< 0.05).**

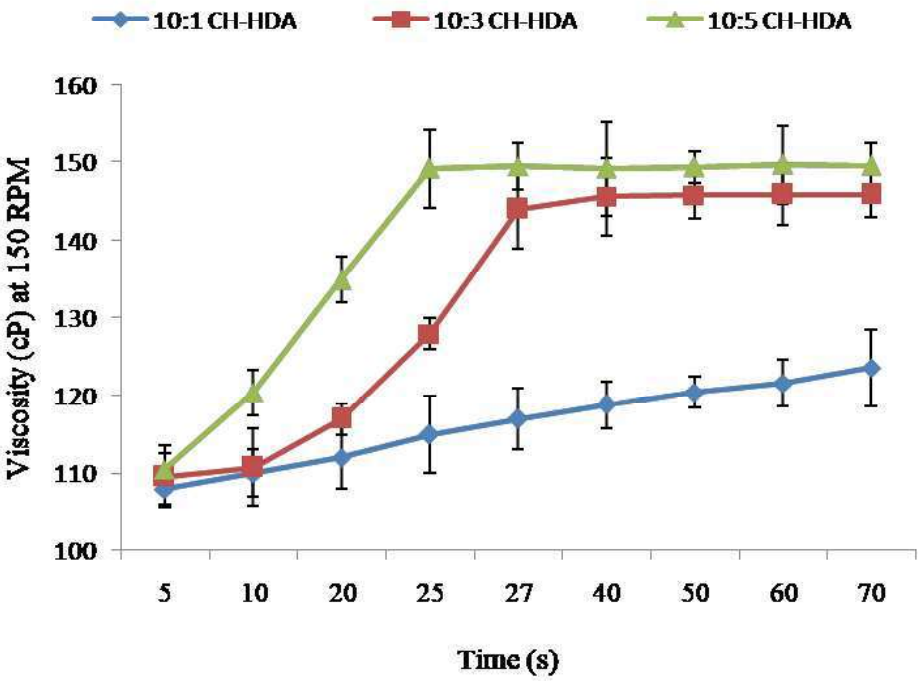


**Figure 4.49. Gelling time of all three compositions of CH-HDA hydrogel by viscosity measurement. Data were presented as mean ± standard deviation (SD)(n = 3) (* p < 0.05).**

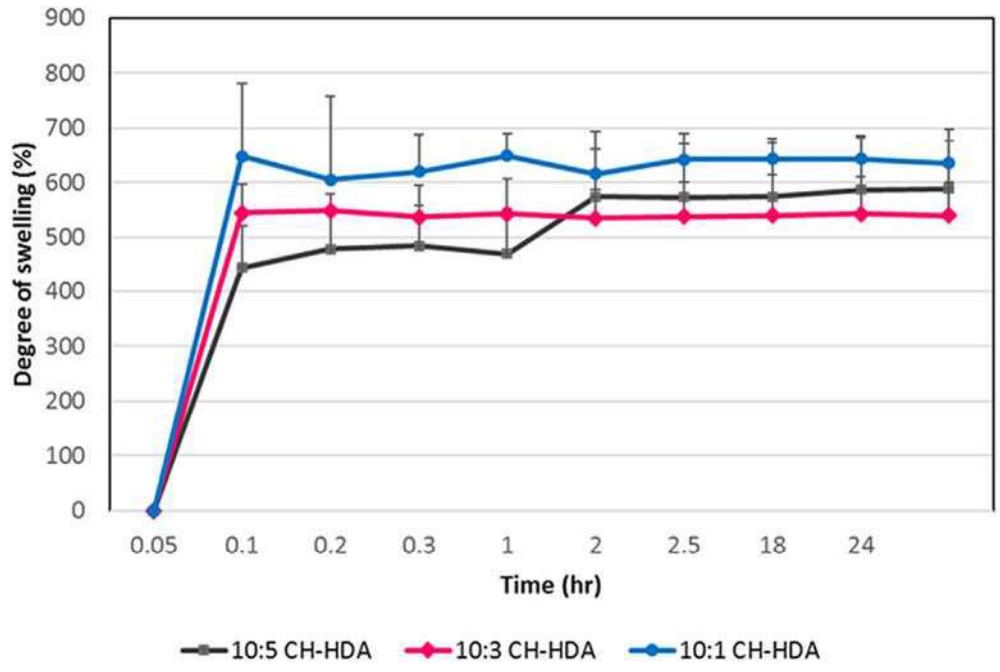


**Figure 4.50. Degree of swelling of all the three ratios of CH-HDA hydrogel. (n = 3).**

### 4.3.3 Thermal characterization of the hydrogel

The thermal decomposition of the hydrogel was studied using thermogravimetric analysis (TGA). The thermal stability of all the three ratios of the CH-HDA hydrogel followed similar decomposition behavior. All the three hydrogels showed decomposition profiles within the decomposition range of their individual components. The decomposition of chitosan started at around 250° C and that of HDA started at 179°C. All the three hydrogels started decomposition at around 179°C and showed more than 50% decomposition at 397° C for 10:1 and 10:3 ratios and 394° C for 10:5 ratio (Fig. 4.51).

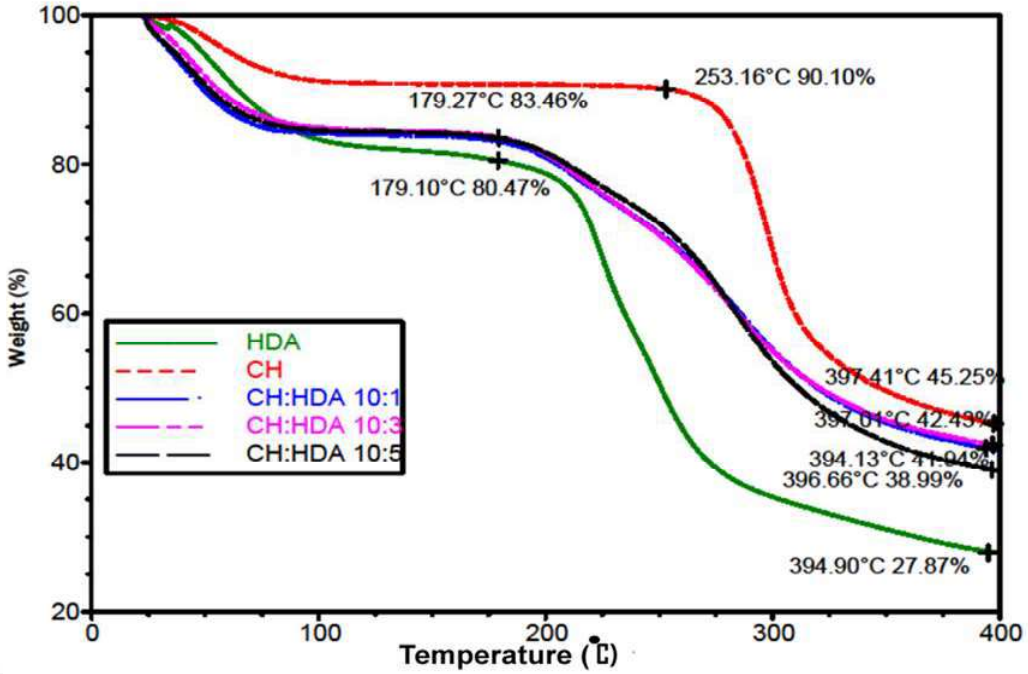


**Figure 4.51. TGA thermogram of CH-HDA hydrogel showing it's thermal stability when heated at a rate of 10° C/min up to 400° C.**

### 4.3.4 Characterization of hydrogel stiffness by AFM

Stiffness of the extracellular matrix plays an important role in cell response. Hence it will definitely help to improve the cell response, by designing a hydrogel system having similar stiffness as that of the native cartilage ECM. Atomic force microscope (AFM) is an efficient tool to measure the mechanical properties of the soft materials. By using the force distance curve generated from the sample, the Young's modulus of the hydrogel can be calculated by mathematical modelling.

With increase in crosslinker ratio the stiffness of the hydrogel is also expected to increase. This was measured using AFM non-contact mode scanning. The Young's modulus of all the three ratios of prepared CH-HDA hydrogel were measured this way and were found to be 130.78±19.83, 199.35±81.57 and 181.47±19.77 kPa respectively. As per the previous studies, the natural human cartilage is reported to have a modulus 0.5-1.5 MPa and that of bovine is reported to be 0.950 MPa and 0.2-0.9 MPa in case of rabbits. It was also observed that the adhesion force decreased with decrease in HDA ratio. The maximum adhesion force was measured to be 476.46±28.36, 322.91±25.80 and 201.16±7.33 for CH-HDA 10:1, 10:3, 10: 5 hydrogels respectively (Fig.4.52). The stiffness of the hydrogel increased with increase in the degree of crosslinking and as expected the 10:5 ratio showed highest stiffness. Thus, the stiffness of the CH-HDA hydrogel system can be tuned by changing the concentration of the crosslinker: HDA.

**Table 15.The mechanical properties of the three hydrogel systems using Force Spectroscopy AFM analysis**

| Sample | Max. Adhesion force (nN) | Young's modulus (kPa) |
|---|---|---|
| 10:1 CH-HDA | 476.46± 28.36 | 130.78±19.83 |
| 10:3 CH-HDA | 322.91±25.80 | 199.35±81.57 |
| 10:5 CH-HDA | 201.16±7.33 | 181.47±19.77 |

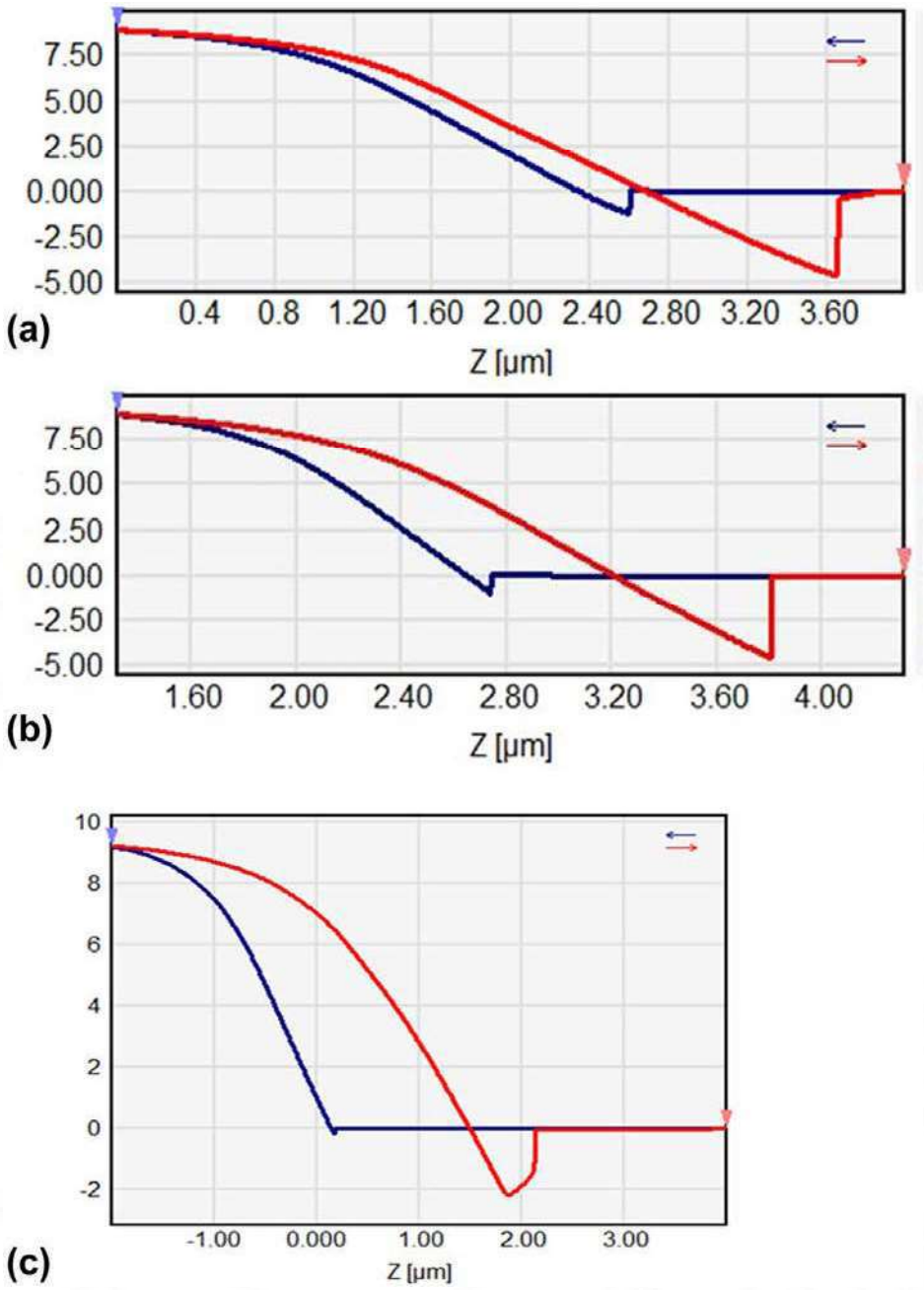


**Figure 4.52. Representative image of force indentation curves obtained for (a) 10:1 CH-HDA (b) 10:3 CH-HDA and (c) 10:5 CH-HDA samples. The data was fitted to Hertz's contact model to calculate the Young's modulus and the maximum adhesion force (n = 3).**

### 4.3.5 The effect of varying stiffness on the encapsulated chondrocytes

The physicochemical properties of the hydrogel play an important role in regulating the activities of the encapsulated chondrocytes. Hence designing a hydrogel having these properties similar to the native system is very crucial for developing a successful hydrogel system. The stiffness of the matrix has been shown to influence the cell migration, cell adhesion and other cellular responses like protein synthesis, proliferation etc.

The effect of varying hydrogel stiffness was studied by encapsulating rabbit articular chondrocytes within the chitosan-HDA hydrogel and cultured for 7, 14 and 28 days at a cell density of 5000 cells/µl. After the culture period the samples were retrieved and tested for its viability by live/dead staining. The live/dead images showed that the cells in all the ratios are viable and did not show any cytotoxicityupto 28 days of culture. However, there was a difference in the cell morphology, which was only observed in the 7 days culture period samples. In the 14 days and 28 days samples, the cells were found to condense and form aggregates and the cells were in spherical morphology (Fig. 4.53). This also indicates the hydrogel system favors cell mobility and hence better cell response.

In a similar study reported by a different group (Jerosch, 2011) the mechanical properties of the cartilage formed improved when the concentration of hyaluronic acid dialdehyde was increased. In a different study, (Wang and Yang, 2017) the ECM cues like chondroitin sulphate and hyaluronic acid were found to play an important role in the neo cartilage formation. Our study suggests that the hydrogels of 10:1 ratio is able to maintain the characteristic spherical morphology of the chondrocytes and viability for a longer period. The stiffness of the hydrogel also influences the ECM synthesis. As per the study by Chen et al., as the substrate stiffness increased from 1 to 90 kPa the secretion of aggrecan and collagen type II also increased. In our study the secretion of the hyaline cartilage marker collagen type II was identified by immunostaining; and collagen type I, which is a negative marker for the hyaline cartilage was absent. Further the synthesized glycosaminoglycan was quantified by DMMB assay.

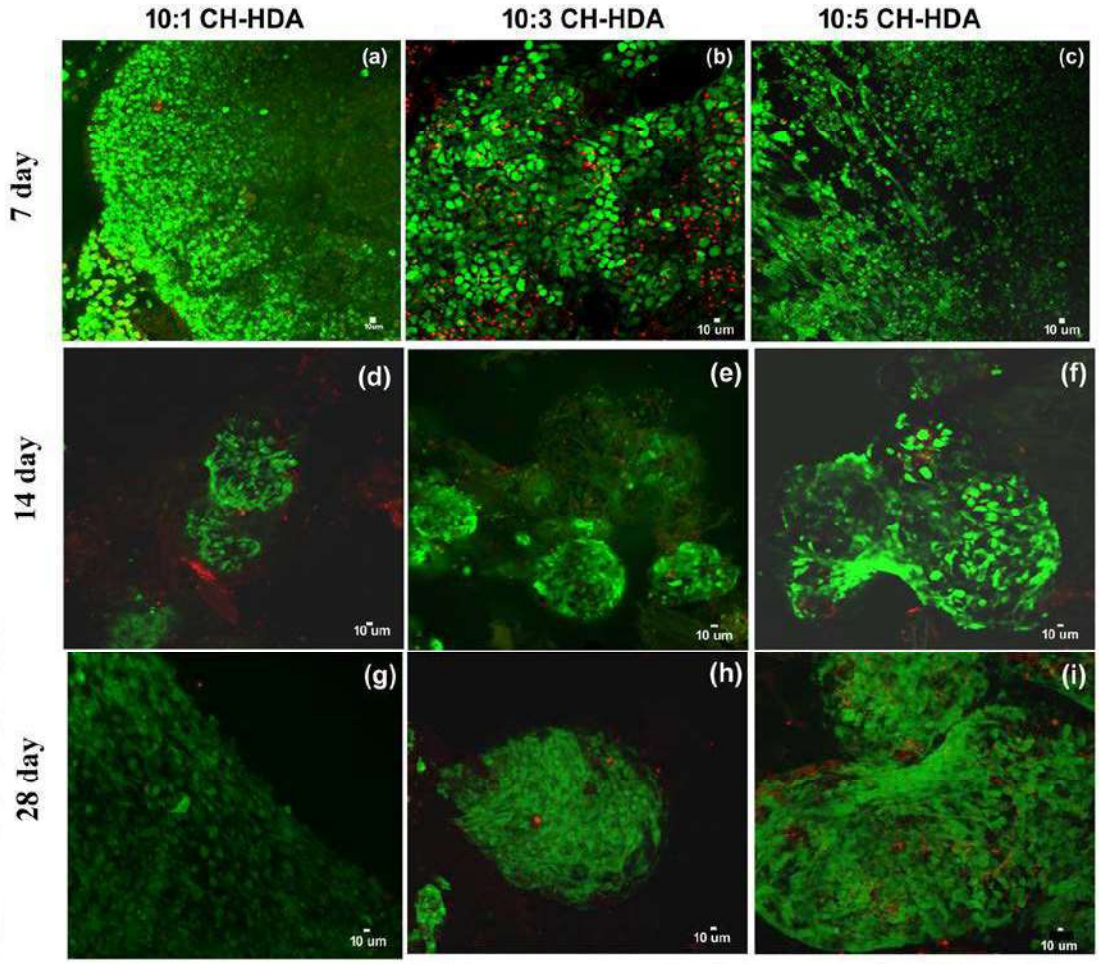


**Figure 4.53. Confocal laser microscopy images of chondrocytes that were stained in the three gels (a)10:1 CH-HDA (b) 10:3 CH-HDA and (c) 10:5 CH-HDA with calcein/ethidium bromide (live/dead) for ascertaining the viability of the cells that were encapsulated. Live cells fluoresce green and red cells fluoresce red. Scale bar = 10 µm.**

### 4.3.6 Immunostaining showed the CH-HDA hydrogel favored chondrogenesis

Further, for the functional studies of the encapsulated chondrocytes. The samples cultured for 7, 14 and 28 days were evaluated for the secretion of hyaline cartilage marker collagen II and collagen I - a negative marker for hyaline cartilage, by immunostaining. Collagen II is a marker for hyaline cartilage and is responsible for the tensile strength of the cartilage. Even though both collagen II and collagen I are fibrillar collagens, collagen I is a marker for fibrocartilage and is not seen in normal healthy hyaline cartilage. Collagen I may be present in hyaline cartilage during injury or during the hypertrophy that occurs during ageing. The presence of collagen I make the hyaline cartilage mechanically inferior. Our study showed that the chitosan-HDA hydrogel system facilitated the secretion of collagen II and collagen I was not seen in the hydrogels of neither the lower stiffness ratio nor in the higher stiffness ratio at any point of the study period up to 28 days (Fig. 4.54 & 4.55). This indicates that the stiffness of the substrate may not have any role in the collagen I expression in chondrocytes derived from hyaline cartilage. The alcian blue staining and the Sirius red staining also corroborated the expression of collagen II by immunostaining. The alcian blue that stains the synthesized glycosaminoglycans, and Sirius red that stains the collagens also stained positive for the samples of all ratio and all time points (Fig. 4.56 & 4.57). The dimethylmethylene blue (DMMB) assay showed a significant ($p < 0.05$) enhancement in the production of glycosaminoglycans for the stiffer gels compared to the less stiff gels (4.58). This may be attributed to the fact that the Young's modulus values of the 10:3 and 10:5 ratios were similar to that of the native cartilage. Hence the results of our study suggest that apart from the compositions of the extracellular matrix, the substrate stiffness plays a major role in determining the cell response.

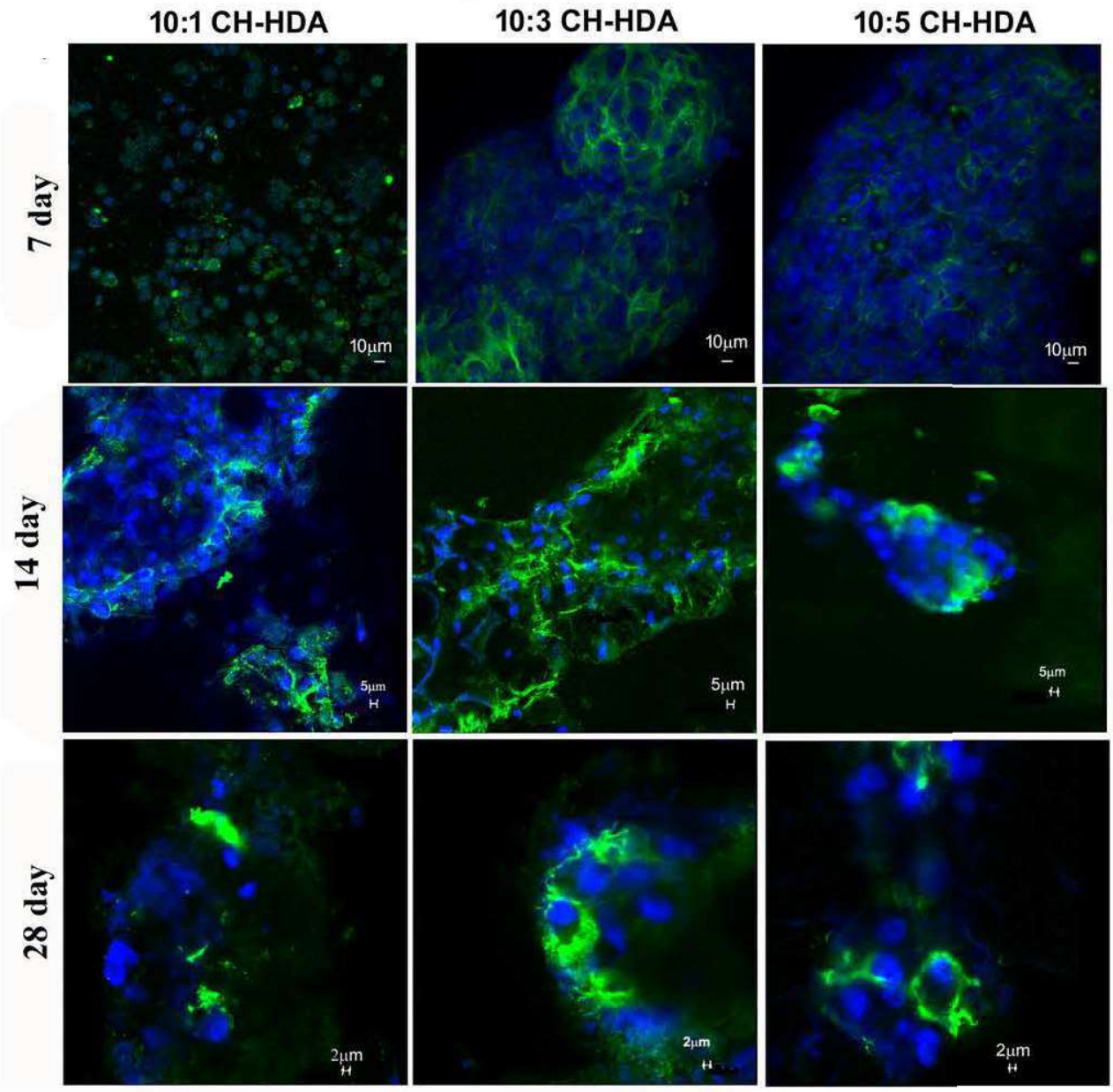


**Figure 4.54. Confocal microscopy images showing type II collagen staining of chondrocytes encapsulated in 10:1 CH-HDA, 10:3 CH-HDA and 10:5 CH-HDA gels at 7$^{th}$ day, 14$^{th}$ day and 28$^{th}$ day. Cells were stained for type II collagen (green) and nuclei (blue). Scale bar for 7$^{th}$ day = 10 µm, 14$^{th}$ days = 5 µm and 28$^{th}$ days = 2 µm.**

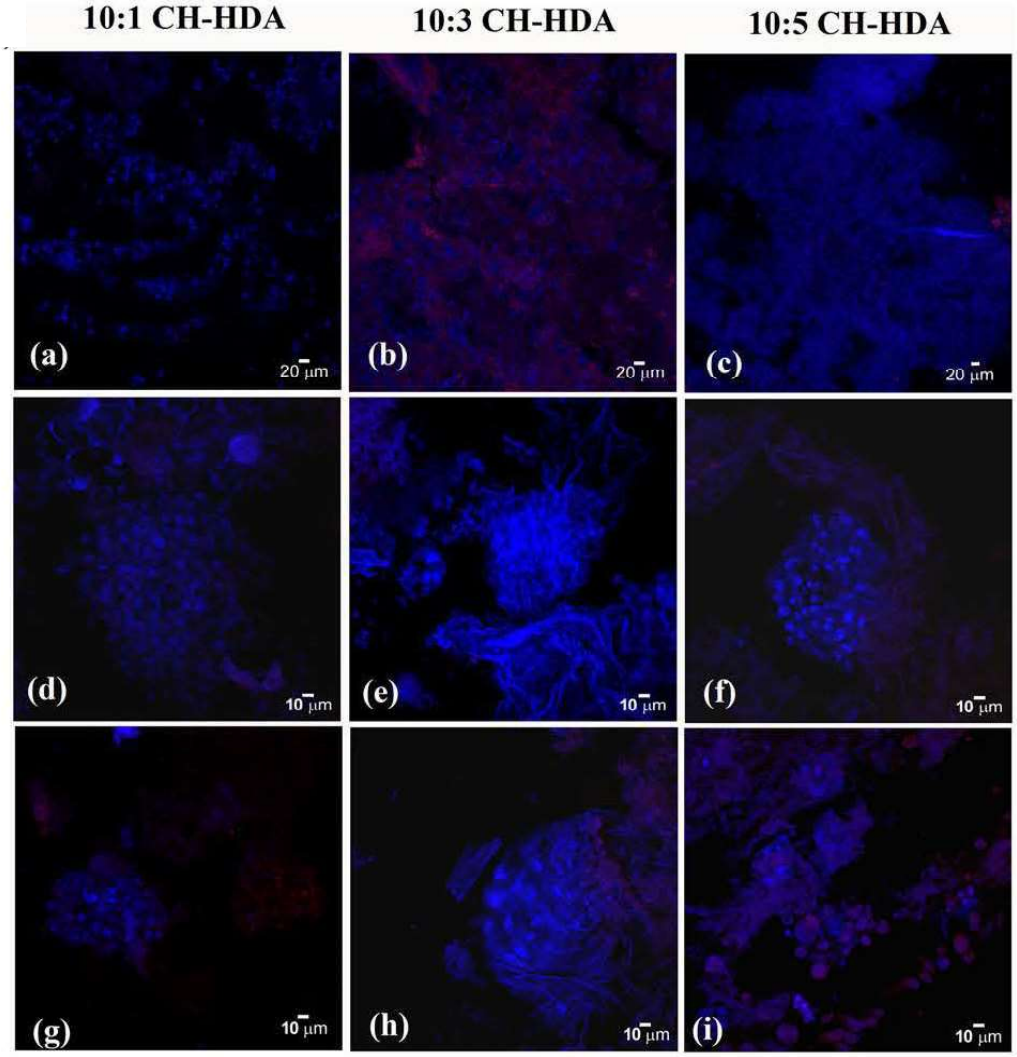


**Figure 4.55. Confocal microscopy images showing type I collagen staining of chondrocytes encapsulated in 10:1 CH-HDA, 10:3 CH-HDA and 10:5 CH-HDA gels at $7^{th}$ day (a, b and c), $14^{th}$ day (d–f) and $28^{th}$ day (g–i). Cells were stained for type I collagen (red) and nuclei (blue).**

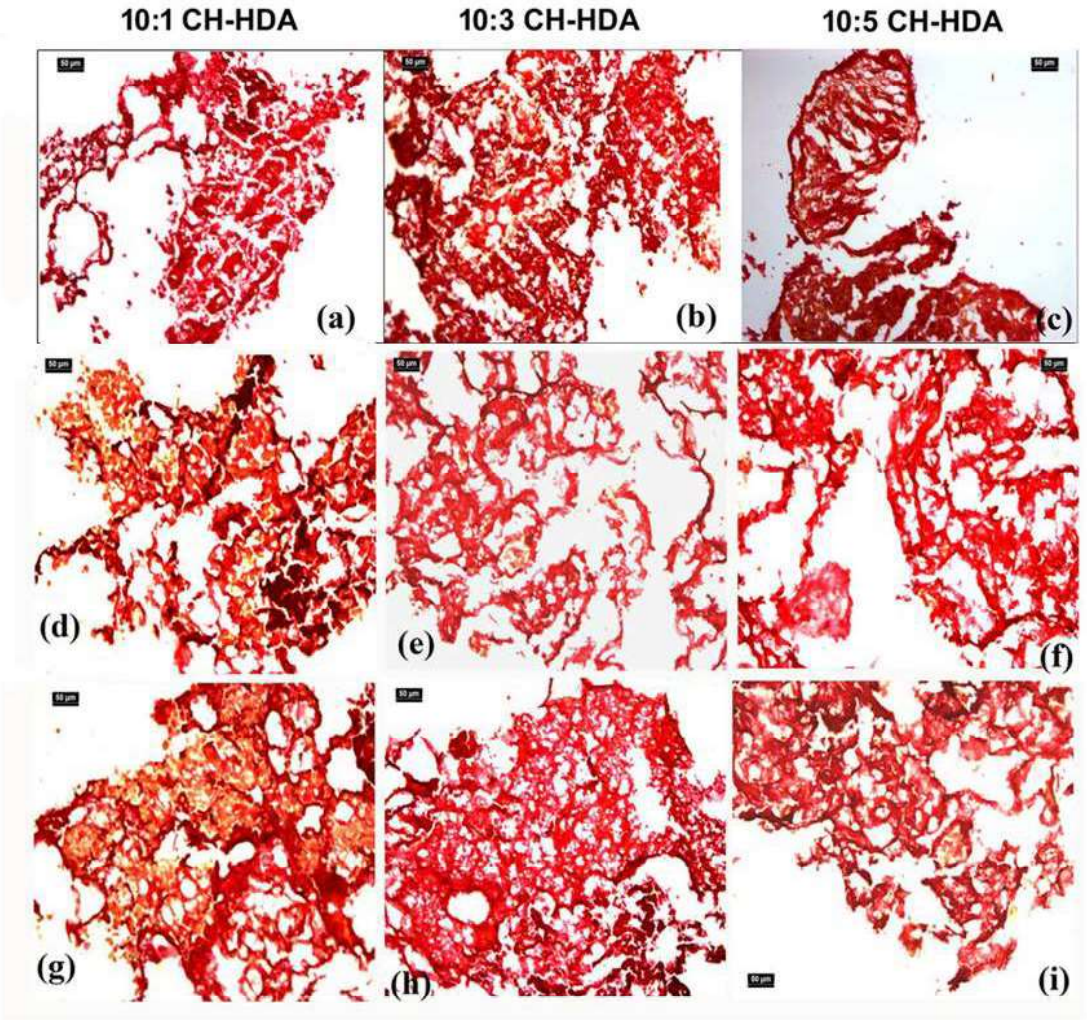


**Figure 4.56. Sirius red staining for collagen performed on the chondrocyte encapsulated gels at 7$^{th}$ day (a, b and c), 14$^{th}$ day (d–f) and 28$^{th}$ day (g–i). Scale bar = 50 µm.**

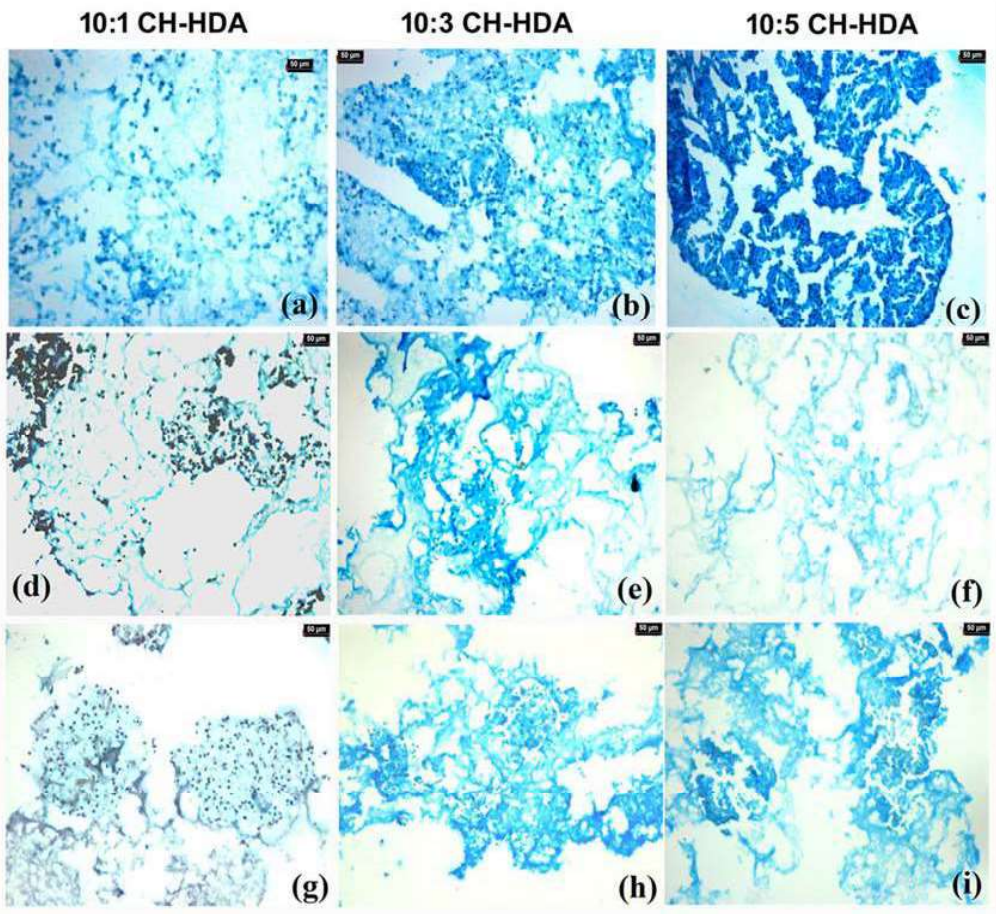


**Figure 4.57. Alcian blue staining for glycosaminoglycan performed on the chondrocyte encapsulated gels at 7$^{th}$ day (a, b and c), 14$^{th}$ day (d, e, f) and 28$^{th}$ day (g, h, i). Scale bar = 50 µm.**

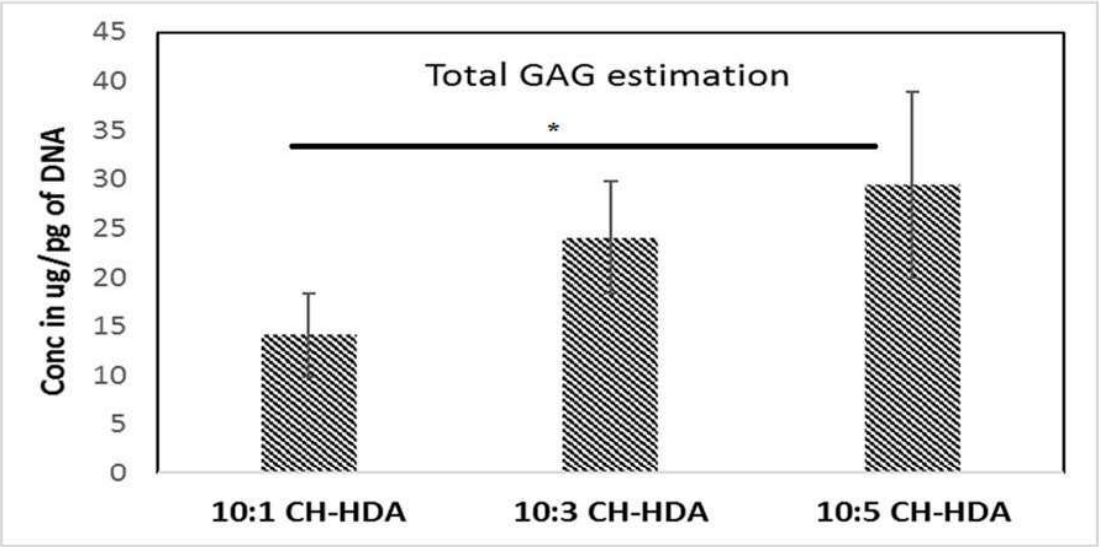


**Figure 4.58. Quantitation of total GAGs by DMMB assay for a 7 days culture period. Mean±SD, n = 3 (*p < 0.05).**

### 4.3.7 Characterization of printability of CH-HDA hydrogel

In order to standardize the printing parameters of the CH-HDA hydrogel, the printing conditions were identified by line drawing method as described previously. Out of the three ratios of the CH-HDA hydrogel, the 10:1 was found to be not good for 3D printing due to lack of shape fidelity. Among the three ratios, 10:2 and 10:3 were tested for its printability and 10:5 was found to have better printability than the 10:3 ratio.

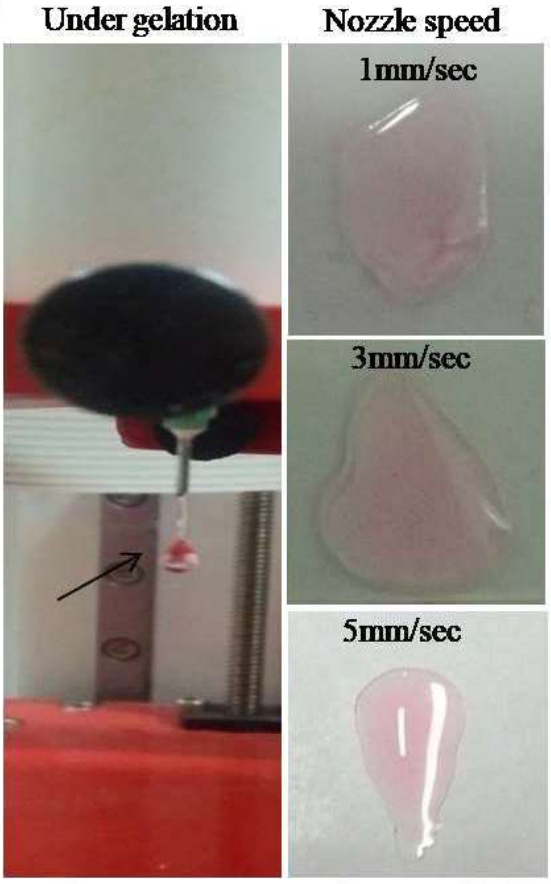


**Figure 4.59. CH-HDA 10:1 ratio failed to form continuous filament during extrusion and had low viscosity due to which it did not form any line in line drawing method.**

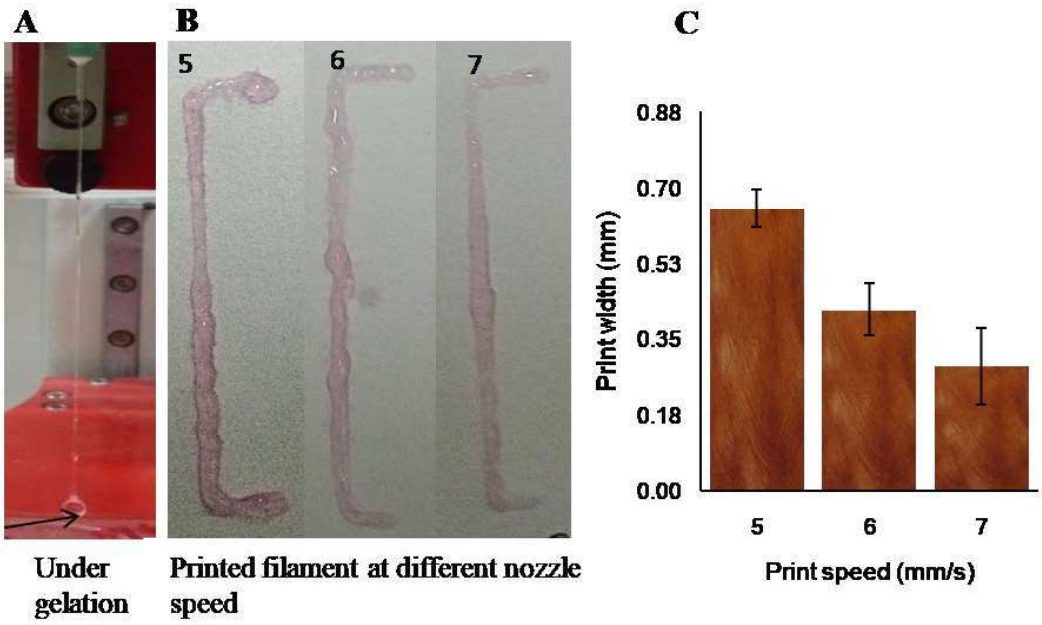


**Figure 4.60. (A) CH-HDA 10:3 forming continues filament while extrusion. (B) Printing characterization of CH-HDA 10:3 hydrogel. (B&C) Line drawing method showing 6 mm/sec as the suitable speed.**

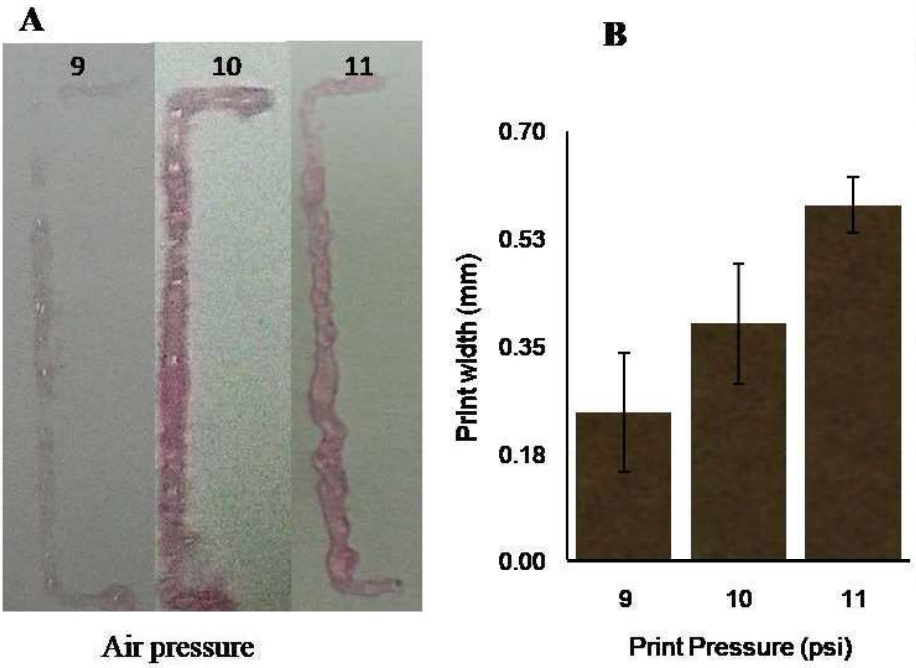


**Figure 4.61. (A) Standardization of print pressure of CH-HDA 10:3 hydrogel. (B) A print pressure of 10psi gave similar filament width as that of the nozzle diameter.**

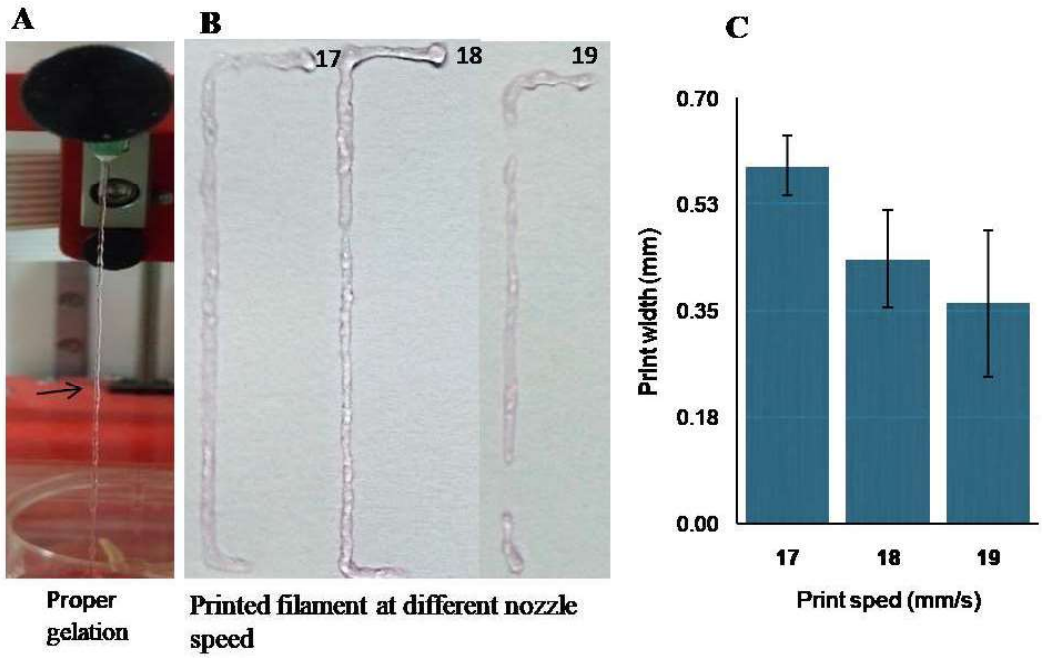


**Figure 4.62. (A) CH-HDA 10:5 forming continues filament while extrusion. (B) Standardization of print speed of CH-HDA 10:5 hydrogel. (C) A print speed of 18 mm/s gave similar filament width as that of the nozzle diameter.**

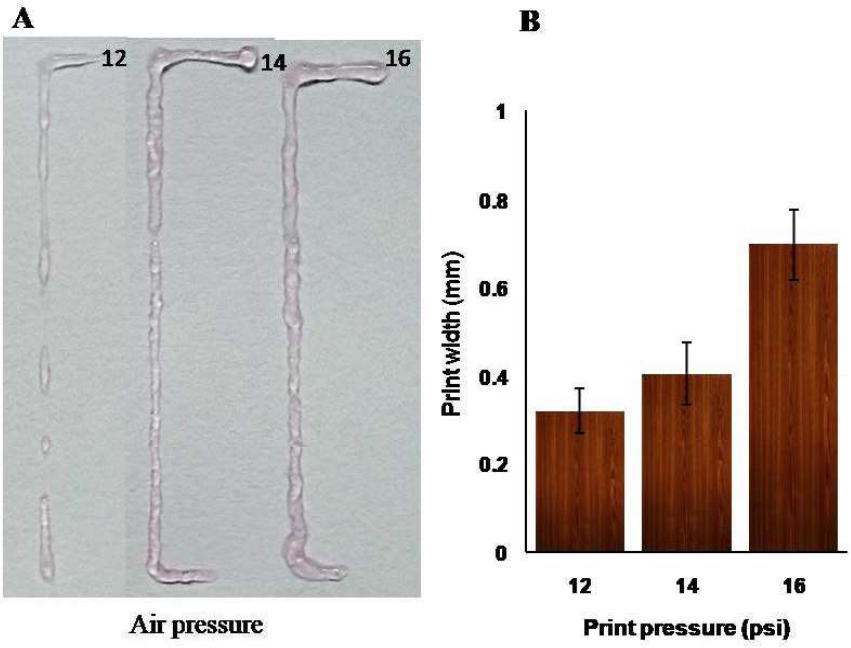


**Figure 4.63. (A) Standardization of print pressure of CH-HDA 10:5 hydrogel. (B) A print pressure of 14 psi gave similar filament width as that of the nozzle diameter.**

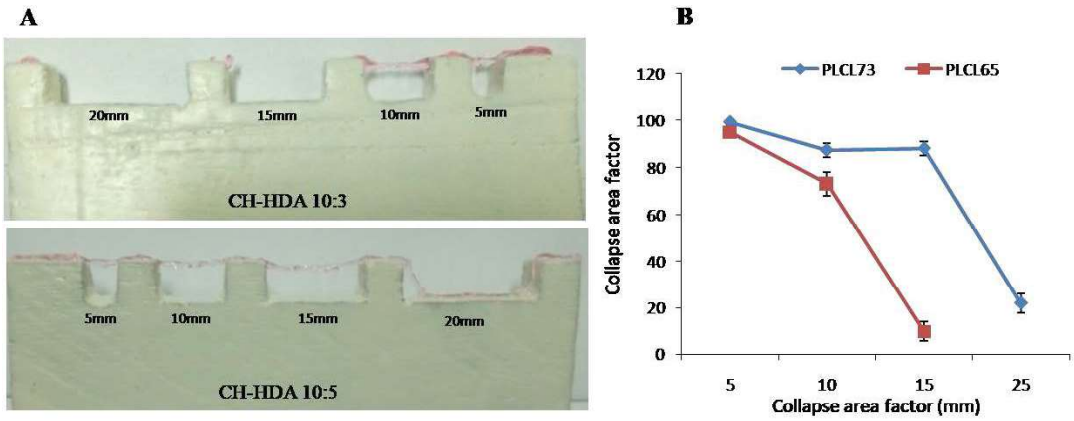


**Figure 4.64. (A&B) Filament collapse test showing better filament stability of CH-HDA 10:5 over 10:3.**

As the lower ratio of 10:1 is least crosslinked and has low viscosity, 3D printing of this ratio was very difficult. (Fig. 4.59) In the line drawing method unlike the other two ratios the 10:1 ratio failed to form a line and was extruding discontinuously even at the low-pressure values, hence we did not proceed with the 10:1 ratio further. Since compared to 10:3, 10:5 is more crosslinked and has high viscosity, the 10:5 ratio required high pressure of 14 psi to print and a speed of 18 mm/s gave line width similar to the nozzle diameter (Fig. 4.62& 4.63). (Fig. 4.60 & 4.61) In case of 10:3 the degree of crosslinking and the viscosity is less compared to the 10:5 ratio, hence the pressure required for its printing has a lower value of 10 psi and a speed of 6mm/s for printing the line of width similar to the nozzle diameter. As the degree of crosslinking increases the mechanical properties of the hydrogel also improves as expected, this was evident in the filament collapse test as well. The 10:5 ratio could form almost a straight filament upto a distance of 15 mm, whereas the less crosslinked 10:3 collapsed at 10 mm distance (Fig. 4.64). This shows the superior mechanical property and print fidelity of 10:5 ratio over the 10:3 ratio. The printability of the 10:3 and 10:5 ratios were also compared and the later was found to have a better printability value of close to 1 compared to the 10:3 ratio which gave a value of 1.13 (Fig. 4.65A). Moreover, the 10:5 ratio showed sharper edges compared to the 10:3 ratio, which shows the ability of the highly crosslinked ratio to print more precise structures (Fig. 4.65B).

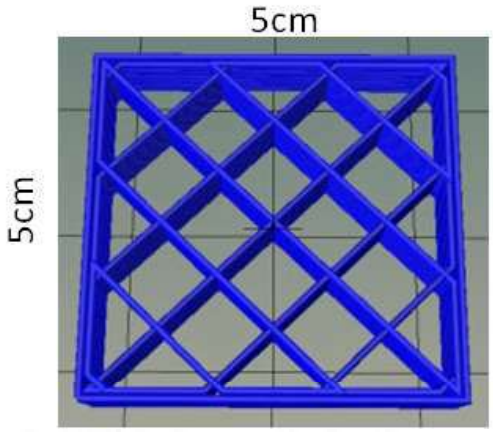


**Eq9,**

$$Pr = \frac{\pi}{4} \times \frac{1}{C} = \frac{L^2}{16A}$$

Pr- Printability
C- Circularity
L- Perimeter
A-Area

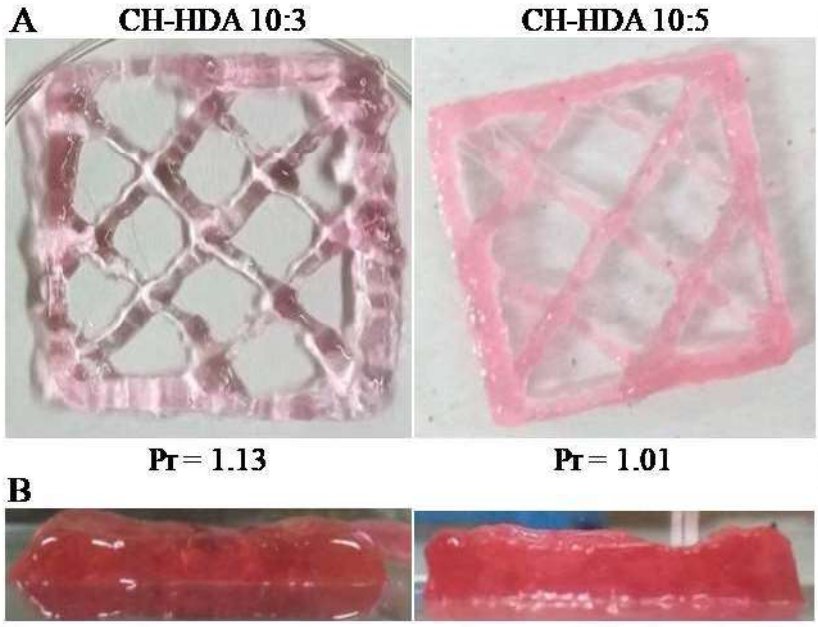


**Figure 4.65. (A) Printability of 10:3 and 10:5 CH:HDA hydrogel. CH:HDA 10:5 ratio showed better printability than 10:3. (B) Side view of the printed structure; 10:5 showed sharp edges compared to 10:3.**

### 4.3.8 Fabrication of 3D printed biphasic tracheal construct

Based on the standardized printing parameters, the biphasic tracheal construct was 3D printed by dual head printing (Fig. 4.66). The PLCL73 was printed at 140$^{o}$ C and the CH-HDA hydrogel mixed with chondrocytes was 3D printed using another printing head. Culturing the construct for 3 days in chondrogenic media and further a live/dead and alcian blue staining showed the 3D printing process is not affecting the viability of the cells and the chondrogenic capacity is also not impaired (Fig. 4.67 & 4.68).

**Figure 4.66. 3D printed PLCL73-CH-HDA biphasic tracheal construct.**

**Table 16. 3D printing parameters of biphasic design**

| | **PLCL73 framework** | **CH-HDA hydrogel** |
|---|---|---|
| **Ratio** | 70:30 | 10:5 |
| **Nozzle dia.** | 0.8 mm | 0.4 mm |
| **Nozzle speed** | 0.8 mm | 9 mm/s |
| **Air pressure** | 0.5 mm/s | 14 psi |
| **Temperature** | 140$^{o}$ C | 25$^{o}$ C |

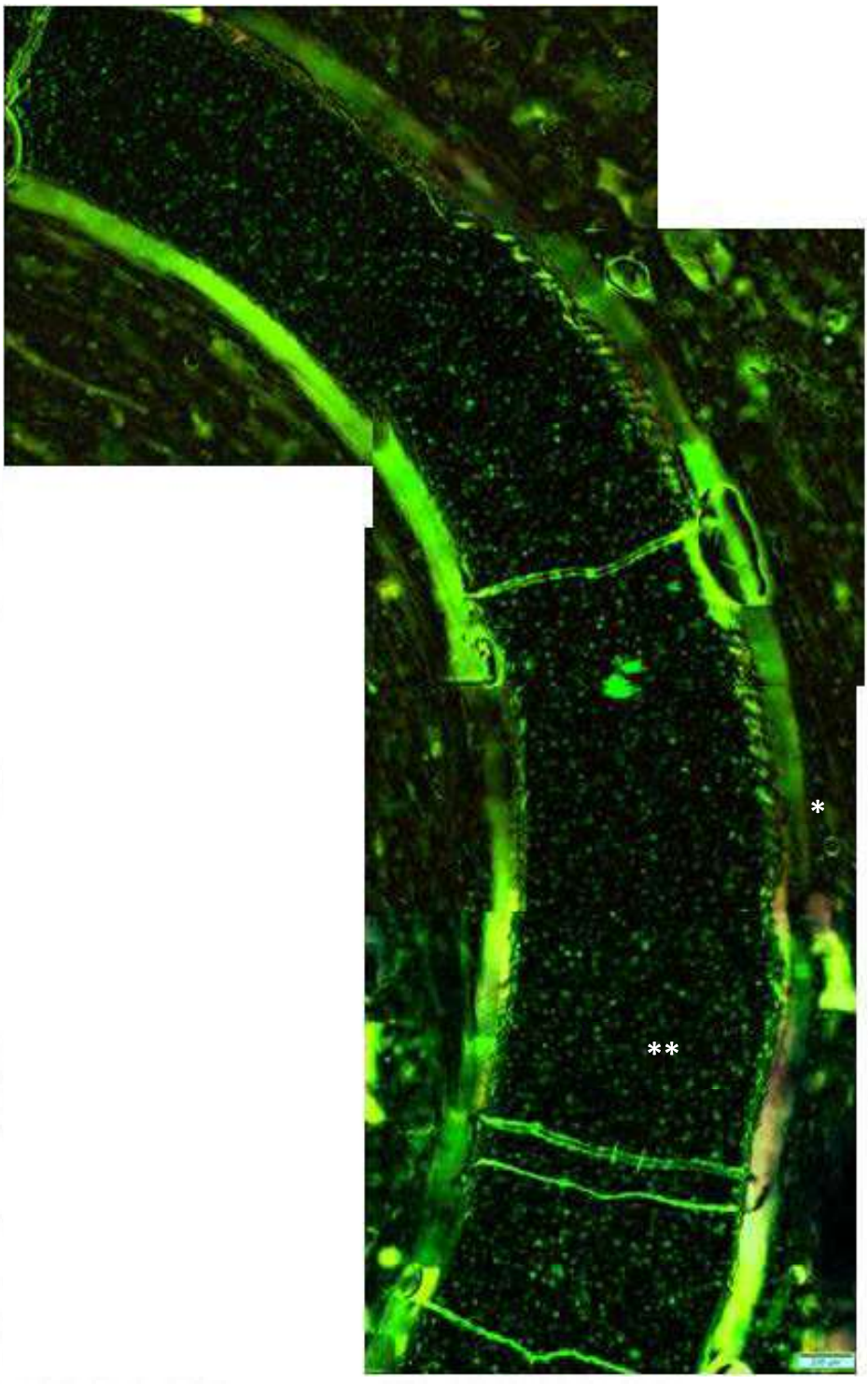


**Figure 4.67. Live dead staining of 3D printed biphasic construct. Showing hydrogel phase with cells (**) and the PLCL (*) solid phase.**

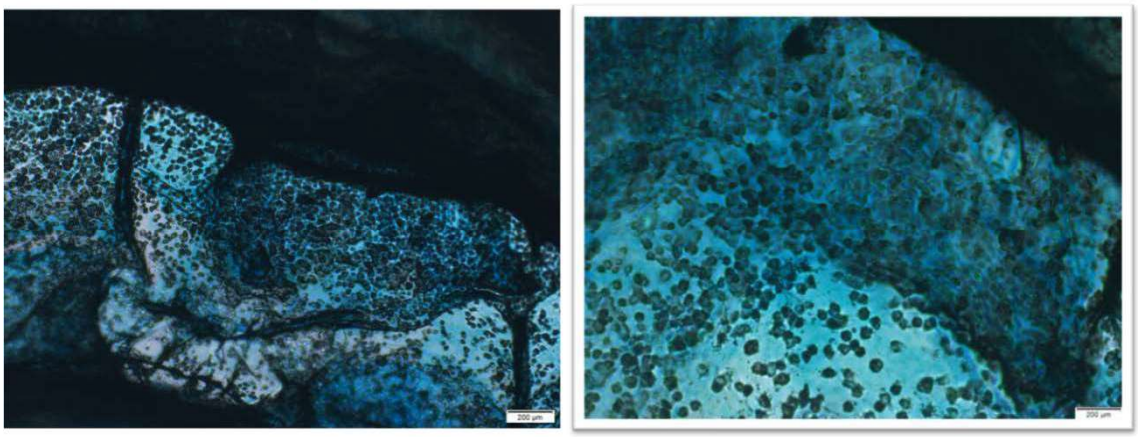

**Figure 4.68. Alcian blue staining of 3 days cultured 3D printed biphasic tracheal construct.**

# CHAPTER 5 |
# DISCUSSION

## 5.1 Synthesis of elastomeric polymers

Trachea has a peculiar design which makes the tissue functionally efficient. The stiffer 'C' shaped cartilage rings prevent the membranous tubular structure from collapsing. At the same time they are placed alternatively, so that the flexibility of the structure is not compromised. While reconstructing this structure artificially, it is very much important to maintain these structural features. The material and the design play a major role in the successful reconstruction of an artificial tracheal substitute. Previous studies in animals have shown severe inflammatory response and graft failure due to mechanical mismatch (Ajalloueian et al., 2014).

Elastomeric polymers are capable of withstanding stress and responding to it by extending from a random coil to a chain extended structure without rupturing its bond. Polymers with low glass transition temperature below room temperature can have chain mobility which will help the polymer to meet these requirements to become flexible. Hence elastomeric polymers are ideal choice for the fabrication of tracheal scaffolds having similar mechanical properties as that of the native trachea. Crystalline polymers have very ordered microstructure and have no enough chain mobility to become flexible like the elastomers. Hence, they fail to respond to the stress and often result in breaking of the polymer structure. Polymers with non-polar chain groups and are amorphous in nature are most preferred for synthesizing elastomers and they have superior elastomeric properties compared to the one with polar groups.

There have been few attempts to reproduce the elasticity of the native structure by using elastic polymers or by using peculiar design. A 3D printed polyurethane based trachea showed comparable elasticity as that of the native trachea, however an improved design or fictionalization of the material would have improved the cell response on the material (Hsieh et al., 2018). In a very recent study, the authors could make flexible 3D printed PCL based tracheal scaffold by using a peculiar design (She et al., 2021).

Polyurethane urea and poly(lactide-co-caprolactone) are two different types of elastomers having different elastic properties. PUU in this study is synthesised using three components polycaprolactonediol as polyol, HDI as diisocyanate and butane diamine as the chain extender. Once they are polymerized, they form a

chain with non-polar groups. The polyol forms the soft segment, HDI and the chain extender forms the hard segment. This results in the segmentation of the microstructure into highly crystalline hard domains and amorphous random coil made of the soft segment. In segmented PUU, the hard segment domain is embedded in the amorphous part and there is non-covalent interaction between these two segments which is responsible for the elasticity of the polymer. When stress is applied, this segmented morphology acts like a spring and enables the polymer to respond to the applied stress. Since there are amorphous domain and highly crystalline hard domain in this, this morphology can be very well studied using DSC and other microscopic techniques. In DSC the two segments give two different melting peaks, the amorphous part formed by PCL was observed at 25$^{o}$ C and the highly crystalline part formed by HDI and butane diamine gave a melting peak at 330$^{o}$ C. These domains can also be visualised by AFM microscopy or using polarizer of light microscope (not included in this study). Polyurethane has been a widely used material for medical devices, even though polyurethane urea has several advantages over polyurethanes; their use in medical applications is limited due difficulty in processing. However, few studies have reported its *in vivo* response in animal models. Electrospun PUU sheet used for abdominal wall reconstruction showed increased M2-type macrophages and better tissue remodelling in rats (Hong, 2016). The limitations in the processing of PUU was evident in this study as well, the material was not suitable for 3D printing due to its high melting point and degradation immediately after its melting point. However, the synthesized polyurethane urea is a promising material for electrospun medical devices.

Since PUU is not suitable for all manufacturing techniques, we further explored other materials suitable for our application. Poly(lactide-co-caprolactone) has recently gained much interest for medical applications because of its biocompatible and hydrolysable nature (Agarwal et al., 2019). PCL is a semicrystalline polymer having elastomeric properties and PLA is a highly crystalline, hard and brittle in nature; hence is not useful for load bearing applications. Combination of the two polymers is expected to have synergistic properties of both the polymers.

The PLCL copolymer is a promising substitute for many medical applications because of its tunable elasticity and mechanical properties based on its change in

the caprolactone and lactide molar ratio. In a very recent study, a highly elastic PLCL sheets were made by melt electrowriting (MEW) and compared its mechanical properties with the PCL. The material showed promising mechanical properties over the conventional PCL (Diaz et al., n.d.). The flexibility and elongation of a polymer is influenced by its crystalline properties. Here we prepared different ratios of PLCL and identified the appropriate ratio having suitable flexibility and 3D printability. The flexibility of the polymer can be easily studied by DSC analysis and further confirmed by mechanical studies using the UTM.

The degree of crystallinity of PLCL depends on the ratio of the lactide content; the melting point of caprolactone is 60$^{o}$ C and that of lactide in 180$^{o}$ C. The resulting PLCL showed a melting peak between 128$^{o}$ C-161$^{o}$ C which is a range between the caprolactone melting point and lactide melting point and as the lactide content increased the melting point moved towards the lactide side. This shows the synthesized polymer is a random copolymer, if it were a block copolymer the melting point would not have changed much. The lower ratios PLCL65 and PLCL73 had a Tg of 18$^{o}$ C and a melting point of 128$^{o}$ C and 133$^{o}$ C respectively and a degree of crystallinity 20% and 39% respectively this indicates that these ratios have both slightly crystalline and amorphous domains, but unlike PUU they are not phase separated and are randomly arranged. Since lactide and caprolactone have different reaction rates during polymerization some part of the lactide bonds with the caprolactone and forms the amorphous part and rest of the lactide part polymerizes to form the crystalline part. These results prove that the synthesized copolymer has semicrystalline properties.

For developing a tissue substitute for elastomeric tissues like trachea, it is important for the polymers to have elastomeric properties. The percentage of extension and tensile strength of the polymer was measured from the stress strain curve. Since the caprolactone contributes to the elasticity of the polymer, the elasticity of the copolymer increases with increase in the caprolactone content. Having mechanical properties similar to the native trachea is important for maintaining the graft patency and its functionality. Previous studies have shown, rigid materials cause granulation at the site of implantation and results in fatal obstruction of the airway. The mechanical mismatch can also cause prolonged

inflammatory response and fibrosis (Boazak and Auguste, 2018). Tracheal flexibility and longitudinal extendibility is important for the normal functioning of the airway. Since this copolymer has comparable mechanical properties as that of the native trachea. It is expected to improve the chances of tissue survival.

A tissue engineered artificial tracheal substitute is a promising strategy for treating long segmental tracheal defects. In a recent study, a tracheal substitute which is mechanically and morphologically similar to the native trachea. The construct when subcutaneously implanted in nude mice showed some promising results. However, the method of fabricating such a scaffold is very complicated and a more detailed in vivo study need to be done in this study (Park et al., 2015).

## 5.2 Preparation of chitosan-HDA hydrogel

A wide variety of hydrogel systems have been used for tracheal tissue engineering. In most of the studies they have been used to improve the cellular response and the regeneration process. Risbud et al., studied the potential of chitosan-gelatin hydrogel system for the regeneration of lumen epithelium (Risbud et al., 2001), and were successful in generating lumen epithelium with functional cilia. By using biphasic structures, it helps to incorporate the desired mechanical properties and cytocompatibility in a single system. In a study by Kim et al., a novel paper based origami strategy was tested for the reconstruction of the tracheal segment. The biphasic structure consisted of paper and cell laden alginate hydrogel which remained patent and replaced the native structure up to 4 weeks when implanted in rabbit (Kim et al., 2015).

As the natural polymers are more cell friendly and nontoxic, they are more preferred for tissue engineering application. They can also be used for cell encapsulation, drug delivery and for delivering other bioactive components (Peers et al., 2020). With the introduction of 3D printing in the tissue engineering field, many efforts have been focused on using these natural polymers for the development of bioinks. For cartilage tissue engineering, polysaccharide based bioink is more preferred due to its similarities with the ECM of the native cartilage (Oliveira and Reis, 2011). Chitosan and hyaluronic acid are polysaccharide based naturally derived biomaterials which have been widely used for tissue engineering applications. Moreover, hyaluronic acid is one of the

components of native cartilage and chitosan has chemistry similar to the native proteoglycans of the cartilage ECM. The chitosan dissolves in acidic pH of less than ~6.5. Polysaccharides polymers degrade faster and have low stability in water. Chitosan based hydrogels are usually prepared using glycerol phosphate based ionic crosslinking mechanisms. But the presence of glycerol phosphate causes mineral deposition and favors bone formation (Gkioni et al., 2010). Hyaluronic acid being one of the components of the cartilage ECM is expected to improve its functional property. The hyaluronic acid in cartilage is responsible for holding the water and is responsible for the cushioning property of cartilage due to which the cartilage is able to bear heavy load.

Schiff's base is an effective strategy to crosslink these two components to form hydrogel. The carbonyl groups of hyaluronic acid are oxidized to form an aldehyde group which reacts with the amino groups of chitosan to form the Schiff's base crosslinks. Unlike other strategies, this one does not involve any toxic agents and can be easily be made in a single step procedure.

The formation of Schiff's base was confirmed by the corresponding peaks of FTIR. Even though all the three ratios of chitosan-HDA 10:1, 10:3 and 10:5 were capable of forming gel, the ratio lower than 10:1 failed to form gel. A change in the intensity of the corresponding peaks was also observed in the FTIR with change in the HDA content. With increase in the HDA ratio the intensity of the amide peak decreased.

To test the water absorption property of the scaffold swelling studies were done in PBS using lyophilized samples. The scaffold was found to take up the water immediately and attain equilibrium. This is because of the OH groups present in the scaffold and also the pores which take up the water by wicking action. Even though the scaffold soaked up water immediately, there was no evident change in the dimensions of the scaffold. The ability of the scaffold to hold water will improve the viability of the cells seeded in it by facilitating better nutrient diffusion (El-Sherbiny and Yacoub, 2013).

## 5.3 Characterization of hydrogel stiffness by AFM

Atomic force microscope (AFM) is a versatile technique that can be used in different modes in different conditions to measure different properties of a

material. The most commonly used modes of AFM are contact mode and non-contact mode. In contact mode the cantilever comes in contact with the sample and can be used for the measurement of its mechanical properties. Whereas in non-contact mode or tapping mode the cantilever comes close to the sample and touches the sample only for a short while and based on the deflection experienced by the cantilever a nanoscale image of the surface of the sample is taken. Even though both modes can be used for the characterization of the chitosan-HDA gel, the appropriate cantilever for that particular mode should be selected. For example, the cantilevers used for the contact mode are of lower resonance frequency cantilevers compared to those used for the non-contact mode.

In this study we have evaluated the effect of the stiffness of CH-HDA hydrogel on the chondrocyte behavior. Our study suggests that apart from the composition of the hydrogel, the hydrogel stiffness also plays a role in determining the cell response. A study from Zang et al., showed that when chondrocytes were seeded on PDMS substrate of decreasing stiffness (135 kPa to 1.4 kPa) the collagen II expression increased. In a different study by Li et al., showed as the stiffness of the gelatin methacrylate gel increased the chondrocytes exhibited increased expression of collagen II and aggrecan. It has been also reported that the polyacrylamide gel of less stiffness (4 kPa) had enhanced collagen II expression compared to the stiffer (100 kPa) gels. Hence, we assume there is an optimum stiffness which favors chondrogenesis, stiffness of lower or higher values may decrease the ECM secretion. Our study shows that it is possible to maintain the cell viability and phenotype in less stiff gels but the secretion of ECM was down regulated. Therefore, an optimum stiffness value of about 200 kpa which is comparable to the native cartilage is preferred for the hydrogel system.

## 5.4 The effect of varying stiffness on the encapsulated chondrocytes

It is well known that the cells change their morphology and gene expression with the change in the substrate rigidity. As a function of the substrate stiffness the internal stiffness of the cell, which is regulated by the cytoskeletal assembly will also change. There have been previous reports which show the elastic modulus of the cell is almost equal to the elastic modulus of the substrate i.e., the cell adjusts

its elastic modulus to make it similar to the substrate's modulus values. The cell does this by regulating the polymerization of its cytoskeletal components like actin. This in turn regulates the cell response.

In native cartilage, the chondrocytes are embedded in extracellular matrices with well-defined elastic modulus. Whereas in case of cells cultured on culturewares, the cells exert a force on the cultureware by attaching on it and pulling it towards the cell. The magnitude of the force is in gigapascal which is much higher than the native ECM. Hence the mechanical properties of the substrate have a great impact on the structure and functions of the cell. Cells cultured on stiff matrices have been reported to have fibrotic morphology, actin stress fibers, enhanced integrin expression, increased contractility, which leads to activation of GTPases and formation of focal adhesion complexes (Selig et al., 2020). These responses depend on the cell type. For example, neurons show elongated morphology at <0.5 kPa and chondrocytes start spreading at 10kPa. The stiffness of the substrate also influences the motility of the cells, cell proliferation and differentiation (Gerardo et al., 2019). In this study we were able to standardize the optimum stiffness required for the substrate for better cell response.

## 5.5 Characterization of printability of chitosan-HDA hydrogel

3D printing was introduced into tissue engineering recently, since then it's been used to fabricate complex tissue constructs with precision as per the design given. 3D printing allows spatial manipulation of the biomaterials and cells and thus helps to develop a 3D tissue like architecture. In this technology the cells are delivered using a biomaterial or bioink (Ouyang et al., 2016). To improve structural and biological functionalities, researchers are more focused on developing new bioinks.

However, the characterization of 3D printing parameters required for this bioink plays a major role in identifying the right bioink and right parameters for printing precise structures. Recently there have been many methods devised for the evaluation and quantification of bioink's properties for 3D printing (Ouyang et al., 2016). The printability and other properties required for 3D printing chitosan-HDA hydrogel of all the three ratios were evaluated by these methods.

The results showed that, out of the three ratios the printability improved with increase in the cross-linker ratio. The 10:1 ratio had poor printability and had difficulty in printing even while standardizing speed and pressure by line drawing method. Since it had more fluidity compared to the other two ratios, it failed to build a 3D structure due to buckling. And 10:1 ratio had less print pressure and high speed to print the lines of desired print width. As the crosslinker ratio increased the crosslinking also increased and the fluidity of the gel decreased which was evident in the stiffness of the gel on AFM analysis. The 10:3 and 10:5 ratios had more stiffness and viscosity compared to the lower ratio 10:1. This was very much influencing the printability and print fidelity of the chitosan–HDA gel. The printability and the print fidelity of the 10:1 ratio was the lowest and that of 10:3 and 10:5 increased with increase in the crosslinker ratio. Out of 10:3 and 10:5 ratios, the 10:5 had better printability and print fidelity compared to the 10:3 and 10:1 ratio. Hence, we selected this ratio for our application. Further the cell viability and the cell response of the 10:5 ratio in terms of chondrogenesis was also found to be satisfactory. This particular ratio is expected to support the growth of the seeded cells and also has the ability to 3D print into a particular structure, hence could be a good candidate to use as a cell delivery system for the biphasic design.

# CHAPTER 6|

# SUMMARY AND CONCLUSION

Clinically, tracheal disorders are still life threatening and require rigorous surgical management. Tracheal pathology includes traumatic injury, tumors, inflammatory diseases etc. Since the airway is membranous, alterations in pressure may lead to remodeling of the system and causes other complications. The gold standard for surgical treatment of tracheal stenosis is tracheal resection and end to end anastomosis. However, a larger stenosis of more than 30% is inoperable due to post-surgical complications.

Initial attempts to replace the defective airway with collagen sponges and stents were not very successful (Okumura et al., 1994). In 2008, there were great hopes and gained worldwide attention for the first decellularized tracheal transplantation (Macchiarini et al., 2008). It was a 30-year-old tuberculosis patient who had hypoplastic left main bronchus. Although initially it showed some promising results, the patient later suffered anastomotic stenosis.

Another group in 2010 (Delaere et al., 2010) attempted allotransplantation using a cadaveric donor trachea after indirect vascularization before the transplantation. Considering the age range and tracheal disorders, broadly applicable tracheal graft which is tissue engineered so that it can be easily available without any risk is required. The concept of tissue engineering involves exploitation of extracellular matrix that gives stiffness and stability using a decellularized trachea or synthetic polymer along with cells that contribute to the regeneration and repair of the tissue and ultimately reproduce the physiological function. However, the determination of the materials, cells and the matrix type still remain as a conundrum.

There have been many attempts to address these problems, each of those studies have their own limitations. Most recently 3D printing was introduced into the field of tissue engineering with an aim to push some of these limitations. This study proposes a model which can address many of the challenges and limitations of the conventional tissue engineering strategies.

The results obtained from the current study emphasize the importance of a material having 3D printability and comparable mechanical properties as that of the native trachea. The study also proposes a model which can improve the tissue regeneration by proper three-dimensional organization of the cells.

So far, the bioprinting was done using aqueous based bioinks, which lack mechanical properties. Hence these types of constructs can only be used for *in vitro* applications not for the clinical use. Even though there are many mechanically strong hydrogel systems, the cytocompatibility of them is compromised.

Here, rather than attempting the chemistry of making a mechanically strong non-cytotoxic hydrogel we have adopted a much simpler yet viable option of tweaking the scaffold design. The proposed biphasic design in this study not only provides superior mechanical properties, it has also taken care of the biocompatibility required for the construct.

The present study demonstrated the potential of 3D printing technology in the medical field which can one day pave the way to solve many complicated problems. The study showed the synthesis of two different types of elastomeric polymers and showed its feasibility to generate a tissue engineered construct by electrospinning and 3D printing. Here the efficiency of the two-fabrication methods electrospinning and the 3D printing technology is also discussed. The advanced 3D printing technology is able to address the limitation in cell penetration which was observed in the electrospinning. Moreover, it can have the advantage of generating any structures with the desired size and shape.

The use of a biphasic design was able to generate a tissue engineered trachea with better three-dimensional cell distribution and mechanical property without compromising the cytocompatibility. Since the polymeric lattice frame work provides ample mechanical support, so that most of the hydrogels can be used for the printing of cells without the concern of mechanical failure. The bioink used here is a natural biomaterial that has proven to have better cell to cell communication and cell mobility which is expected to improve the regeneration potential of the tissue. This design strategy could be a better alternative for generating cytocompatible scaffolds with desired mechanical properties.

## Future prospects

This study was majorly focused on the identification of the suitable biomaterial for 3D printing, its designing and *in vitro* studies. The *in vivo* response of the material and the construct needs to be explored. Implantation of the construct in a heterotrophic location for vascularization and then implanting it in the defect location could be a promising strategy that needs to be tested.

## References


Agarwal R, Blum KM, Musgrave A, et al. (2019) Degradation and in vivo evaluation of polycaprolactone, poly(ε-caprolactone-co-L-lactide), and poly-L-lactic acid as scaffold sealant polymers for murine tissue-engineered vascular grafts. *Regenerative Medicine* 14(7): 627–637. DOI: 10.2217/rme-2018-0069.

Ahn CB, Son KH, Yu YS, et al. (2019) Development of a flexible 3D printed scaffold with a cell-adhesive surface for artificial trachea. *Biomedical Materials* 14(5). IOP Publishing: 055001. DOI: 10.1088/1748-605X/ab2a6c.

Ajalloueian F, Lim ML, Lemon G, et al. (2014) Biomechanical and biocompatibility characteristics of electrospun polymeric tracheal scaffolds. *Biomaterials* 35(20): 5307–5315. DOI: 10.1016/j.biomaterials.2014.03.015.

Allen MS (2003) Surgical anatomy of the trachea. *Chest Surgery Clinics of North America* 13(2): 191–199. DOI: 10.1016/S1052-3359(03)00037-1.

Al-Qadi MO, Artenstein AW and Braman SS (2013) The 'forgotten zone': acquired disorders of the trachea in adults. *Respiratory Medicine* 107(9): 1301–1313. DOI: 10.1016/j.rmed.2013.03.017.

Boazak EM and Auguste DT (2018) Trachea Mechanics for Tissue Engineering Design. *ACS Biomaterials Science & Engineering* 4(4). American Chemical Society: 1272–1284. DOI: 10.1021/acsbiomaterials.7b00738.

Borthwick DW, Shahbazian M, Todd Krantz Q, et al. (2001) Evidence for Stem-Cell Niches in the Tracheal Epithelium. *American Journal of Respiratory Cell and Molecular Biology* 24(6): 662–670. DOI: 10.1165/ajrcmb.24.6.4217.

Brand-Saberi BEM and Schäfer T (2014) Trachea. *Thoracic Surgery Clinics* 24(1): 1–5. DOI: 10.1016/j.thorsurg.2013.09.004.

Burton LV and Silberman M (2020) Bacterial Tracheitis. In: *StatPearls*. Treasure Island (FL): StatPearls Publishing. Available at: http://www.ncbi.nlm.nih.gov/books/NBK470240/ (accessed 9 November 2020).

Cassandras M, Wang C, Kathiriya J, et al. (2020) Gli1 + mesenchymal stromal cells form a pathological niche to promote airway progenitor metaplasia in the fibrotic lung. *Nature Cell Biology* 22(11). 11. Nature Publishing Group: 1295–1306. DOI: 10.1038/s41556-020-00591-9.

Chistiakov DA (2010) Endogenous and exogenous stem cells: a role in lung repair and use in airway tissue engineering and transplantation. *Journal of Biomedical Science* 17(1): 92. DOI: 10.1186/1423-0127-17-92.

Cole BB, Smith RW, Jenkins KM, et al. (2010) Tracheal Basal Cells. *The American Journal of Pathology* 177(1): 362–376. DOI: 10.2353/ajpath.2010.090870.

Cole P, Savard P, Miljeteig H, et al. (1993) Resistance to respiratory airflow of the extrapulmonary airways. *The Laryngoscope* 103(4 Pt 1): 447–450. DOI: 10.1002/lary.5541030415.

Croisier F and Jérôme C (2013) Chitosan-based biomaterials for tissue engineering. *European Polymer Journal* 49(4). Biobased Polymers and Related Materials: 780–792. DOI: 10.1016/j.eurpolymj.2012.12.009.

D'Andrilli A, Venuta F and Rendina EA (2016) Subglottic tracheal stenosis. *Journal of Thoracic Disease* 8(Suppl 2): S140–S147. DOI: 10.3978/j.issn.2072-1439.2016.02.03.

Delaere P and Van Raemdonck D (2016) Tracheal replacement. *Journal of Thoracic Disease* 8(Suppl 2): S186–S196. DOI: 10.3978/j.issn.2072-1439.2016.01.85.

Dhasmana A, Singh A and Rawal S (2020) Biomedical grafts for tracheal tissue repairing and regeneration "Tracheal tissue engineering: an overview". *Journal of Tissue Engineering and Regenerative Medicine* 14(5): 653–672. DOI: https://doi.org/10.1002/term.3019.

Diaz RS, Park J-R, Rodrigues LL, et al. (n.d.) Highly Elastic Scaffolds Produced by Melt Electrowriting of Poly(L-lactide-co-ε-caprolactone). *Advanced Materials Technologies* n/a(n/a): 2100508. DOI: 10.1002/admt.202100508.

Drevet G, Conti M and Deslauriers J (2016) Surgical anatomy of the tracheobronchial tree. *Journal of Thoracic Disease* 8(Suppl 2): S121–S129. DOI: 10.3978/j.issn.2072-1439.2016.01.69.

Elliott MJ, Speggiorin S, Vida VL, et al. (2009) Slide Tracheoplasty as a Rescue Technique After Unsuccessful Patch Tracheoplasty. *The Annals of Thoracic Surgery* 88(3): 1029–1031. DOI: 10.1016/j.athoracsur.2009.01.024.

Elliott MJ, De Coppi P, Speggiorin S, et al. (2012) Stem-cell-based, tissue engineered tracheal replacement in a child: a 2-year follow-up study. *Lancet (London, England)* 380(9846): 994–1000. DOI: 10.1016/S0140-6736(12)60737-5.

El-Sherbiny IM and Yacoub MH (2013) Hydrogel scaffolds for tissue engineering: Progress and challenges. *Global Cardiology Science and Practice* 2013(3): 38. DOI: 10.5339/gcsp.2013.38.

Ershadi R, Rahim M, Jahany S, et al. (2018) Transplantation of the decellularized tracheal allograft in animal model (rabbit). *Asian Journal of Surgery* 41(4): 328–332. DOI: 10.1016/j.asjsur.2017.02.007.

Etienne H, Fabre D, Caro AG, et al. (2018) Tracheal replacement. *European Respiratory Journal* 51(2). European Respiratory Society. DOI: 10.1183/13993003.02211-2017.

Fang S, Zhang S, Dai H, et al. (2019) The role of pulmonary mesenchymal cells in airway epithelium regeneration during injury repair. *Stem Cell Research & Therapy* 10(1): 366. DOI: 10.1186/s13287-019-1452-1.

Firth AL, Dargitz CT, Qualls SJ, et al. (2014) Generation of multiciliated cells in functional airway epithelia from human induced pluripotent stem cells. *Proceedings of the National Academy of Sciences of the United States of America* 111(17): E1723-1730. DOI: 10.1073/pnas.1403470111.

Fletcher A, Stowell J and Jamoulis S (n.d.) Congenital Tracheobronchomegaly (Mounier-Kuhn Syndrome) in a Woman with Human Immunodeficiency Virus: A Case Report. *Cureus* 9(4). DOI: 10.7759/cureus.1136.

Folch E and Keyes C (2018) Airway stents. *Annals of Cardiothoracic Surgery* 7(2): 273–283. DOI: 10.21037/acs.2018.03.08.

Frejo L and Grande DA (2019) 3D-bioprinted tracheal reconstruction: an overview. *Bioelectronic Medicine* 5(1): 15. DOI: 10.1186/s42234-019-0031-1.

Furlow PW and Mathisen DJ (2018) Surgical anatomy of the trachea. *Annals of Cardiothoracic Surgery* 7(2): 255–260. DOI: 10.21037/acs.2018.03.01.

Ganesan S and Sajjan US (2013) Repair and Remodeling of airway epithelium after injury in Chronic Obstructive Pulmonary Disease. *Current respiratory care reports* 2(3). DOI: 10.1007/s13665-013-0052-2.

Gerardo H, Lima A, Carvalho J, et al. (2019) Soft culture substrates favor stem-like cellular phenotype and facilitate reprogramming of human mesenchymal stem/stromal cells (hMSCs) through mechanotransduction. *Scientific Reports* 9(1): 9086. DOI: 10.1038/s41598-019-45352-3.

Gkioni K, Leeuwenburgh SCG, Douglas TEL, et al. (2010) Mineralization of Hydrogels for Bone Regeneration. *Tissue Engineering Part B: Reviews* 16(6). Mary Ann Liebert, Inc., publishers: 577–585. DOI: 10.1089/ten.teb.2010.0462.

Grillo HC (1994) Slide tracheoplasty for long-segment congenital tracheal stenosis. *The Annals of Thoracic Surgery* 58(3): 613-619 discussion 619-621. DOI: 10.1016/0003-4975(94)90714-5.

Grillo HC (2002) Tracheal replacement: a critical review. *The Annals of Thoracic Surgery* 73(6). Elsevier: 1995–2004. DOI: 10.1016/S0003-4975(02)03564-6.

Harris C, Cao C, Croce B, et al. (2018) Tracheal tumors. *Annals of Cardiothoracic Surgery* 7(2): 317. DOI: 10.21037/acs.2018.02.02.

Haykal S, Soleas JP, Salna M, et al. (2012) Evaluation of the structural integrity and extracellular matrix components of tracheal allografts following cyclical decellularization techniques: comparison of three protocols. *Tissue Engineering. Part C, Methods* 18(8): 614–623. DOI: 10.1089/ten.TEC.2011.0579.

Haykal S, Salna M, Waddell T, et al. (2014) Advances in Tracheal Reconstruction. *Plastic and reconstructive surgery. Global open* 2: e178. DOI: 10.1097/GOX.0000000000000097.

Hong Y (2016) 19 - Electrospun fibrous polyurethane scaffolds in tissue engineering. In: Cooper SL and Guan J (eds) *Advances in Polyurethane Biomaterials*. Woodhead Publishing, pp. 543–559. DOI: 10.1016/B978-0-08-100614-6.00019-6.

Hsieh C-T, Liao C-Y, Dai N-T, et al. (2018) 3D printing of tubular scaffolds with elasticity and complex structure from multiple waterborne polyurethanes for tracheal tissue engineering. *Applied Materials Today* 12: 330–341. DOI: 10.1016/j.apmt.2018.06.004.

Hurley JJ and Hensley JL (2020) Physiology, Airway Resistance. In: *StatPearls*. Treasure Island (FL): StatPearls Publishing. Available at: http://www.ncbi.nlm.nih.gov/books/NBK542183/ (accessed 9 November 2020).

Ito JT, Lourenço JD, Righetti RF, et al. (2019) Extracellular Matrix Component Remodeling in Respiratory Diseases: What Has Been Found in Clinical and Experimental Studies? *Cells* 8(4). DOI: 10.3390/cells8040342.

Khazraee SP, Marashi SM, Kaviani M, et al. (2018) Stem Cell-Based Therapies and Tissue Engineering of Trachea as Promising Therapeutic Methods in Mustard Gas Exposed Patients. *International Journal of Organ Transplantation Medicine* 9(4): 145–154.

Kim IG, Park SA, Lee S-H, et al. (2020) Transplantation of a 3D-printed tracheal graft combined with iPS cell-derived MSCs and chondrocytes. *Scientific Reports* 10(1). 1. Nature Publishing Group: 4326. DOI: 10.1038/s41598-020-61405-4.

Kim JK, Vinarsky V, Wain J, et al. (2012) In Vivo Imaging of Tracheal Epithelial Cells in Mice during Airway Regeneration. *American Journal of Respiratory Cell and Molecular Biology* 47(6): 864–868. DOI: 10.1165/rcmb.2012-0164OC.

Kim S-H, Lee HR, Yu SJ, et al. (2015) Hydrogel-laden paper scaffold system for origami-based tissue engineering. *Proceedings of the National Academy of Sciences* 112(50): 15426–15431. DOI: 10.1073/pnas.1504745112.

Kim WS, Chang JW, Jang WS, et al. (2017) Tracheal reconstruction with a free vascularized myofascial flap: preclinical investigation in a porcine model

to human clinical application. *Scientific Reports* 7(1). 1. Nature Publishing Group: 10022. DOI: 10.1038/s41598-017-10733-z.

Kojima K and Vacanti CA (2014) Tissue Engineering in the Trachea. *The Anatomical Record* 297(1): 44–50. DOI: https://doi.org/10.1002/ar.22799.

Kojima K, Bonassar LJ, Ignotz RA, et al. (2003) Comparison of tracheal and nasal chondrocytes for tissue engineering of the trachea. *The Annals of Thoracic Surgery* 76(6). Elsevier: 1884–1888. DOI: 10.1016/S0003-4975(03)01193-7.

Lenot B, Macchiarini P, Dulmet E, et al. (1993) Tracheal allograft replacement. An unsuccessful method. *European Journal of Cardio-Thoracic Surgery: Official Journal of the European Association for Cardio-Thoracic Surgery* 7(12): 648–652. DOI: 10.1016/1010-7940(93)90261-9.

Liu H-C, Lee K-S, Huang C-J, et al. (2002) Silicone T-tube for complex laryngotracheal problems. *European Journal of Cardio-Thoracic Surgery* 21(2). Oxford Academic: 326–330. DOI: 10.1016/S1010-7940(01)01098-3.

Liu Z and Zhang X (2017) A vascularized tissue-engineered trachea with ectopic pedicled muscle flap. *Biomedical Research* 28(3). Allied Academies. Available at: https://www.alliedacademies.org/abstract/a-vascularized-tissueengineered-trachea-with-ectopic-pedicled-muscle-flap-6460.html (accessed 9 November 2020).

Lopes MS, Jardini AL and Filho RM (2012) Poly (Lactic Acid) Production for Tissue Engineering Applications. *Procedia Engineering* 42. CHISA 2012: 1402–1413. DOI: 10.1016/j.proeng.2012.07.534.

Mabrut JY, Adham M, Bourgeot JP, et al. (2001) Mechanical and histological characteristics of human trachea before and after cryopreservation: an opportunity for tracheal tissue banking. *Transplantation Proceedings* 33(1–2): 609–611. DOI: 10.1016/S0041-1345(00)02166-7.

Macchiarini P, Jungebluth P, Go T, et al. (2008) Clinical transplantation of a tissue-engineered airway. *Lancet (London, England)* 372(9655): 2023–2030. DOI: 10.1016/S0140-6736(08)61598-6.

Madariaga MLL and Gaissert HA (2018) Overview of malignant tracheal tumors. *Annals of Cardiothoracic Surgery* 7(2). 2: 244-254–254. DOI: 10.3978/16457.

Maughan EF, Hynds RE, Proctor TJ, et al. (2017) Autologous Cell Seeding in Tracheal Tissue Engineering. *Current Stem Cell Reports* 3(4): 279–289. DOI: 10.1007/s40778-017-0108-2.

Mete A and Akbudak İ (2018) Functional Anatomy and Physiology of Airway. DOI: 10.5772/intechopen.77037.

Morrisey EE, Cardoso WV, Lane RH, et al. (2013) Molecular Determinants of Lung Development. *Annals of the American Thoracic Society* 10(2): S12–S16. DOI: 10.1513/AnnalsATS.201207-036OT.

Nakanishi R (2007) Revascularization of trachea in lung and tracheal transplantation. *Clinical Transplantation* 21(5): 668–674. DOI: 10.1111/j.1399-0012.2007.00752.x.

Nandakumar R, Jagdish C, Prathibha C, et al. (2011) Tracheal resection with end-to-end anastomosis for post-intubation cervical tracheal stenosis: Study of 14 cases. *The Journal of laryngology and otology* 125: 958–61. DOI: 10.1017/S002221511100137X.

Nettesheim P, Jetten AM, Inayama Y, et al. (1990) Pathways of differentiation of airway epithelial cells. *Environmental Health Perspectives* 85: 317–329.

Neville WE, Bolanowski PJP and Bentley D (1991) Tracheal Reconstruction: Success with A Silicone Tracheal Prosthesis. *AORN Journal* 54(3): 470–482. DOI: 10.1016/S0001-2092(07)66766-0.

O'Brien FJ (2011) Biomaterials & scaffolds for tissue engineering. *Materials Today* 14(3): 88–95. DOI: 10.1016/S1369-7021(11)70058-X.

Okumura N, Nakamura T, Natsume T, et al. (1994) Experimental study on a new tracheal prosthesis made from collagen-conjugated mesh. *The Journal of Thoracic and Cardiovascular Surgery* 108(2): 337–345.

Oliveira JT and Reis RL (2011) Polysaccharide-based materials for cartilage tissue engineering applications. *Journal of Tissue Engineering and Regenerative Medicine* 5(6): 421–436. DOI: 10.1002/term.335.

Ouyang L, Yao R, Zhao Y, et al. (2016) Effect of bioink properties on printability and cell viability for 3D bioplotting of embryonic stem cells. *Biofabrication* 8(3): 035020. DOI: 10.1088/1758-5090/8/3/035020.

Park H, Gong M-S and Knowles JC (2013) Catalyst-free synthesis of high elongation degradable polyurethanes containing varying ratios of isosorbide and polycaprolactone: physical properties and biocompatibility. *Journal of Materials Science: Materials in Medicine* 24(2): 281–294. DOI: 10.1007/s10856-012-4814-0.

Park JH, Hong JM, Ju YM, et al. (2015) A novel tissue-engineered trachea with a mechanical behavior similar to native trachea. *Biomaterials* 62: 106–115. DOI: 10.1016/j.biomaterials.2015.05.008.

Peers S, Montembault A and Ladavière C (2020) Chitosan hydrogels for sustained drug delivery. *Journal of Controlled Release* 326: 150–163. DOI: 10.1016/j.jconrel.2020.06.012.

Perl A-KT, Wert SE, Loudy DE, et al. (2005) Conditional Recombination Reveals Distinct Subsets of Epithelial Cells in Trachea, Bronchi, and

Alveoli. *American Journal of Respiratory Cell and Molecular Biology* 33(5): 455–462. DOI: 10.1165/rcmb.2005-0180OC.

Pj B (1986) Neural control of human airways in health and disease. *The American Review of Respiratory Disease* 134(6): 1289–1314. DOI: 10.1164/arrd.1986.134.5.1289.

Puchelle E, Zahm J-M, Tournier J-M, et al. (2006) Airway Epithelial Repair, Regeneration, and Remodeling after Injury in Chronic Obstructive Pulmonary Disease. *Proceedings of the American Thoracic Society* 3(8). American Thoracic Society - PATS: 726–733. DOI: 10.1513/pats.200605-126SF.

Rawlins EL and Hogan BLM (2008) Ciliated epithelial cell lifespan in the mouse trachea and lung. *American Journal of Physiology. Lung Cellular and Molecular Physiology* 295(1): L231–L234. DOI: 10.1152/ajplung.90209.2008.

Reynolds SD, Pinkerton KE and Mariassy AT (2015) Epithelial Cells of Trachea and Bronchi. In: *Comparative Biology of the Normal Lung*. Elsevier, pp. 61–81. DOI: 10.1016/B978-0-12-404577-4.00006-0.

Risbud M, Endres M, Ringe J, et al. (2001) Biocompatible hydrogel supports the growth of respiratory epithelial cells: possibilities in tracheal tissue engineering. *Journal of Biomedical Materials Research* 56(1): 120–127. DOI: 10.1002/1097-4636(200107)56:1<120::aid-jbm1076>3.0.co;2-w.

Rodríguez-Vázquez M, Vega-Ruiz B, Ramos-Zúñiga R, et al. (2015) Chitosan and Its Potential Use as a Scaffold for Tissue Engineering in Regenerative Medicine. Hindawi. DOI: https://doi.org/10.1155/2015/821279.

Santiago-Rosado LM, Sigmon DF and Lewison CS (2020) Tracheal Trauma. In: *StatPearls*. Treasure Island (FL): StatPearls Publishing. Available at: http://www.ncbi.nlm.nih.gov/books/NBK500015/ (accessed 9 November 2020).

Seguin A, Baccari S, Holder-Espinasse M, et al. (2013) Tracheal regeneration: evidence of bone marrow mesenchymal stem cell involvement. *The Journal of Thoracic and Cardiovascular Surgery* 145(5): 1297-1304.e2. DOI: 10.1016/j.jtcvs.2012.09.079.

Selig M, Lauer JC, Hart ML, et al. (2020) Mechanotransduction and Stiffness-Sensing: Mechanisms and Opportunities to Control Multiple Molecular Aspects of Cell Phenotype as a Design Cornerstone of Cell-Instructive Biomaterials for Articular Cartilage Repair. *International Journal of Molecular Sciences* 21(15): E5399. DOI: 10.3390/ijms21155399.

She Y, Fan Z, Wang L, et al. (2021) 3D Printed Biomimetic PCL Scaffold as Framework Interspersed With Collagen for Long Segment Tracheal Replacement. *Frontiers in Cell and Developmental Biology* 0. Frontiers. DOI: 10.3389/fcell.2021.629796.

Shin Y, Choi J, Park J-K, et al. (2014) Tissue-Engineered Tracheal Reconstruction Using Mesenchymal Stem Cells Seeded on a Porcine Cartilage Powder Scaffold. *Annals of biomedical engineering* 43. DOI: 10.1007/s10439-014-1126-1.

Singhvi MS, Zinjarde SS and Gokhale DV (2019) Polylactic acid: synthesis and biomedical applications. *Journal of Applied Microbiology* 127(6): 1612–1626. DOI: https://doi.org/10.1111/jam.14290.

Snijders D and Barbato A (2015) An Update on Diagnosis of Tracheomalacia in Children. *European Journal of Pediatric Surgery: Official Journal of Austrian Association of Pediatric Surgery ... [et Al] = Zeitschrift Fur Kinderchirurgie* 25(4): 333–335. DOI: 10.1055/s-0035-1559816.

Tiddens H a. WM, Hofhuis W, Bogaard JM, et al. (1999) Compliance, Hysteresis, and Collapsibility of Human Small Airways. *American Journal of Respiratory and Critical Care Medicine* 160(4). American Thoracic Society - AJRCCM: 1110–1118. DOI: 10.1164/ajrccm.160.4.9709004.

Turcatel G, Rubin N, Menke DB, et al. (2013) Lung mesenchymal expression of Sox9plays a critical role in tracheal development. *BMC Biology* 11(1): 117. DOI: 10.1186/1741-7007-11-117.

Venkatesan J, Kim S-K and Wong TW (2015) Chapter 9 - Chitosan and Its Application as Tissue Engineering Scaffolds. In: Thomas S, Grohens Y, and Ninan N (eds) *Nanotechnology Applications for Tissue Engineering*. Oxford: William Andrew Publishing, pp. 133–147. DOI: 10.1016/B978-0-323-32889-0.00009-1.

Wang T and Yang F (2017) A comparative study of chondroitin sulfate and heparan sulfate for directing three-dimensional chondrogenesis of mesenchymal stem cells. *Stem Cell Research & Therapy* 8. DOI: 10.1186/s13287-017-0728-6.

Zhang H, Fu W and Xu Z (2015) Re-epithelialization: a key element in tracheal tissue engineering. *Regenerative Medicine* 10(8): 1005–1023. DOI: 10.2217/rme.15.68.

Zhao Z, Zhang T, Yin X, et al. (2017) Update on the diagnosis and treatment of tracheal and bronchial injury. *Journal of Thoracic Disease* 9(1): E50–E56. DOI: 10.21037/jtd.2017.01.19.

Zhou Y, Horowitz JC, Naba A, et al. (2018) Extracellular Matrix in Lung De5.velopment, Homeostasis and Disease. *Matrix biology : journal of the International Society for Matrix Biology* 73: 77–104. DOI: 10.1016/j.matbio.2018.03.00

## Publications

1) Lynda V Thomas, **Rahul V G**, Prabha D Nair (2017) Effect of stiffness of chitosan-hyaluronic acid dialdehyde hydrogels on the viability and growth of encapsulated chondrocytes. Int J BiolMacromol 104(Pt B):1925-1935.

2) **Rahul V.G**, Jijo Wilson, Lynda V Thomas, Prabha D. Nair Assessing the 3D printability of elastomeric poly(caprolactone-co-lactide) copolymer as a potential material for 3D printing tracheal scaffolds DOI 10.1021/acsomega. 1c06679 in *ACS Omega.*

## Patents

3D printed biphasic scaffold for tracheal reconstruction, Indian patent Application no: 201941042440.

## Design registration

3D printed biphasic scaffold for tracheal reconstruction, design application number 323114-001.

## Book chapter

**Rahul V G**, Prabha D Nair (2016) Biomaterials and Designs Supporting Cartilage Regeneration. CRC Press.ISBN 978-1-4987-4373-0.

## Conference Attended

1)11$^{th}$ Asia Pacific Chitin and Chitosan Symposium & 5$^{th}$ Indian Chitin and Chitosan Society Symposium, 2016, India.

**Oral presentation:** Effect of stiffness of chitosan-hyaluronic acid dialdehyde hydrogels on the viability and growth of encapsulated chondrocytes.

2)International Conference on Biomaterials, BioEngineering&BioTheranostics, 2018, India.

**Poster presentation:** A comparative study on 3D printed and electrospun elastomeric tracheal constructs

# CURRICULUM VITAE

## ACADEMIC PROFILE

| | |
|---|---|
| 2014- Present | PhD Scholar at SreeChitraTirunal Institute for Medical Sciences and Technology,.Biomedical Technology Wing, Thiruvananthpuram, Kerala, India.<br>Advisor: Dr. Prabha D. Nair |
| 2010-2012 | Master of Science in Biomedical Genetics, VIT University, Tamil Nadu. |
| 2006-2009 | Bachelor of Science in Biotechnology, Bangalore University. |

## Awards and Honours

| | |
|---|---|
| 2016 | **Best oral presentation award:** Effect of stiffness of chitosan-hyaluronic acid dialdehyde hydrogels on the viability and growth of encapsulated chondrocytes. |
| 2014 | Institute fellowship, SCTIMST. |